The Pennsylvania State University

The Graduate School

College of Earth and Mineral Sciences

GRAIN SIZE CONTROLS ON PLANFORM MORPHOLOGY AND STRATIGRAPHY OF RIVER-DOMINATED DELTAS

A Thesis in

Geosciences

by

Alexander P. Burpee

Submitted in Partial Fulfillment
of the Requirements
for the Degree of

Master of Science

December 2012

The thesis of Alexander P. Burpee was reviewed and approved* by the following:

Rudy L. Slingerland
Professor of Geology
Thesis Adviser

Douglas A. Edmonds
Assistant Professor of Geological Sciences
Indiana University

Elizabeth Hajek
Assistant Professor of Geosciences

Michael Arthur
Professor of Geosciences

Chris Marone
Professor of Geosciences
Head of the Graduate Program

*Signatures are on file in the Graduate School.

ABSTRACT

The proportions of sand and mud that make up a river-dominated delta strongly determine its topset morphology, which in turn controls its internal facies and clinoforms. These relationships allow one to predict the stratigraphy of a delta from the character of its topset or reconstruct its planform from measures of clinoform geometry. We used Delft3D to simulate nine self-formed deltas having different sediment loads and critical shear stresses required for re-entrainment of mud. The deltas prograded into a shallow basin absent of waves, tides, Coriolis forcing, and buoyancy. Model results indicate that sand-dominated deltas are more fan-shaped and mud-dominated deltas are more bird's foot in planform because the sand-dominated deltas have more active distributaries and a smaller variance of topset elevations, and thereby experience more equitable distribution of sediment to their perimeters. This results in a larger proportion of channel facies and autogenic parasequences in sand-dominated deltas, and more uniformly-distributed clinoform dip directions, steeper dips, and greater clinoform concavity. These conclusions are consistent with data collected from the Goose River Delta, a coarse-grained fan delta prograding into Goose Bay, Labrador, Canada. These results allow a re-interpretation of the Kf-1 parasequence set of the Cretaceous Last Chance Delta, a unit of the Ferron Sandstone near Emery, UT. Inversion of Ferron grain size data, clinoform dips, clinoform concavity, and variance of dip directions suggests that the Kf-1 Last Chance Delta was more fan-delta than bird's foot, and therefore more consistent with Cotter (1976) and Thompson (1986) than Gardner (1995a, 1995b) and Anderson and Ryer (2004). It likely possessed numerous distributaries with at least five orders of bifurcation.

TABLE OF CONTENTS

LIST OF TABLES

LIST OF FIGURES

ACKNOWLEDGEMENTS

First and foremost, I must express my sincerest gratitude to Dr. Rudy Slingerland for his advising of my graduate studies. This project was born out of his passion for deltas and his passion is contagious. It has been an absolute privilege to work with such a formidable and creative scientist. Thank you for the opportunity. Thank you for teaching me how to think and how to approach problems. Thank you for being a mentor and a true friend.

Thank you to my thesis committee: Dr. Rudy Slingerland, Dr. Michael Arthur, Dr. Elizabeth Hajek, and Dr. Douglas Edmonds. You have all provided the necessary comments and criticisms to keep this project moving in the right direction. In many ways, Dr. Edmonds' previous work in the numerical modeling of deltas set the stage for this project and he has made numerous contributions to this body of work.

I have learned much while studying in the Geosciences Department and I want to thank Dr. Donald Fisher, Dr. Chris Marone, Dr. Charles Ammon, Dr. Rudy Slingerland, Dr. Sridhar Anandakrishnan, Dr. Elizabeth Hajek, and Dr. Lee Kump for their instruction. Thank you to my fellow graduate students, too numerous to mention, for your positive influence on my time at Penn State.

Thank you to the Labrador field party: Dr. Rudy Slingerland, Dr. Douglas Edmonds, Dr. James Best, Dr. Daniel Parsons, James Cederberg, Andrew McGuffin, Rebecca Caldwell, Austin Nijhuis, and Jordan Royce. Your contributions to this project are significant and it is to your credit that I was able to use the Goose River Delta as a test of the numerical models. I also appreciate the time and energy spent by Leo Peters, Peter Burkett, Lucas Zoet, and Dr. Sridhar Anandakrishnan helping with ground-penetrating radar and seismic data acquisition and

processing. While those data are not presented in this thesis they will be valuable for our research group in the future.

I would not have been able to measure clinoforms of the Last Chance Delta without the help of Sarah Prozeller. Her dedication and attitude made for both a successful and enjoyable field campaign. Also, thank you to Waylon and Tara Ivie, the Ranch Motel, Mom's Café, and the rest of Salina, Utah, for making us feel at home.

Thank you to James Cederberg, Andrew McGuffin, and Travis Call for reviewing this thesis. Thank you to Matt Herman for our conversation about measuring clinoform concavity.

This research has been funded by the National Science Foundation grant OCE – 1061495 awarded to R.L. Slingerland and D.A. Edmonds, and grant EAR – 0809653 awarded to R.L. Slingerland and J. Best.

To my mother and father.

INTRODUCTION

Deltas are the link between source terrains and basins, and their planform and internal characteristics should reflect influences of both domains. Traditionally, the morphologies of the world's deltas were thought to be determined mainly by river discharge, tidal range, and wave climate (Fig. 1) as summarized in the well-known ternary classification of deltas (Galloway, 1975). In this classification wave-dominated deltas, like the Rhone River Delta, are said to have smooth shorelines that are constantly reworked by waves and longshore transport, thereby producing a fan shape. Tide-dominated deltas, like the Niger Delta, are trumpet-shaped because ebbing and flooding tides create flow-parallel bars within the sub-tidal estuary. And river-dominated deltas, like the Mississippi, are thought to be shaped by the energy of the river and prograde offshore with well-defined levees and digitate shorelines. Postma (1990) modified the Galloway classification by suggesting that the morphology and facies of the delta plain, prodelta, and delta front are governed at the first-order level by basinal processes and at the second-order level by the feeder system. He recognized the importance of the catchment and proposed 12 prototype deltas that reflect the interaction of the feeder system and the basin. Then in a landmark paper, Orton and Reading (1993) argued that "the amount, mode of emplacement, and grain size of the sediment load to a delta have a considerable effect on the physical processes, environments, and the shape and size of the delta (p. 476)." Orton and Reading (1993) specifically discussed the role of grain size in determining delta morphology and they recognized its influence on the feeder channel, the type of shoreline, and processes on the subaequeous delta front. They called upon the delta community for predictive models that incorporate better understanding of the feeder system. Recently, Edmonds and Slingerland (2010) used numerical experiments to quantify the effect of grain size on delta planform. They showed that sediment cohesion, and by implication sediment size and vegetation type, play a major role in determining

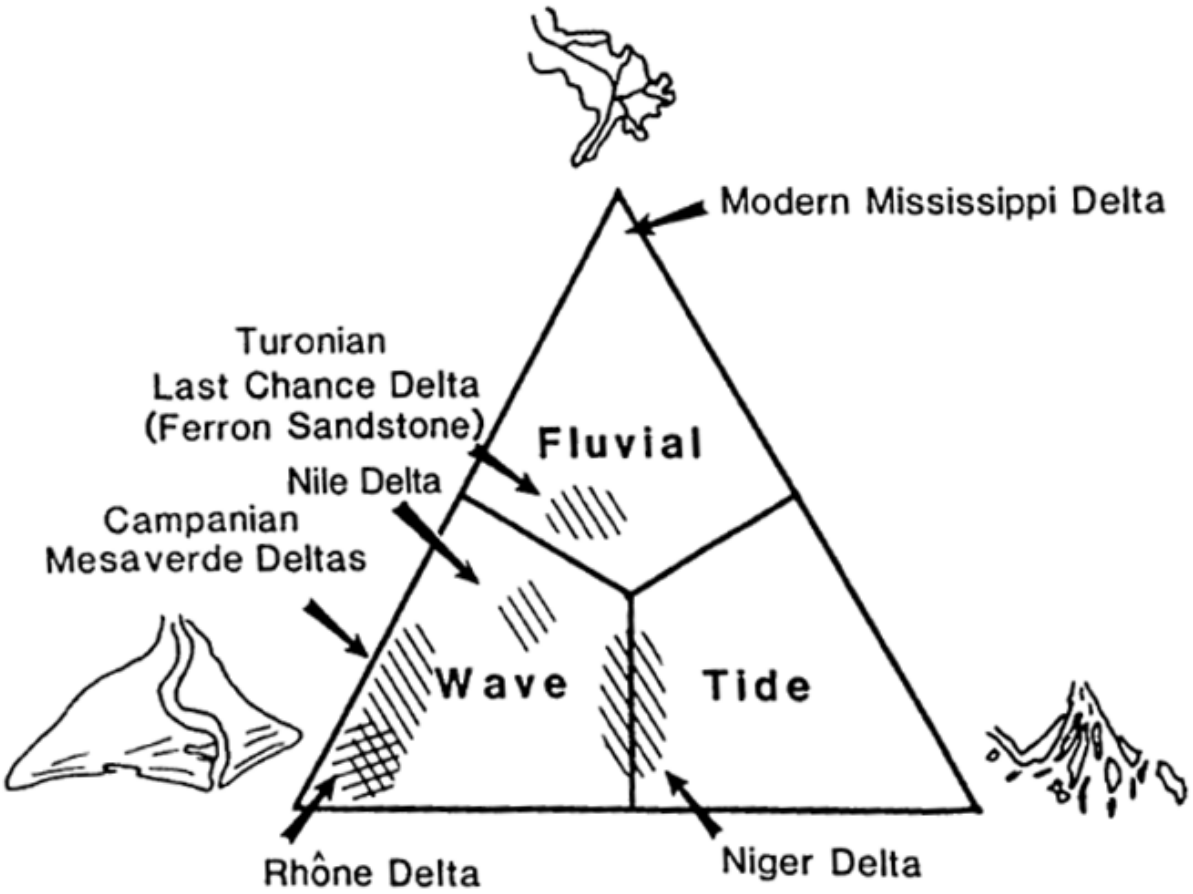

Figure 1. The ternary diagram is useful for qualitatively representing the relative importance of waves, tides, and river discharge in shaping delta planform morphology (modified from Galloway, 1975 by Thompson et al., 1986).

the shapes, cumulative number of distributaries, and wetland areas of river-dominated deltas. In their experiments elongate deltas with rugose shorelines and topographically rough floodplains were created if the incoming sediment was highly cohesive. Fan-like deltas with smooth shorelines and flat floodplains were created by less cohesive sediment.

Research Objective

The objective of this research is to better quantify the functional relationships between the sediment creating a delta, the resulting delta morphology, and the delta's internal stratigraphy. We specifically include delta facies and stratal architecture because these are more observable in the rock record than delta planform. Our work plan consists of three parts: 1) a suite of nine numerical experiments using Delft3D to predict delta morphologies, facies, and stratigraphy as a function of various sediment types, thereby extending the work of Edmonds and Slingerland (2010); 2) a test of the model predictions using the modern Goose River Delta of Labrador, Canada, through field observations of its planform, facies, and stratigraphy; and 3) an application of the results to an ancient delta, the Last Chance Delta of the Ferron Sandstone, Utah, US.A. We aim to show that there are predictable relationships between sediment type and delta planform, and between delta planform and clinoform morphology, facies partitioning, and reservoir morphology. Furthermore, we conjecture that this novel approach of numerically modeling a depositional system, validating the model results using a modern analog, and applying the model results to an ancient depositional system will provide a more accurate interpretation than current methodology permits.

Background

Current research into the sufficient conditions necessary to produce delta morphology and stratigraphy remains limited (Giosan et al., 2005; Syvitski and Saito, 2007, Syvitski, 2006;

Syvitski, 2008). While some studies have recognized that internal stratigraphy can differ from what would be expected from facies models dependent upon shoreline geometry (Lambiase et al., 2003; Rodriguez et al., 2000; Fielding et al., 2005a, 2005b), most current depositional models of deltas are strongly dependent upon interpretations of a delta's planform morphology (Coleman and Wright, 1975; Bhattacharya and Walker, 1991b; Bhattacharya, 2006). This belief has driven the hypothesis that delta sand body geometries are a function of river, wave, and tide influence (Bhattacharya, 2006; Coleman and Wright, 1975; Coleman, 1976; Galloway, 1975). Such facies models dependent upon these classic ternary forces can be incorrect as in the case of a delta with a wave- or tide-dominated morphology that is internally dominated by fluvial facies (Fielding et al., 2005; Lambiase et al., 2003; Rodriguez et al., 2000).

Like Postma (1990) and Orton and Reading (1993) we argue that sediment type and load (mass of sediment delivered to the delta head per unit time) exert more influence on delta morphology and stratigraphy than is currently appreciated. While it is generally accepted that non-cohesive deltas are fan-like, constructed by few simultaneously active distributaries, and their stratigraphy is characterized by angle of repose foresets (McPherson et al., 1987; Postma, 1990), and finer-grained deltas are constructed by more simultaneously active distributaries, it is challenging to identify the role of sediment properties and tease out cause and effect. Postma (1990) and Orton and Reading (1993) hypothesized that the steepness of a delta foreset and coastal plain increase with increasing grain size, and that these conditions predispose coarse-grained systems to feedbacks whereby they are more susceptible to strong wave influence due to deep bathymetry caused by steep foresets, and they resist tidal influence because of the steep coastal plain. To the best of our knowledge, there has been no systematic inventory of delta

stratigraphy as a function of sediment load and type while holding all other external forcing factors constant.

The dependency of clinoform geometry upon sediment properties and delta morphology is even less well known. We define a clinoform as a chronostratigraphic horizon cutting obliquely through a heterolithic, coarsening upward sequence (Mitchum et al., 1977), such as commonly observed in a single basin-ward dipping seismic reflector, and we define the term clinothem as the deposits separated by clinoforms. Clinoform geometries are thought to be a function of four semi-independent variables: rate of creation of accommodation space, type and mass of sediment flux to the delta, distributive processes on the delta topset, and stage of development. Researching these relationships has been attempted using theory (Driscoll and Karner, 1999; Kostic and Parker, 2003a; Kostic and Parker, 2003b), experimentation (Paola et al., 2001; Pratson et al., 2004; Niedoroda et al., 2005), and observation. Observational studies conducted on many modern clinothems around the world provide specific realizations of the functional relationship between clinothem characteristics and the controlling independent variables (Kuehl et al., 1986; Nittrouer et al., 1986; Nittrouer et al., 1995), but the relative importance of each variable remains unknown.

Approach

This study seeks to quantify the link between a delta's sediment feed and its topset, and the link between a delta's topset and its stratigraphy. Specifically, we will test the following hypotheses:

(1) *If a relatively non-cohesive delta is constructed by a sand-dominated sediment load, then it will have more active distributaries, a less rugose shoreline morphology, less topset complexity, and a foreset with smaller uniformity than a highly cohesive delta constructed by a mud-dominated sediment load;*

(2) If a relatively non-cohesive delta is constructed by a sand-dominated sediment load then its stratigraphy will have greater clinoform dip magnitudes, greater clinoform concavity, more channel facies, more autogenic parasequences, and less rugose sand bodies than a highly cohesive delta constructed by a mud-dominated sediment load;

(3) If we have a priori knowledge of a fluvial catchment and its geology, then we can predict delta planform morphology and vice versa; and

(4) If we have a priori knowledge of delta planform morphology, then we can predict stratigraphy and vice versa.

These hypotheses may be falsified if geomorphological relationships with stratigraphy become disconnected as a result of accommodation, sediment supply, or other boundary condition changes occurring independent of sediment properties. We test these hypotheses by creating nine experimental deltas of differing sediment grain sizes and cohesion in the absence of waves, tides, and eustatic base level changes. The deltas are predicted by Delft3D, a morphodynamic model used extensively in coastal engineering studies (Lesser et al., 2004). We next quantify the morphology of the experimental delta topsets, foresets, and internal stratigraphy in order to generate a predictive facies model for each delta type. These predictive models are tested by comparing one of them, a coarse-grained end-member, to a modern coarse-grained delta, the Goose River Delta of Labrador, Canada, that experiences minimal waves and tides. Finally, we apply the predictive model to reinterpret the Cretaceous Last Chance Delta of the Ferron Sandstone of Utah, U.S.A.

Controlling Variables

We define four metrics to quantify differences in delta topsets: 1) number of active distributaries (d), 2) shoreline rugosity (IQ), 3) topset roughness (T), and 4) foreset dip azimuth uniformity

(U^2). We define five metrics to quantify delta stratigraphy: 1) average clinoform dip magnitude (α), 2) average clinoform concavity (c), 3) facies proportion (F), 4) number of autogenic parasequences (P), and 5) reservoir rugosity (R). The experiment is conceived as a multiple regression problem where this set of variables is a function of the independent variables sediment grain size (D_{50}) and cohesion (C):

$$(d, IQ, T, U^2, \alpha, c, F, P, R) = f(D_{50}, C)$$

Number of Active Distributaries (d)---. The number of active distributaries is defined as the number of distributaries participating in sediment deposition at the delta shoreline. Distributaries are the conduits through which sediments are deposited on the delta topset and foreset, and as such, we believe they are important for organizing delta stratigraphy. Distributaries incise previously deposited strata, and they are easily recognized in stratigraphy. The number of active distributaries and their avulsion frequencies should influence the occurrence of channel facies in the stratigraphic record. Deltas with numerous distributaries should have more uniform fan-like shapes and highly mobile distributaries will also make deltas more prone to take a fan shape. As a delta progrades, the foreset should reflect the nature of the distributaries because the foreset derives its sediments from the distributaries.

In this study, we count distributaries where they influence the shoreline and create visual morphodynamic change (Fig. 2). Distributaries passing water and sediment but not participating in morphodynamic evolution at the shoreline are not counted.

Shoreline Rugosity (IQ)---. Shoreline rugosity is defined as the roughness of the geomorphic shoreline (Fig. 3). The geometry of the shoreline is thought to be a reflection of the receiving basin and delta distributaries. Shorelines are an important metric to include because they are inarguably the most easily recognizable feature of modern deltas, yet, they are the most difficult

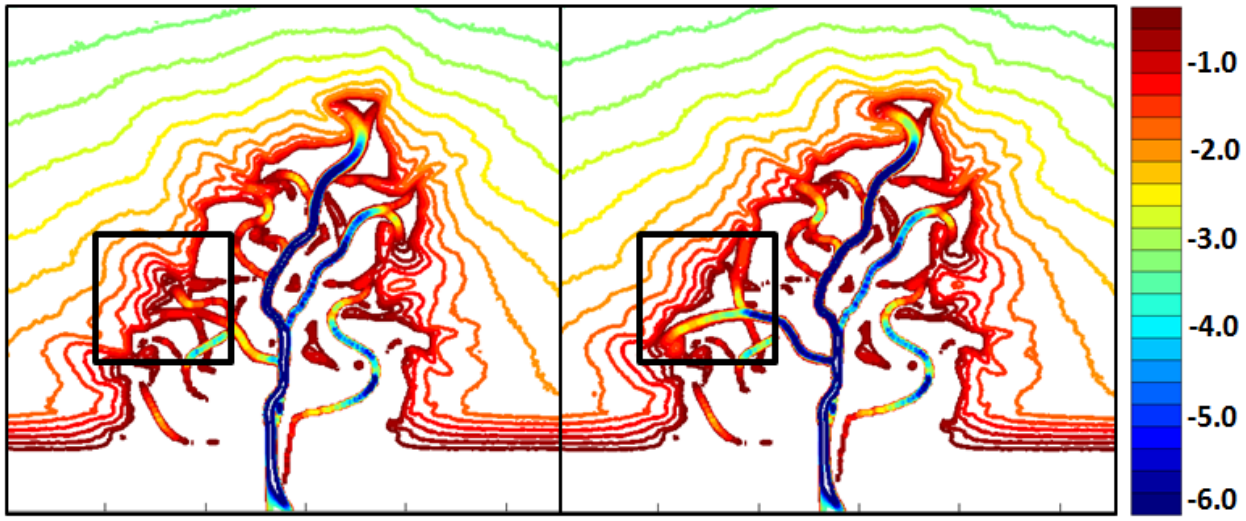

Figure 2. Active distributaries (above is an example from Delta E in Fig. 9) are counted where distributaries create visual morphodynamic change over time. The image on the left shows an earlier point of delta growth than the image on the right, and the black boxes highlight some of the most pronounced morphodynamic changes through time where distributary bifurcation has caused a large mouth bar to form.

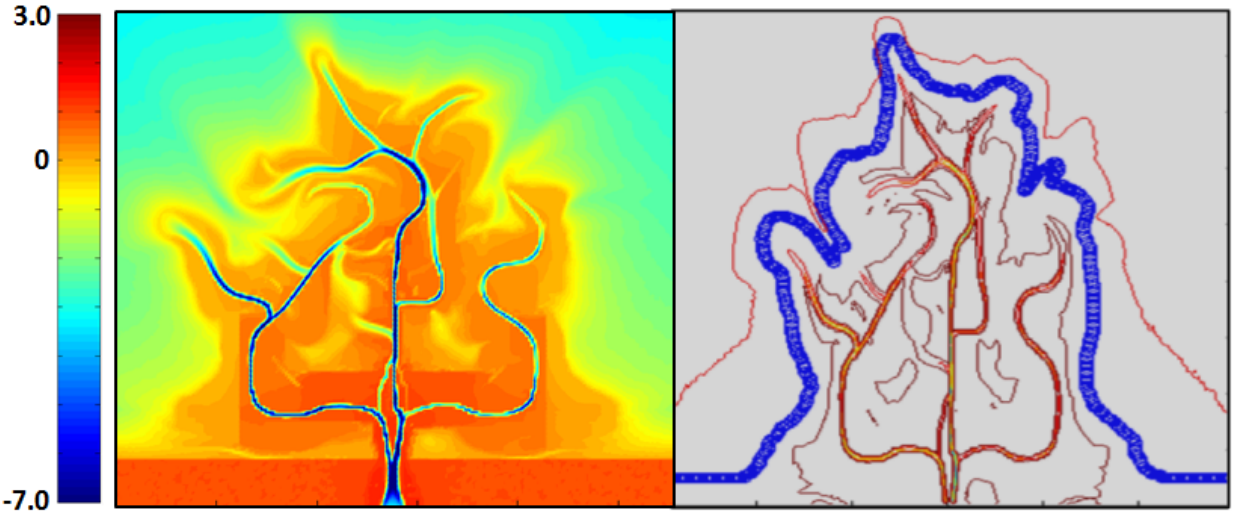

Figure 3. A delta shoreline (above is an example from Delta H in Fig. 9) is approximated by using the open angle method (Shaw et al., 2008). The blue line in the image on the right is the open angle method result of the delta shoreline from the image on the left. The area inside the blue line and the perimeter of the blue line are used to calculate rugosity.

feature to recover from an ancient delta. Here, we postulate that the shoreline geometry is a manifestation of the behavior of delta distributaries.

There is no widely accepted method for quantifying delta shoreline rugosity; here we propose the isoperimetric quotient (IQ) given by:

$$IQ = 4 \pi A / P^2$$

where A = the area [m^2] of the plane figure enclosed by a line and P = the figure's perimeter [m]. Notice that IQ is dimensionless and is devised such that a circle has the value of one. Highly rugose, complex shorelines with shapes that deviate from a circle have low IQ's while low rugosity, uniform shorelines that approximate a fan have IQs nearer to 1. We measure shoreline rugosity by fitting a polygon to the delta topset and computing the area and wetted perimeter of the polygon. Shoreline points are selected using the open angle method, with the angle being 25° (Shaw et al., 2008). The open angle method standardizes a shoreline cut-off for contour points inside distributaries.

Topset Roughness (T)---. The roughness of a delta topset is defined as the standard deviation of topset bed elevation points (Fig. 4). Topset elevations are defined as bed elevation points with magnitudes greater than -0.1 m. The roughness of a delta topset should control distributary avulsion frequency because topset roughness is thought to be primarily controlled by distributary levee aggradation. In systems with a high proportion of fine-grained sediments, distributary levees typically aggrade and stabilize making it more difficult for distributaries to avulse than in coarser-grained systems. Topset roughness is an important metric for this study because levee stability acts as a control on distributaries and distributaries impact delta stratigraphy.

F-tests of topset roughness measurements from random line orientations indicate that topset roughness is not a function of position of strike or dip line on the delta. As the position of

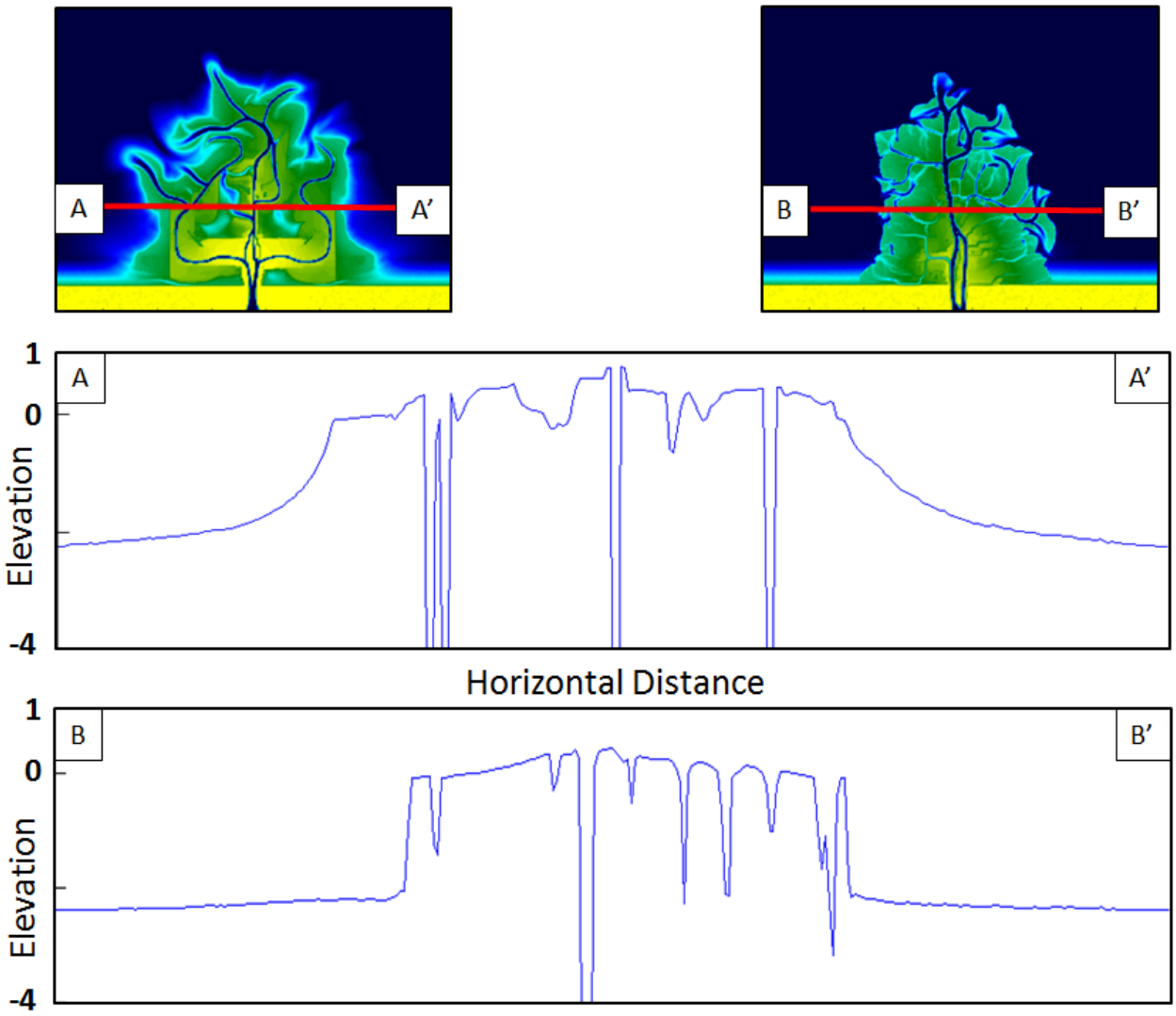

Figure 4. The roughness of a delta topset is demonstrated through levee aggradation. The topographic cross-section A to A' of a mud-dominated delta (Delta H in Fig. 9) shows higher elevation levees and undulatory topography and the topographic cross-section B to B' of a sand-dominated delta reveals a smoother topography with relatively little levee aggradation and less undulation.

a strike line on the delta becomes more proximal or distal, the average and maximum elevations change, but the standard deviation does not appreciably change.

Foreset Dip Azimuth Uniformity (U^2)---. Delta foresets are variable in their progradation directions, but they can be broadly estimated to approximate a 180° progradation spread. The foreset is thought to mimic the orientation of distributary channels which can range from 123° as in the Volga Delta to 248° as in the Lena Delta (Olariu et al., 2006). We believe that the variability in foreset dip directions is a reflection of the distributaries on the delta topset and that the variability should correlate with the geometry of the shoreline. While a measure of the active delta foreset is not truly a measure of the topset, we include it as a topset metric because foreset evolution reflects the number and azimuth of distributary channels on the topset.

Foreset dip azimuth uniformity is defined as a measure of the sum of the deviations of clinoform dip azimuths from a theoretical uniform distribution, and is given by:

$$U^2 = \sum_{i=1}^{N} \left[U_i - \overline{U} - \frac{i - 1/2}{N} + \frac{1}{2} \right]^2 + \frac{1}{12N},$$

where $\overline{U}$ is the simple mean of azimuthal data (U_i) ordered from i = 1 to N (Jones, 2006). Fan delta fronts that grow self similarly in all directions should have smaller U^2 values because azimuthal distributions will approximate a uniform distribution and have fewer deviations from the theoretical uniform distribution compared to a delta with lobes growing in multiple directions. Foreset dip azimuth uniformity (U^2) can most readily be measured in numerical or modern deltas where the entire foreset is known (Fig. 5). In ancient deltas it can be measured from high quality 3D seismic data and 3D outcrops.

Clinoform Dip Magnitude (α)---. Clinoform dip magnitude is defined as the angle between a clinoform bed and the horizontal. It may be a true dip or apparent dip. Clinoform dip magnitudes are readily measurable for ancient systems in outcrops and seismic data and they

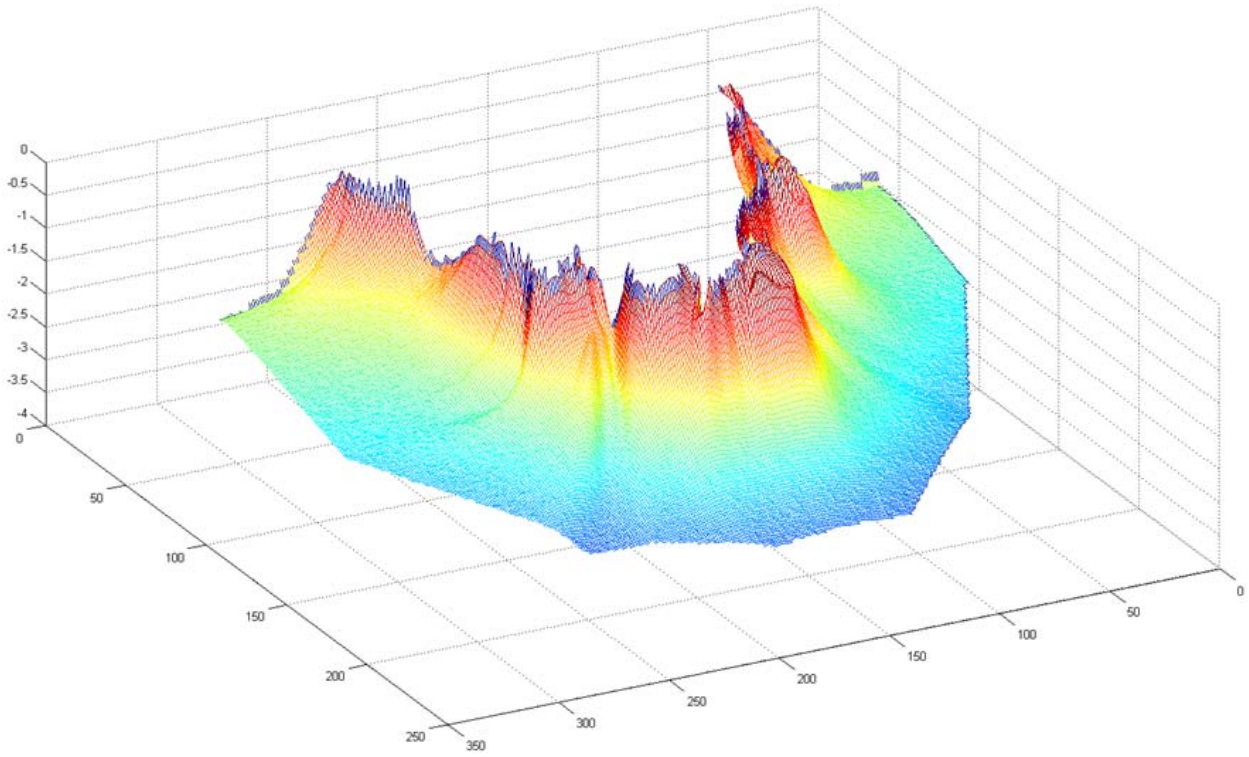

Figure 5. The delta foreset (above is an example from Delta H in Fig. 9) grows in numerous directions. Dip azimuth uniformity is designed to capture the variation in foreset growth.

may be measured in modern systems from bathymetric data. Clinoform dip magnitudes are set by the basin geometry and depth, the sediment type, and the velocity of the flow. The process controlling the clinoform dip is thought to be set by grain particle trajectories of sediments falling out of suspension and bedload deposition at the clinoform rollover. Accessibility of clinoforms and their direct relevance to sediment deposition makes them an ideal subject for this study.

Dip magnitude measurements were collected in three ways: the two-point method, the concavity method, and the bathymetry method. The two-point method calculates the slope between the rollover point and the clinoform toe. The concavity method (Fig. 6) incorporates more than five points along a clinoform surface between the rollover point to the toe to compute the average of all slopes measured between adjacent points. The bathymetry method uses the 3D bathymetry of the foreset to calculate the average slope between adjacent cells along the clinoform from the rollover to the toe. The rollover point is defined as the inflection point between the convex and concave portions of a clinoform, or when this point has been eroded, the rollover point is defined as the highest elevation on the clinoform. The clinoform toe is defined as the point where bedding surfaces become so condensed that it no longer is possible to follow an individual clinoform.

Clinoform Concavity (c)---. Concavity is defined as the second derivative of any function. Here, clinoform concavity is defined as a measure of the rate of change of the slope along the clinoform surface from the rollover point to the toe. Concavity should depend upon the relative proportions of grains deposited on the delta front as bedload and the grains deposited towards the clinoform toe as they fall out of suspension. With increasing bedload, sedimentation should increase near the clinoform rollover promoting increased concavity. Pure bedload dumping at

the rollover should produce Gilbert-type planar foresets. We measured concavity by fitting a second-order polynomial to a minimum of five equally spaced points along a geo-referenced clinoform surface (Fig. 6). Clinoform concavity can be measured in outcrop and seismic cross-sections in addition to modern delta bathymetry, and concavity is valuable for connecting stratigraphy to depositional processes.

Because various lobes prograde in different directions, some of the traces of clinoforms record apparent dips and some record true dips. We argue that this does not appreciably affect the concavity measurement. Concavities were calculated along four random cross-sections of a single numerically-modeled delta, resulting in concavities of 3.51×10^{-6}, 3.52×10^{-6}, 3.25×10^{-6}, and 4.10×10^{-6}. This variation is small compared to the range of concavities among the nine deltas from 9.14×10^{-7} to 3.87×10^{-4}.

Facies Partitioning (F)---. The relative proportion of distributary channel and delta foreset facies is an important attribute of delta stratigraphy insofar as it reflects the mobility and number of distributaries in addition to basin geometry and depth. Their volumetric proportions are estimated here by the relative cross-sectional area of each facies computed as a proportion of the total cross-sectional area of a vertical face (Fig. 7). The relative proportion of these facies is measured by assigning polygons in ArcGIS to each facies in a line-of-section, summing their areas, and dividing by the total area of the line-of-section.

Number of Autogenic Parasequences (P)---. A parasequence is defined as "a relatively conformable succession of genetically related beds or bedsets bounded [above and below] by marine-flooding surfaces" (van Wagoner, 1990). Autogenic events in deltas, including large-scale lobe switching and smaller-scale distributary avulsion can result in a condensed mud drape separating two coarser-grained clinothems (Fig. 7). This apparent abrupt basinward shift in

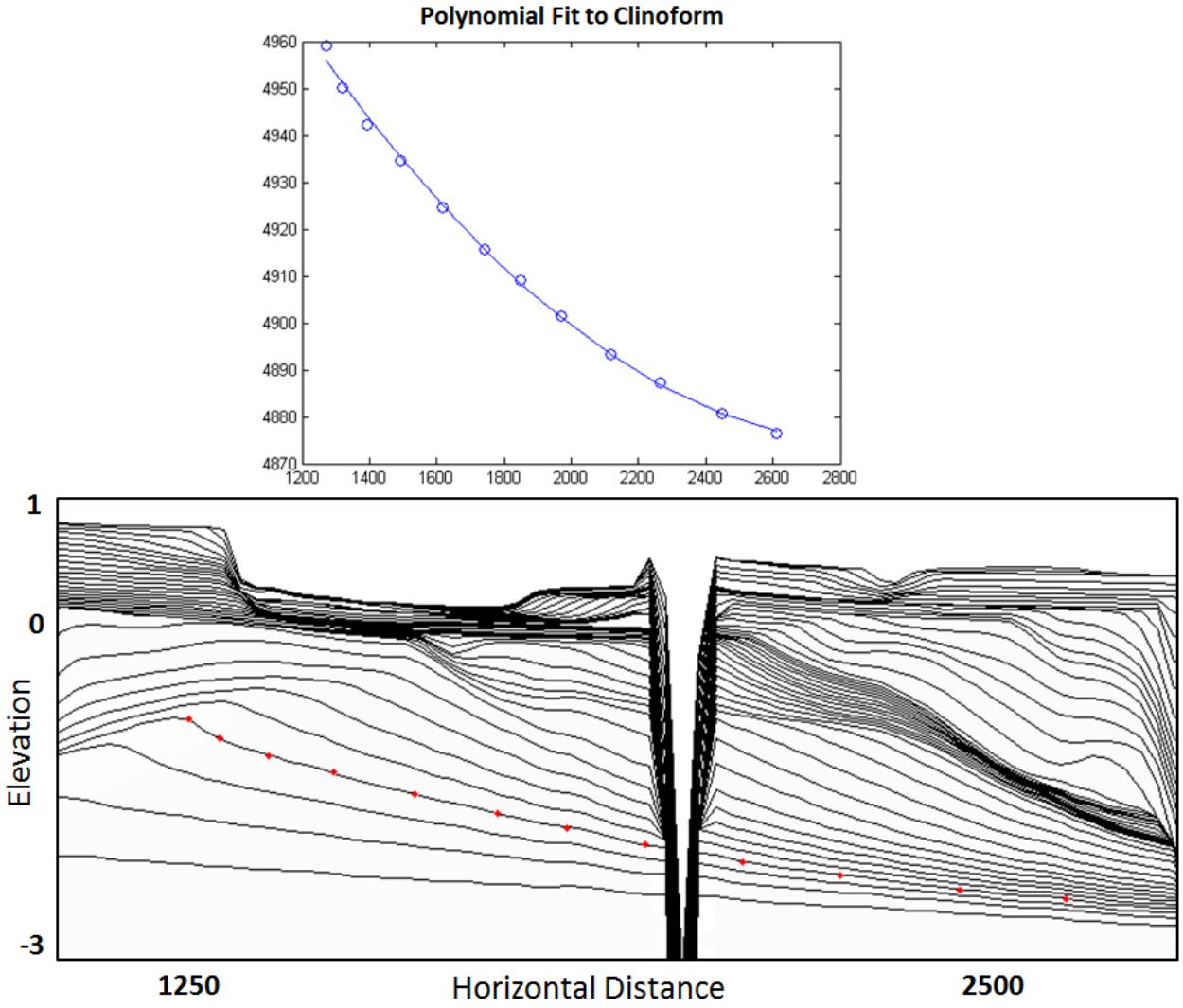

Figure 6. Clinoform concavity is calculated by fitting a second order polynomial (top) to a digitized clinoform (bottom) and taking the second derivative of the polynomial. Clinoform dip is calculated by averaging the slopes between adjacent points along the clinoform (bottom).

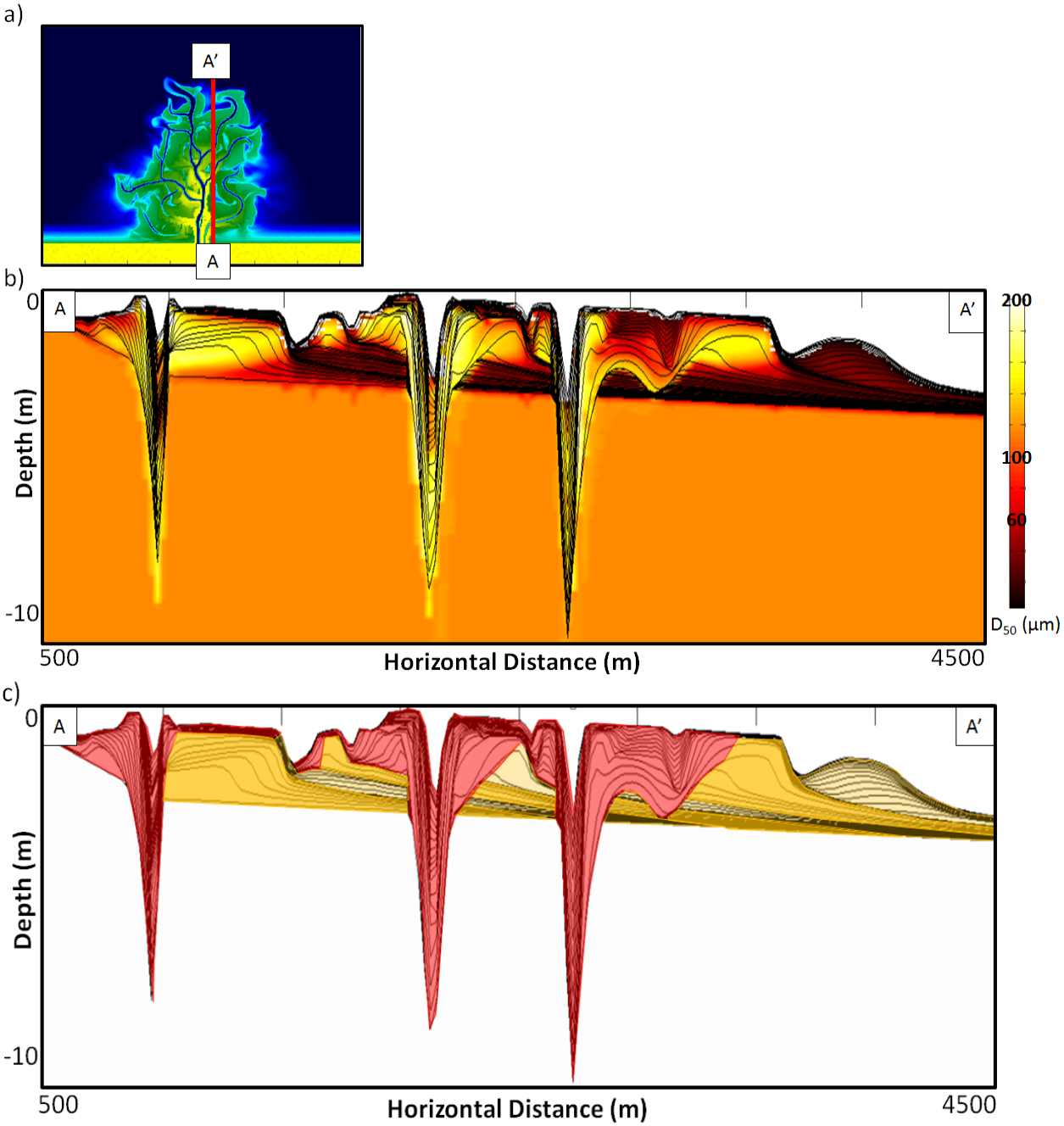

Figure 7. a) An example of numerically modeled stratigraphy from Delta E, a medium-cohesion, 50% sand delta. b) A dip line showing chronostratigraphic surfaces (black lines) and D_{50} grain size magnitudes (scale bar on the right in μm). Notice the coarsening upward yellow portions, the clinoforms dipping from left to right, and the fine-grained clinoform toes. c) The same dip line has been interpreted to show channel (red) and foreset (orange) facies. Foreset parasequences are indicated by different shades of orange. Parasequences change from older to younger from left to right. Notice the onlap of the youngest parasequence onto an older parasequence (far right).

facies could be interpreted as a flooding surface, and consequently we call the clinothems they separate "autogenic parasequences." These apparent flooding surfaces are important because they often act as baffles to flow in deltaic sand reservoirs and the number of autogenic parasequences in a delta can have a significant impact on reservoir compartmentalization.

Reservoir Rugosity (R)---. Reservoir rugosity is defined as the planform complexity of a sand body deposited by a delta (Fig 8). This is an important attribute to measure because high rugosity reservoirs are poor targets for hydrocarbon exploration. As a measure of reservoir rugosity we propose using the isoperimetric quotient to determine an area/perimeter relationship that will describe the complexity of a sand body shape (see "Shoreline Rugosity" in "Controlling Variables" section).

NUMERICAL EXPERIMENTS

The experimental deltas are simulated using Delft3D (v. 4.00.01), an engineering-grade numerical fluid flow and sediment transport model. Model computations solve the depth averaged, nonlinear, shallow-water equations which are derived from Reynolds-averaged Navier-Stokes equations in a basin consisting of 300 x 225 computational cells each of which is 25 m x 25 m. A time step of 9 s is used in order to preserve numerical stability. To adapt the model for longer time scales a morphologic scale factor of 175 is applied. Small-scale horizontal eddy viscosity is calculated by means of a horizontal large-eddy simulator. Sediments are categorized as being either "cohesive" or "non-cohesive". Non-cohesive sediments, defined as greater than 64 μm, may travel as suspended or bedload material. Transport of non-cohesive sediments is governed by the Van Rijn equation with erosion and deposition determined from the Shields curve. Cohesive sediments, finer than 64 μm, are treated as suspended material and sediment transport is governed by the Partheniades-Krone formula with erosion and deposition

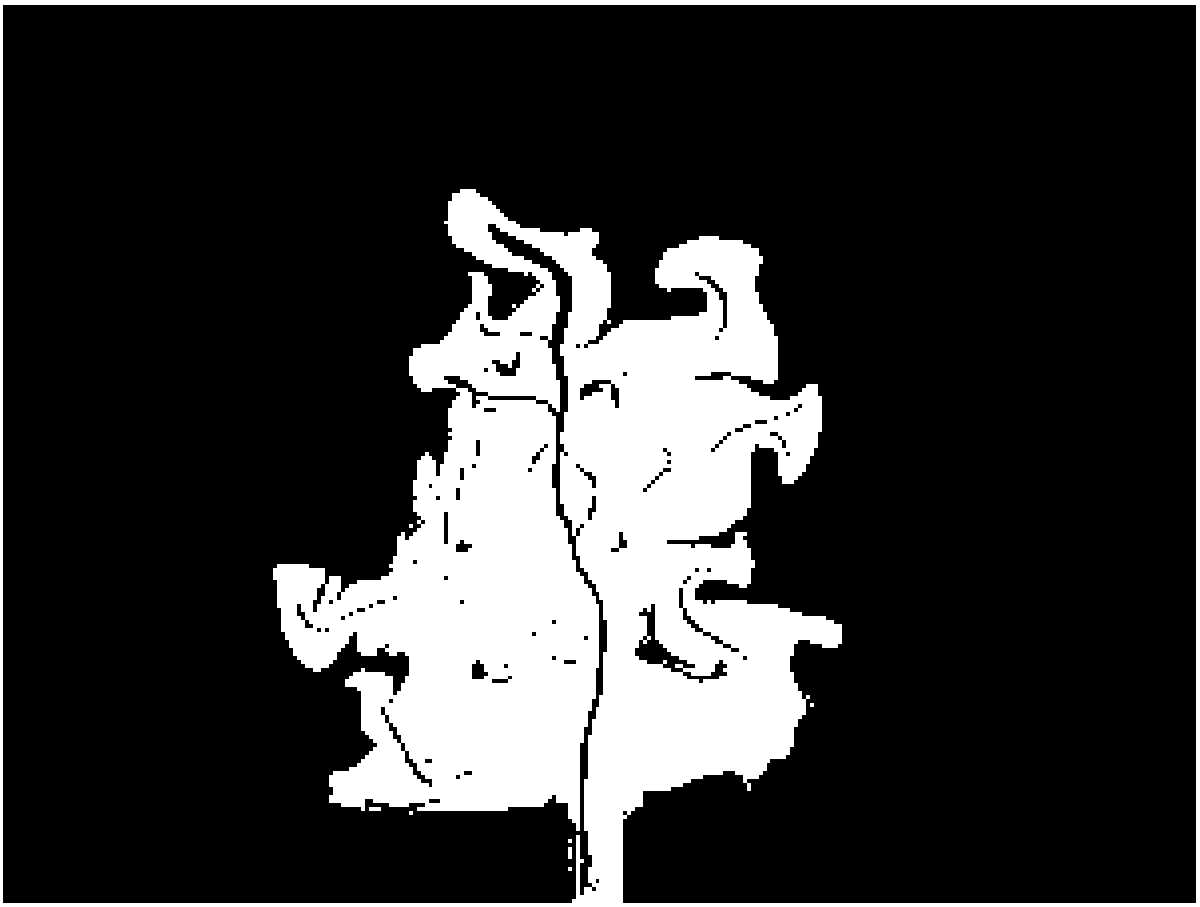

Figure 8. Reservoir rugosity is a measure of the complexity of a sand body perimeter for a given area. White cells above denote areas with greater than 0.5 m of net sand and areas in black denote areas with less than 0.5 m of net sand.

calculated as source and sink terms in an advection diffusion equation. Cohesive sediment erosion arises when the bed shear stress (τ_o) exceeds the critical shear stress required for re-erosion of cohesive sediments (τ_{cre}). The latter is set by the user. In our experiments τ_{cre} is also used as a proxy for vegetation on the topset, where a high value represents a highly vegetated environment.

Experimental Design

Three different ratios of non-cohesive to cohesive sediment (90:10, 50:50, 10:90) and three different critical shear stresses for re-erosion of cohesive sediment (0.25, 1.75, 3.25 N m^{-2}) are used in combination to create nine deltas. Deltas comprised of 90%, 50%, and 10% sand are respectively referred to as "sand-dominated," "sand-mixed," and "mud-dominated," while deltas experiencing a critical shear stress required for re-erosion of cohesive sediments (τ_{cre}) of 0.25, 1.75 and 3.25 N m^{-2} are respectively referred to as "low-cohesion," "medium-cohesion," and "high-cohesion" deltas. The nine self-formed deltas prograde into a shallow basin absent of waves, tides, Coriolis acceleration, temperature, and salinity variations. Thus they are representative of deltas prograding into fetch-limited lakes. Initial basin bathymetry for each numerical experiment slopes seaward from 0 m to 3.5 m. White noise is initially created on the bed to provide more realistic variations in water depth. A rectangular trunk stream 250 m wide, 1000 m long, and having an initial depth of 2.5 m deep flows seaward into the basin through a 500 m wide sandy shoreline trending perpendicular to the trunk stream. Open boundaries on the other three sides of the computation grid allow both water and sediment to pass and are defined with a constant water elevation equal to zero. The initial bed and the sediment in the river consist of three non-cohesive and three cohesive size-classes with grain diameters of 300, 150, 80, 32, 13, and 7.5 μm. The six sediment fractions sum to a relatively normal distribution with

the smallest and largest fractions always comprising the smallest proportion of the total sediment load. Available bed material in each model run consists of 20 m of evenly mixed sediment. All grain particles have a density of 2,650 kg m^{-3}. Dry bed densities are 500 kg m^{-3} for cohesive sediments and 1600 kg m^{-3} for non-cohesive sediments. The model precludes deposition of sediment in water depths shallower than 10 cm. To simulate channel-widening into dry cells 25% of the sediment in a cell experiencing erosion is taken from the adjacent dry cell.

Model stratigraphy is constructed from chronostratigraphic surfaces and sediment layers. The chronostratigraphic surfaces are generated from bed elevation data recorded at evenly-spaced time steps during delta growth. Sedimentary facies are recorded in 100 subsurface sediment layers that store the D_{50} grain size in each layer in each cell. Each sediment layer is 10 cm thick. The matrix of sediment layers is combined with the chronostratigraphic surfaces to generate stratigraphy.

Application of Methods

Measurements for each numerical delta were made after an identical volume of sediment had passed into the basin. Metrics were not measured at stages of delta growth when distributaries prograded to an open boundary. The number of active distributaries was measured at ten sequential time steps of delta growth at points in time when between 80% and 90% of the total sediment volume had entered the basin. Distributaries that showed progradation and obvious morphodynamic change between time steps were counted and averaged through time. Because Delft3D does not transport sediment in water shallower than 10 cm, we used -0.1 m bed elevation level as our definition of the land-water interface to determine the shoreline using the open angle method. The area of each delta was computed from a polygon comprising the shoreline points and a straight line connecting the two end points of the shoreline. To understand

the evolution of shoreline rugosity through time we computed an IQ at equally spaced time intervals during delta growth and averaged them to obtain a representative shoreline rugosity. We measured topset roughness for numerical deltas by sampling bed elevation data every 25 m along a strike line at y = 2000 m. Uniformity of the delta foreset was computed from bathymetric data after topset and bottomset elevations were removed. Dip magnitudes for numerical deltas were measured in a 2D dip line cross-section at x = 4000 m using both the concavity and bathymetry methods. It is often difficult to see clinoform dips and concavity without vertical exaggeration, so we set the vertical exaggeration of each numerical delta to 50. Concavity of a second order polynomial is linearly proportional to vertical exaggeration, so the final concavity data are presented as the measured concavity divided by the vertical exaggeration. This provides a concavity magnitude independent of the vertical exaggeration. Clinoform concavity measurements were acquired from a single dip line at x = 4000 m. To account for variations in progradation style, stratal stacking patterns, and oblique angles along each dip line, every other clinoform was measured, with the exception of clinoforms occurring at condensed horizons. For dip lines with less than 20 clinoforms, a minimum of 12 were measured. For each of the numerically-modeled deltas, facies proportions were determined along one stratigraphic dip-section (at x = 4000 m) and one stratigraphic strike section (at y = 2000 m). Channel facies were recognized as "U" shaped sedimentary bodies deeply eroded into previously deposited strata. They consist of coarse-grained prograding bars and laterally aggrading channel deposits, as well as fine-grained channel fills. For channel facies, we assumed that all active channels will eventually be filled and preserved in the stratigraphy, so the active channels were included as channel facies. Foreset facies were recognized as shallow- to steeply-dipping concave strata that coarsen upward. We identified as flooding surfaces all of

those condensed time horizons on the delta foreset where there was a prominent accumulation of fine-grained material (< 63 μm) along a foreset time horizon. Parasequences were counted on the same strike and dip lines used in the facies partitioning measurements. To measure reservoir rugosity, net sand thickness maps for thicknesses greater than 0.5 m were generated, the areas of which were measured in km^2. These maps were generated using D_{50} = 63 μm as the boundary between a reservoir sand and non-reservoir sediment. We then applied a strong Gaussian filter ([10 10], 3) to the net sand thickness maps to enhance the edges of the sand body. With well-defined sand body edges, a polygon was then fit to the reservoir in ArcGIS to calculate its area and perimeter.

Results

The numerical experiments resulted in nine self-formed deltas constructed by different sediment loads (90%, 50%, and 10% sand) and critical shear stresses for re-erosion of cohesive sediments (0.25, 1.75, 3.25 N m^{-2}). The nine deltas show unique shoreline shapes and bathymetry for each combination of sediment load and cohesion (Fig. 9), with the greatest difference occurring as expected between the 90% sand, low-cohesion delta and the 10% sand, high-cohesion delta. Duplicate model iterations of any single delta reveal no observable differences in planform or stratigraphy. Attributes of the nine numerical deltas are summarized in Table 1.

Delta Topset Characteristics--. The number of active distributaries on each delta topset increases with increasing proportion of sand delivered to the delta (Fig. 10; Table 1). Sand-dominated deltas average 11 active distributaries, while sand-mixed deltas average 9.3, and mud-dominated deltas average 4.3 active distributaries. Low-cohesion results in the greatest number of active distributaries for mud-dominated, sand-mixed, and sand-dominated deltas, and high-

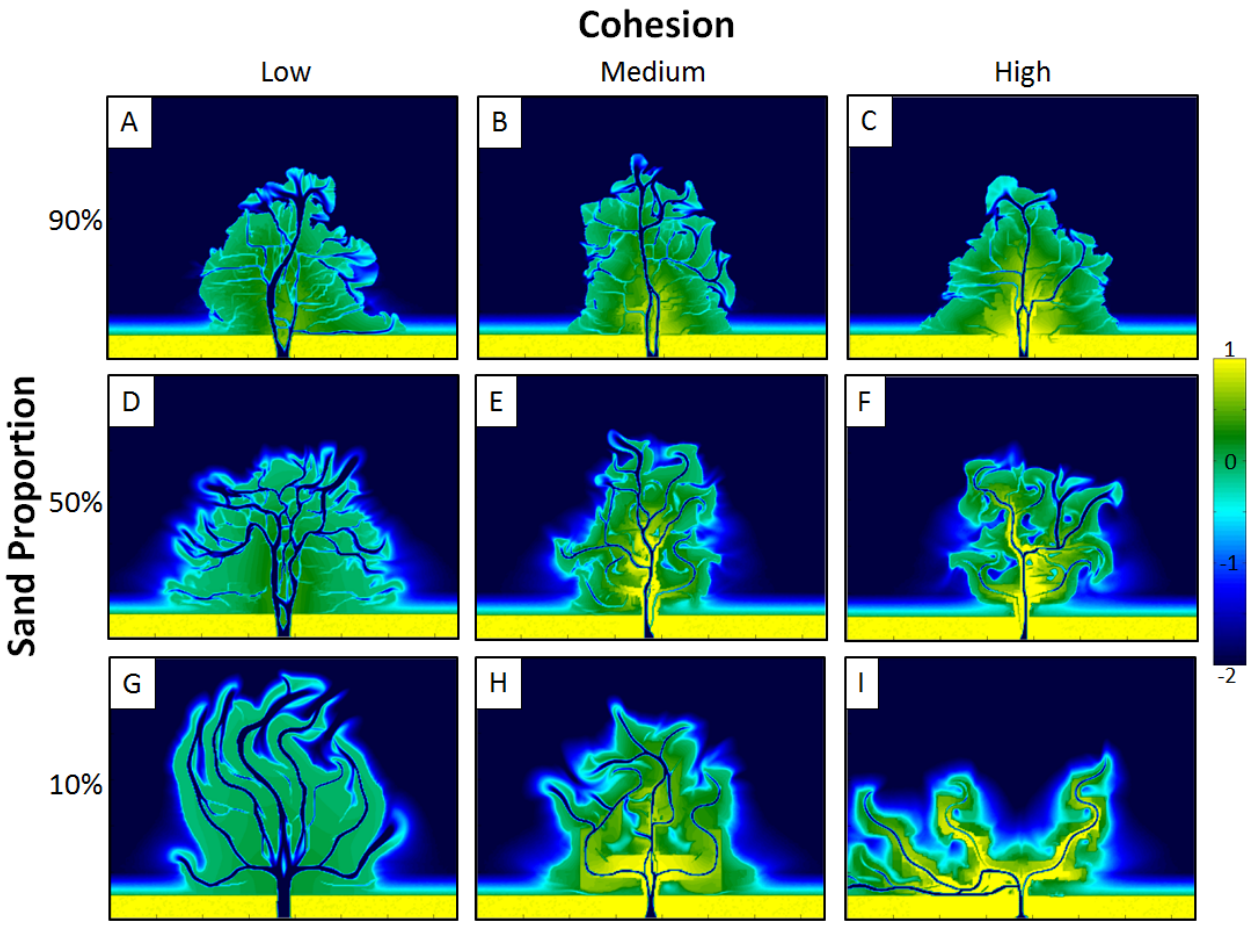

Figure 9. The numerical deltas show a wide range of shapes. The scale bar on the right shows elevations from 1 to -2 m. Areas in blue are all less than -2 m. The sand-dominated deltas (upper row) tend to take a fan-shape over the three degrees of cohesion (A-C), but the mouth-bar size appears to decrease with increasing cohesion. The sand-mixed (middle row) and mud-dominated deltas (bottom row) develop irregular complex shorelines with increasing cohesion (D-F; G-I). Topset elevations increase with increasing cohesion for all deltas.

ID	Sand (%)	τ_{cre}	d	IQ	T	U^2	α	c	F (Channel)	P	R
A	90	0.25	12	0.29	0.11	17.4	0.92	2.9×10^{-4}	70.0	15	0.43
B	90	1.75	11	0.29	0.15	14.9	0.92	3.4×10^{-4}	69.1	12	0.53
C	90	3.25	10	0.27	0.24	44.9	1.22	3.9×10^{-4}	62.1	10	0.40
D	50	0.25	11	0.20	0.09	101.5	0.12	3.5×10^{-6}	60.8	14	0.27
E	50	1.75	10	0.29	0.33	104.4	0.16	3.5×10^{-6}	53.5	12	0.29
F	50	3.25	7	0.27	0.43	62.3	0.23	3.1×10^{-6}	53.0	13	0.24
G	10	0.25	6	0.20	0.04	106.8	0.11	3.0×10^{-6}	52.5	8	0.10
H	10	1.75	3	0.28	0.23	131.2	0.10	1.9×10^{-6}	46.7	9	0.09
I	10	3.25	4	0.18	0.33	176.3	0.07	9.1×10^{-7}	29.1	7	0.07
GRD	~ 90	low	14	0.47	0.11	n/a	13.3	1.7×10^{-3}	n/a	n/a	n/a
LCD	~ 80	med	n/a	n/a	n/a	1.1	7.40	1.3×10^{-4}	12.1	7	n/a
LCDm	80	1.75	12	0.28	0.20	32.5	0.86	1.8×10^{-4}	65.1	13	0.41

Table 1. Parameters for each numerical delta are given with their corresponding topset and stratigraphic attribute values. Letters provided for "ID" correspond to those given in Figure 9. Other delta ID's include "GRD" for the Goose River Delta, "LCD" for the Cretaceous Last Chance Delta, and "LCDm" for the numerical model of the Last Chance Delta. "Sand (%)" is the proportion of sand delivered to the delta (unitless) and τ_{cre} is the critical shear stress required for re-erosion of cohesive sediment (N m^{-2}). Topset variables include "d" for number of active distributaries (unitless), "IQ" for shoreline rugosity (dimensionless), "T" for topset roughness (m), and "U^2" for foreset dip azimuth uniformity (degrees). Stratigraphic variables include "α" for clinoform dip magnitude (degrees), "c" for clinoform concavity (unitless), "F (Channel)" for channel facies proportion (dimensionless), "P" for number of parasequences (unitless), and "R" for rugosity of net sand thickness maps (dimensionless). Values for any variable that show "n/a" denote variables that were not measured.

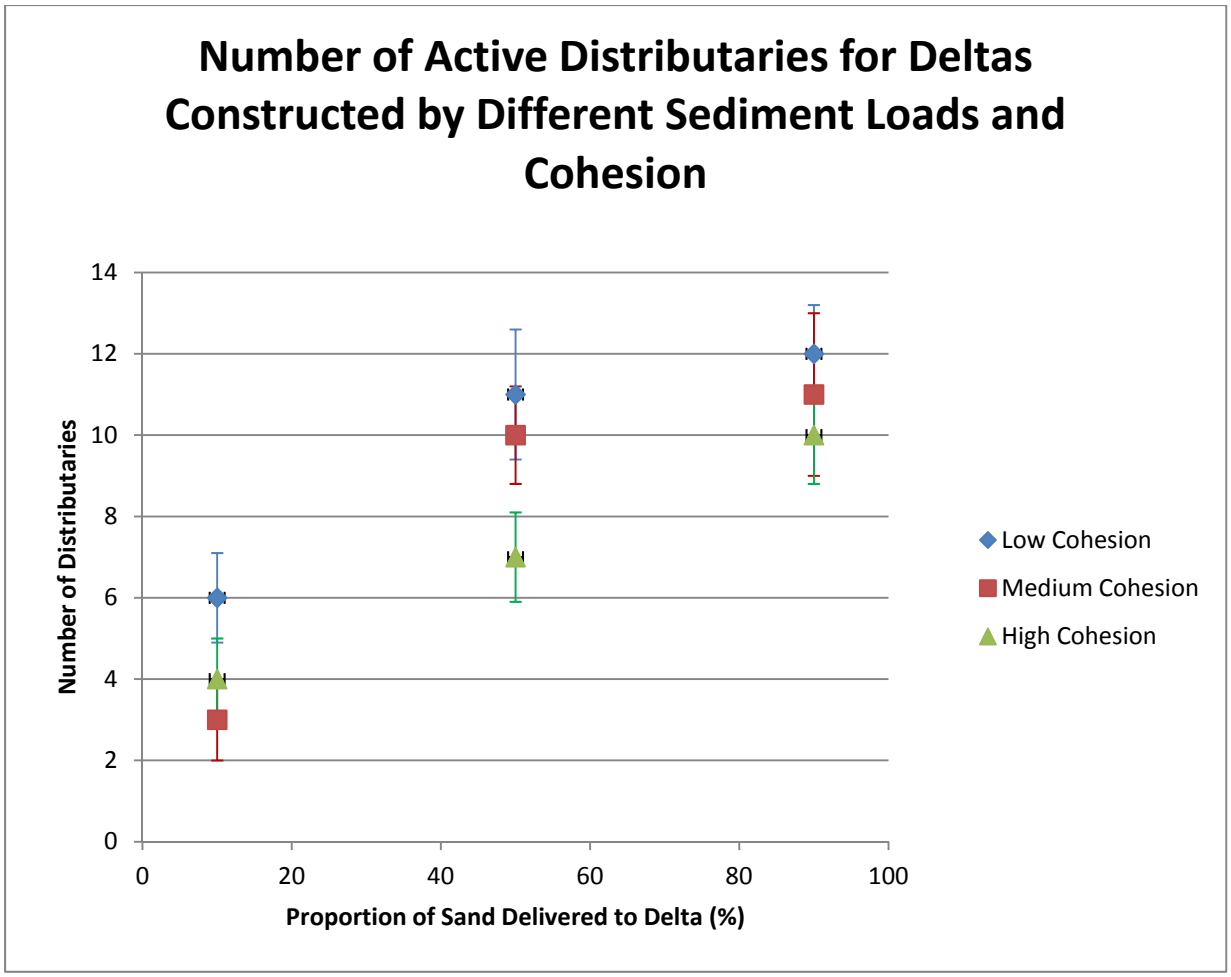

Figure 10. The number of active distributaries increases with increasing proportion of sand delivered to the delta. The number of distributaries also increases with decreasing cohesion, except for mud-dominated deltas.

cohesion results in the fewest number of active distributaries for sand-mixed and sand-dominated deltas.

The proportion of sand delivered to a delta has a significant impact on its shape and the rugosity of its shoreline. Sand-dominated deltas tend to have the smoothest shorelines, and with decreasing sand proportion, the shorelines increase in rugosity. Mud-dominated deltas display more meander-like behavior in their distributaries than the sand-dominated and sand-mixed deltas, and this leads to complex shoreline shapes. The isoperimetric quotient (IQ) generally increases with increasing proportion of sand delivered to the delta (Fig. 11). The delta having the most rugose, bird's-foot shoreline is the high-cohesion, mud-dominated delta (IQ = 0.18), and the delta having the least rugose, most fan-like shoreline is the low-cohesion, sand-dominated delta (IQ = 0.29). Sand-dominated deltas have the greatest average rugosity (IQ = 0.28), sand-mixed deltas have intermediate average rugosity (IQ = 0.26), and mud-dominated deltas have the smallest average rugosity (IQ = 0.22). Average standard deviation of shoreline rugosity is greatest for mud-dominated deltas (0.055), intermediate for sand-dominated deltas (0.047), and smallest for sand-mixed deltas (0.037).

As cohesion is increased, topsets become higher (Fig. 12) and increasingly variable in their elevation (Fig. 13). Average topset elevations are greatest for sand-mixed deltas (0.29 m), intermediate for mud-dominated deltas (0.21 m), and smallest for sand-dominated deltas (0.16 m). The roughness of topset elevations is greatest for sand-mixed deltas (0.28), intermediate for mud-dominated deltas (0.20), and smallest for sand-dominated deltas (0.17).

Delta foreset dip-azimuth uniformity (the sum of deviations from a theoretical uniform distribution) systematically decreases with increasing sand proportion delivered to the delta

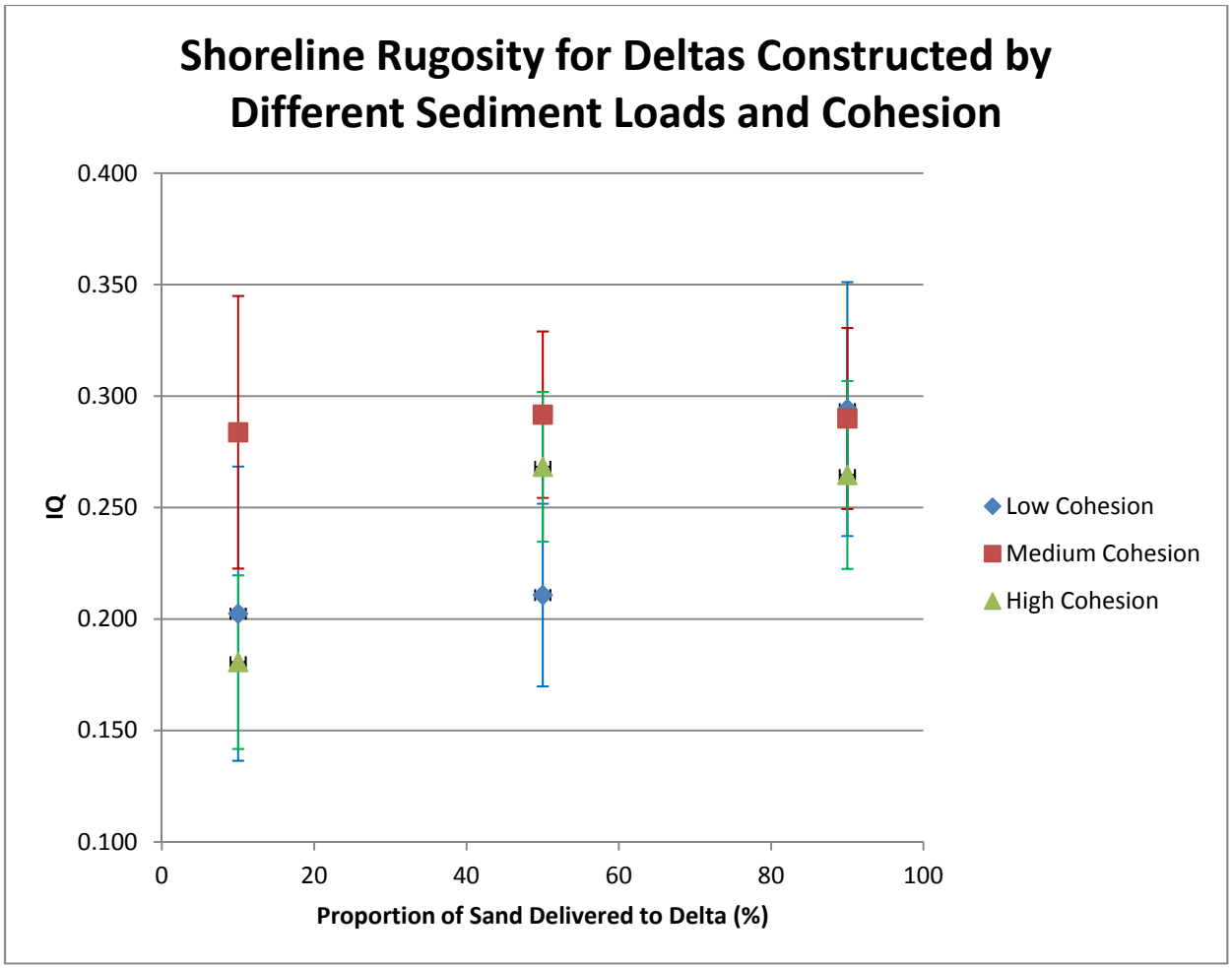

Figure 11. Rugosity values calculated from the isoperimetric quotient (IQ) range from 0.18 to 0.29 and averaged over all cohesion types they increase with increasing proportion of sand delivered to the delta. The high-cohesion, mud-dominated delta has the greatest rugosity (lowest IQ) and the low-cohesion, sand-dominated delta has the smallest rugosity.

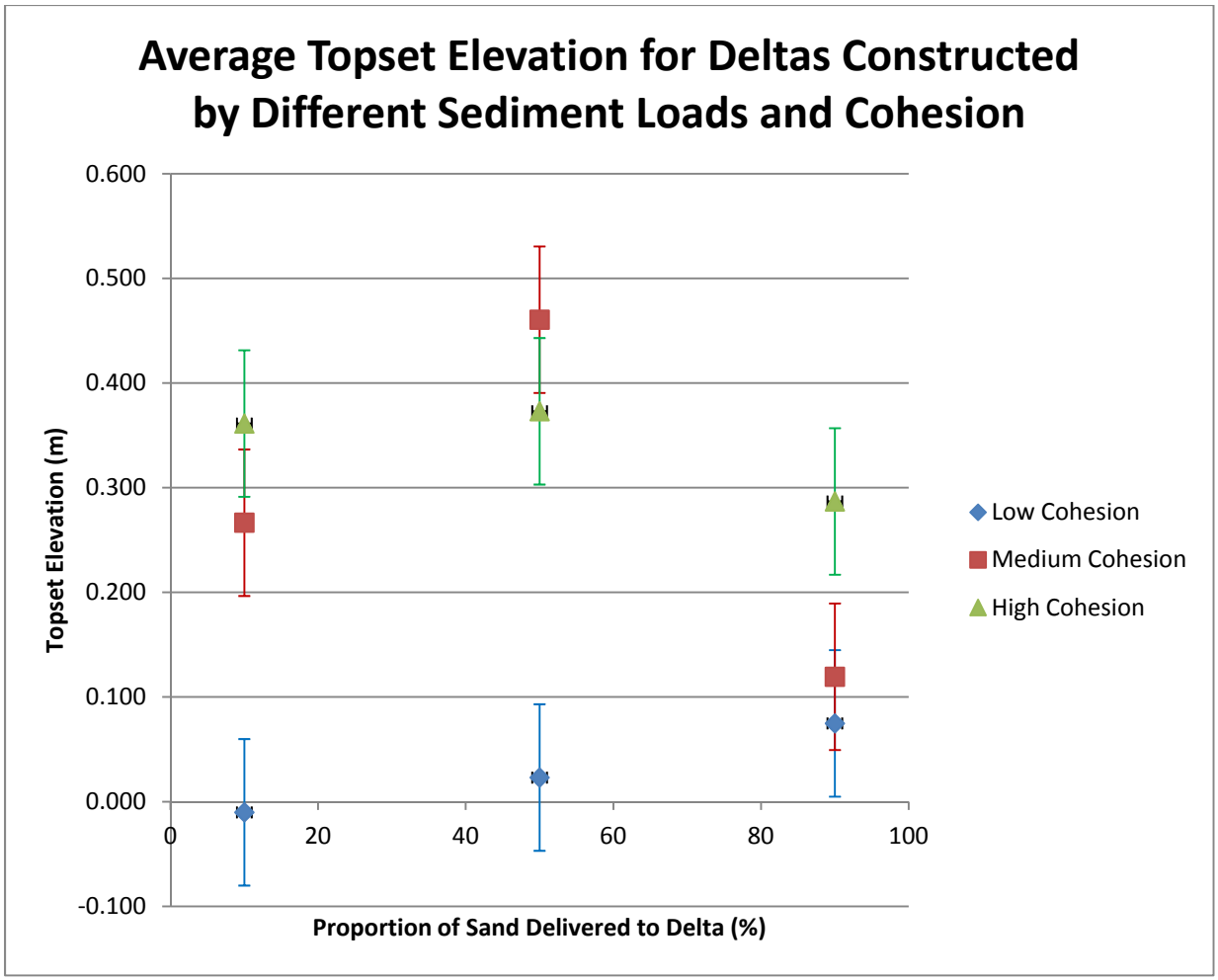

Figure 12. The average elevation of a delta topset (elevations greater than -0.1 m) increases with increasing cohesion. Sand-mixed deltas have topsets with the highest elevation.

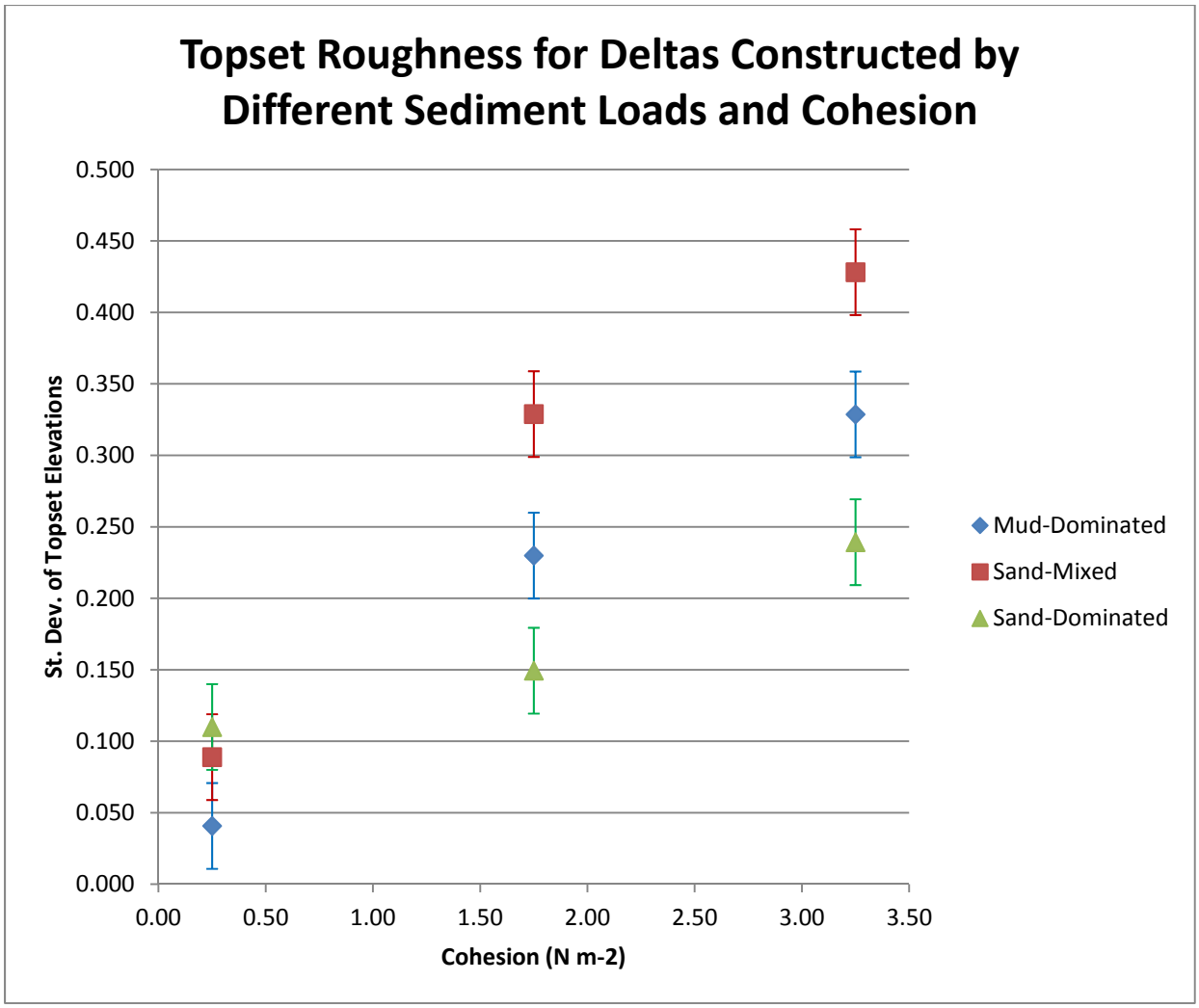

Figure 13. The roughness of a delta topset (elevations greater than -0.1 m) increases with increasing cohesion. Sand-mixed deltas develop the roughest topsets.

(Fig. 14). Mud-dominated deltas have the highest average uniformity (144.0), that is to say they are the most modal. Sand-mixed deltas have intermediate average uniformity (79.3), and sand-dominated deltas have the lowest average uniformity (26.9). With the exception of sand-mixed deltas, high-cohesion leads to higher foreset uniformity. The high-cohesion, mud-dominated delta has the highest uniformity and the medium-cohesion, sand-dominated delta has the lowest uniformity.

Delta Stratigraphy--. Clinoform dip magnitudes for the numerical deltas were computed from a 3D matrix of the entire active foreset (Fig. 15; Table 1). They show an increase in average clinoform dip magnitude from 0.19 degrees for mud-dominated deltas to 0.27 degrees to sand-mixed deltas to 0.59 degrees for sand-dominated deltas. The standard deviation of clinoform dip magnitudes increases similarly, with an increase from 0.22 to 0.27 for mud-dominated to sand-mixed deltas, and 0.27 to 0.73 for sand-mixed to sand-dominated deltas. Cohesion does not seem to influence clinoform dip magnitudes as measured from the entire foreset. Average clinoform dip magnitudes computed from vertically exaggerated (VE = 50) stratigraphic dip cross-sections were included to compare model results to seismic and outcrop dip lines. These also show increases in dip magnitude and standard deviation with increasing proportion of sand delivered to the delta. Vertically exaggerated dip magnitudes increase from 4.7° for mud-dominated deltas to 8.4° for sand-mixed deltas, to 38.1° for sand-dominated deltas. Standard deviations increase from 1.9° for mud-dominated deltas to 6.3° for sand-mixed deltas, to 15.1° for sand-dominated deltas. For sand-mixed and sand-dominated deltas higher cohesion leads to greater clinoform dip magnitudes. At 90% confidence, there is a statistically significant difference between mud-dominated and sand-mixed delta clinoform dips for 6 of 9 cases, and at 80% confidence there is a statistically significant difference between mud-dominated and sand-

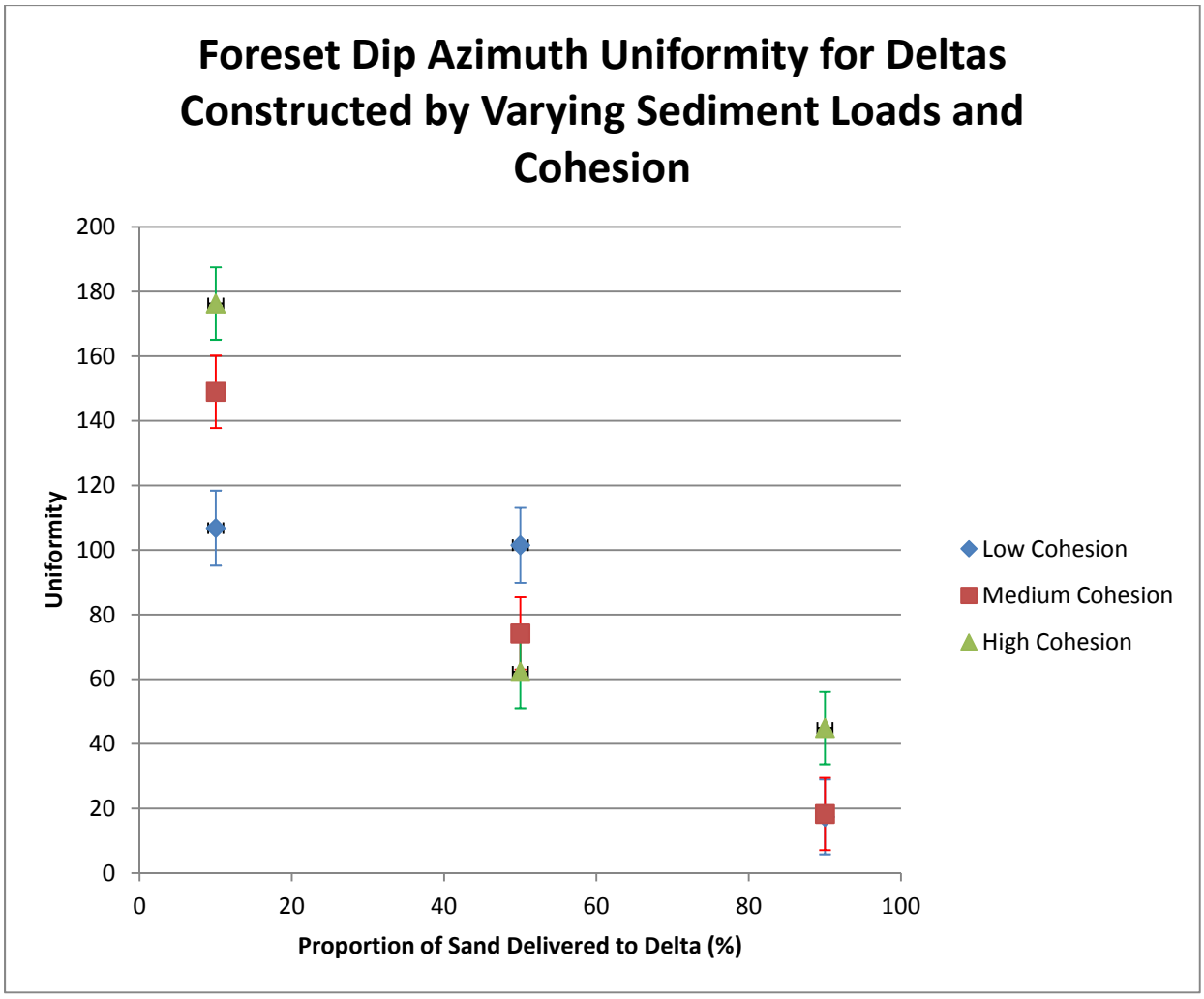

Figure 14. Delta foreset dip azimuth uniformity decreases with increasing proportion of sand delivered to the delta. The foreset with the greatest uniformity is the high-cohesion, mud-dominated delta.

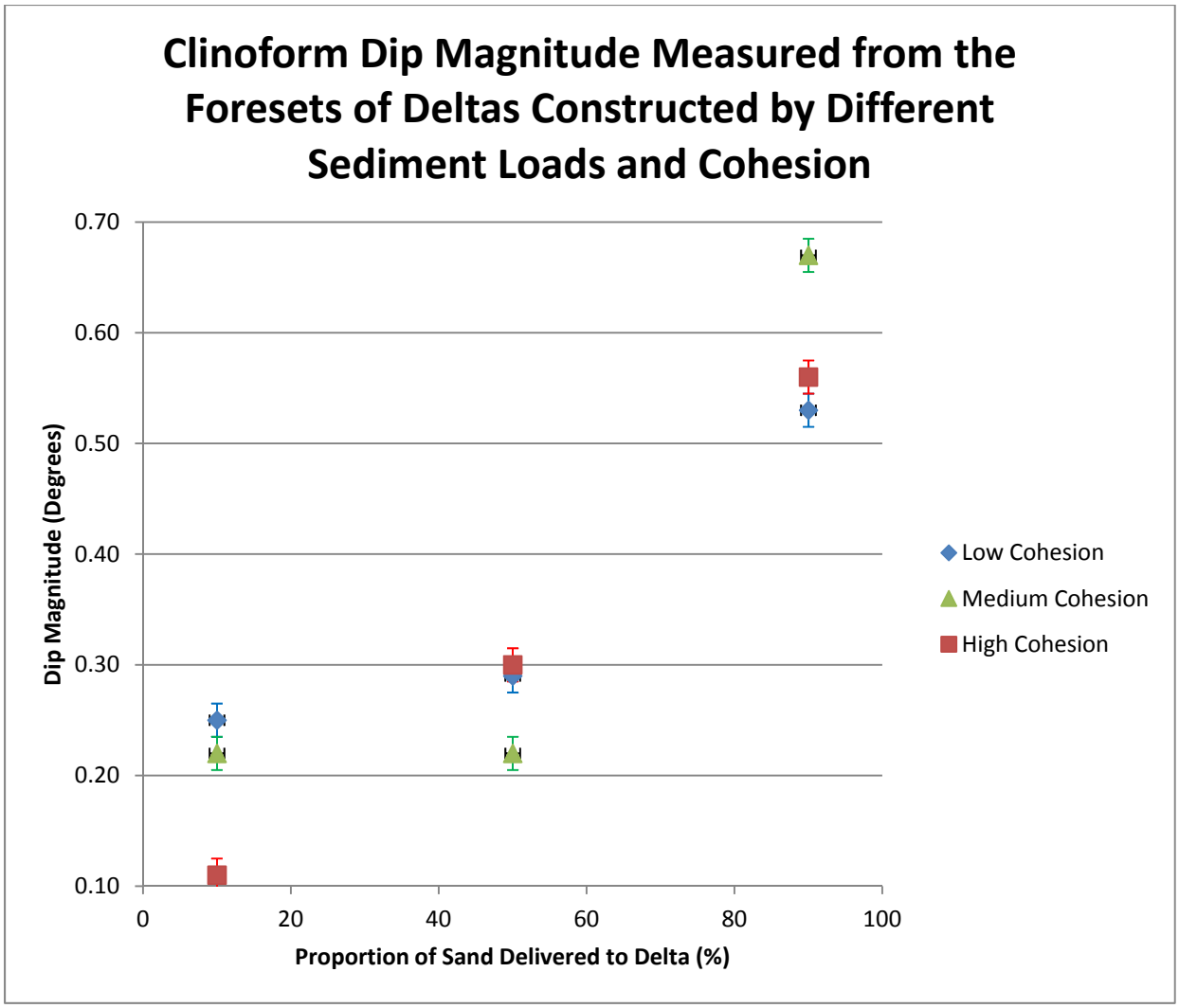

Figure 15. Clinoform dip magnitudes measured from foreset bathymetry increase with increasing proportion of sand delivered to a delta. Cohesion does not participate strongly in determining clinoform dip magnitude because it is a depositional feature not an erosive feature.

mixed delta clinoform dips for 8 of 9 cases. At 95% confidence, there is a statistically significant difference between mud-dominated and sand-dominated clinoform dips for 9 of 9 cases. At 95% confidence, there is a statistically significant difference between sand-mixed and sand-dominated clinoform dips for 9 of 9 cases.

Clinoform concavity, measured from stratigraphic dip cross-sections, increases with increasing proportion of sand delivered to the delta (Fig. 16). Mud-dominated deltas have the smallest average clinoform concavity, averaging 2.0×10^{-6}, sand-mixed deltas average 3.4×10^{-6}, and sand-dominated deltas have the highest average clinoform concavity, averaging 3.4×10^{-4}. Cohesion does not seem to systematically control clinoform concavity. Standard deviation of clinoform concavity increases with increasing proportion of sand delivered to the delta, from 1.3×10^{-6} to 3.1×10^{-6} for mud-dominated to sand-mixed deltas, and 3.1×10^{-6} to 3.4×10^{-4} for sand-mixed to sand-dominated deltas. At 90% confidence, there is a statistically significant difference between mud-dominated and sand-mixed delta clinoform concavity for 6 of 9 cases. At 95% confidence, there is a statistically significant difference between sand-mixed and sand-dominated delta clinoform concavity for 9 of 9 cases. At 95% confidence, there is a statistically significant difference between mud-dominated and sand-dominated delta clinoform concavity for 9 of 9 cases. For four arbitrarily drawn cross-sections of a single delta, there is no statistically significant difference in clinoform concavity at 95% confidence.

The proportion of channel and foreset facies, measured in strike and dip cross-sections, is a function of the proportion of sand delivered to the delta and sediment cohesion. The average proportion of channel facies increases with increasing proportion of sand delivered to the delta and with decreasing cohesion (Fig. 17). Inversely, foreset facies increase with decreasing proportion of sand delivered to the delta and with increasing cohesion. The low-cohesion, sand-

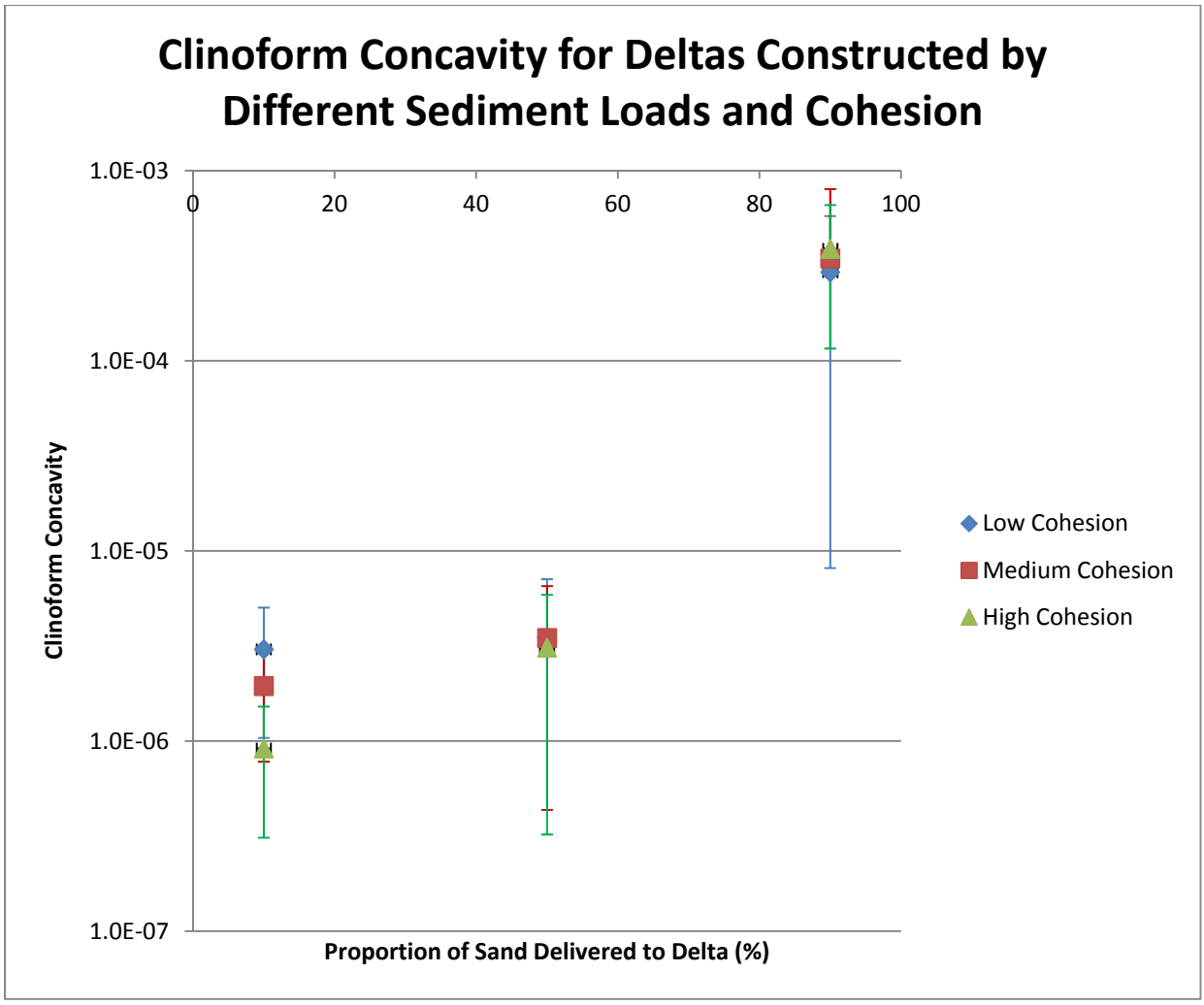

Figure 16. Clinoform concavity increases with increasing proportion of sand delivered to the delta. Cohesion does not seem to control clinoform concavity.

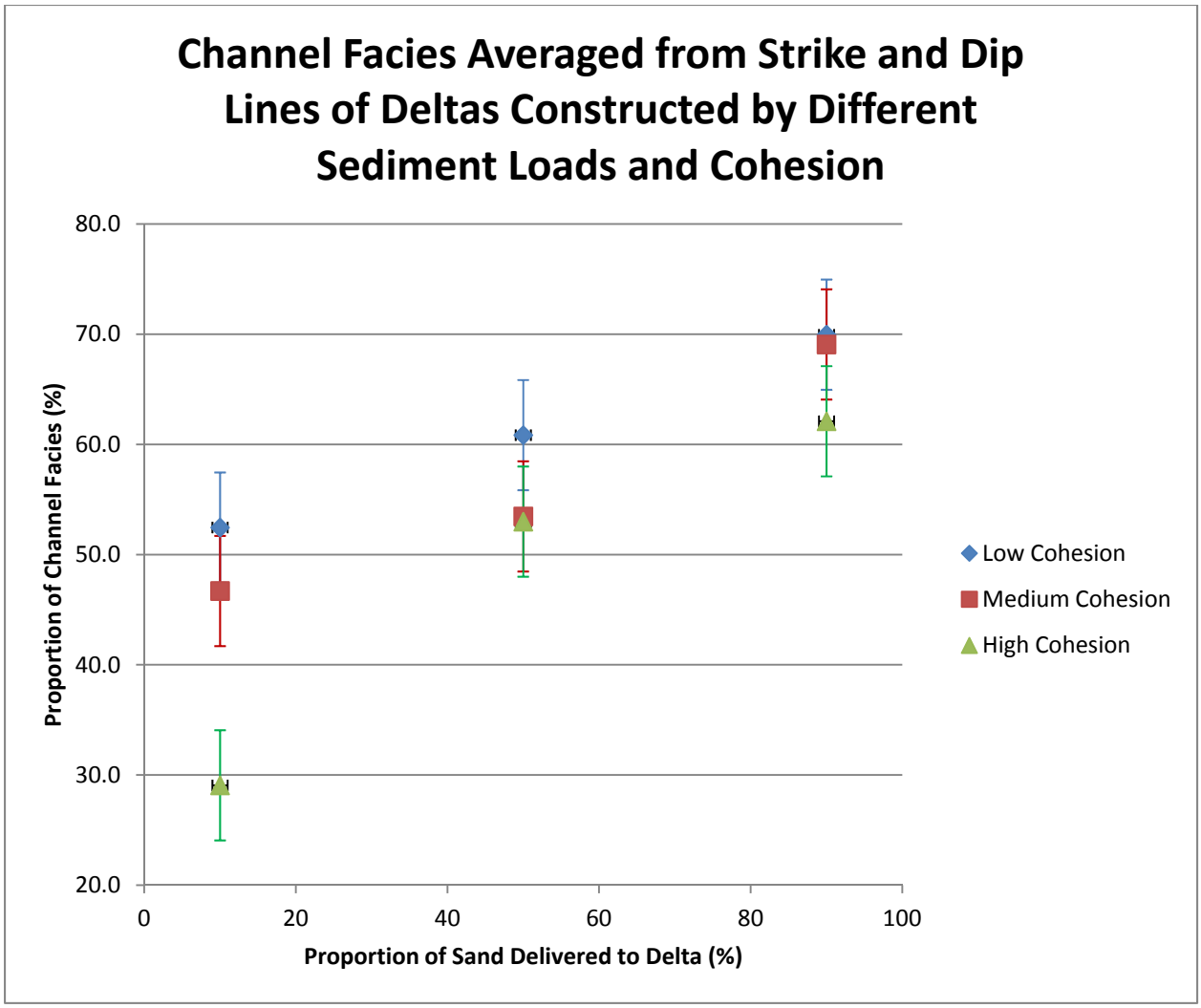

Figure 17. The proportion of channel facies relative to foreset facies increases with increasing proportion of sand delivered to the delta and with decreasing cohesion.

dominated delta is comprised of the largest proportion of channel facies (70.0%) and the high-cohesion, mud-dominated delta contains the largest proportion of foreset facies (70.9%).

The number of autogenic parasequences produced over a fixed period of delta growth was measured from strike and dip cross-sections. Strike lines typically exhibit more parasequences than dip lines. The total number of parasequences occurring in both lines increases from an average of 8 for mud-dominated deltas to 13 for sand-mixed deltas, then decreases slightly to 12.3 for sand-dominated deltas (Fig. 18). The decrease from sand-mixed deltas to sand-dominated deltas may not be statistically significant. Low-cohesion increases the number of parasequences observed in sand-mixed and sand-dominated deltas. The delta having the most parasequences is the low-cohesion, sand-dominated delta, and the delta with the least number of parasequences is the high-cohesion, mud-dominated delta. The lowest numbers of parasequences occur in the mud-dominated deltas.

Reservoir rugosity of the numerical deltas depends heavily on the proportion of sand delivered to the delta and on cohesion. The 0.5 m or greater isopach maps of net sand show that sand-dominated deltas contain large, continuous sand bodies as expected. Mud-dominated deltas contain elongate discontinuous sand bodies reminiscent of shoe-string sands, and sand mixed-deltas contain a combination of the two types (Fig. 19). The low-cohesion, sand-dominated delta creates the largest coherent sand body whereas the low-cohesion, mud-dominated delta creates the smallest. For sand-dominated deltas, isopach area decreases with increasing cohesion. Sand body rugosity is a function of both proportion of sand delivered to the delta and cohesion (Fig. 20). The average IQ of sand bodies increases from 0.09 for mud-dominated deltas to 0.27 for sand-mixed deltas to 0.46 for sand-dominated deltas. For all three types of deltas, high-cohesion leads to the greatest sand isopach rugosity. The delta having the sand isopach with the least

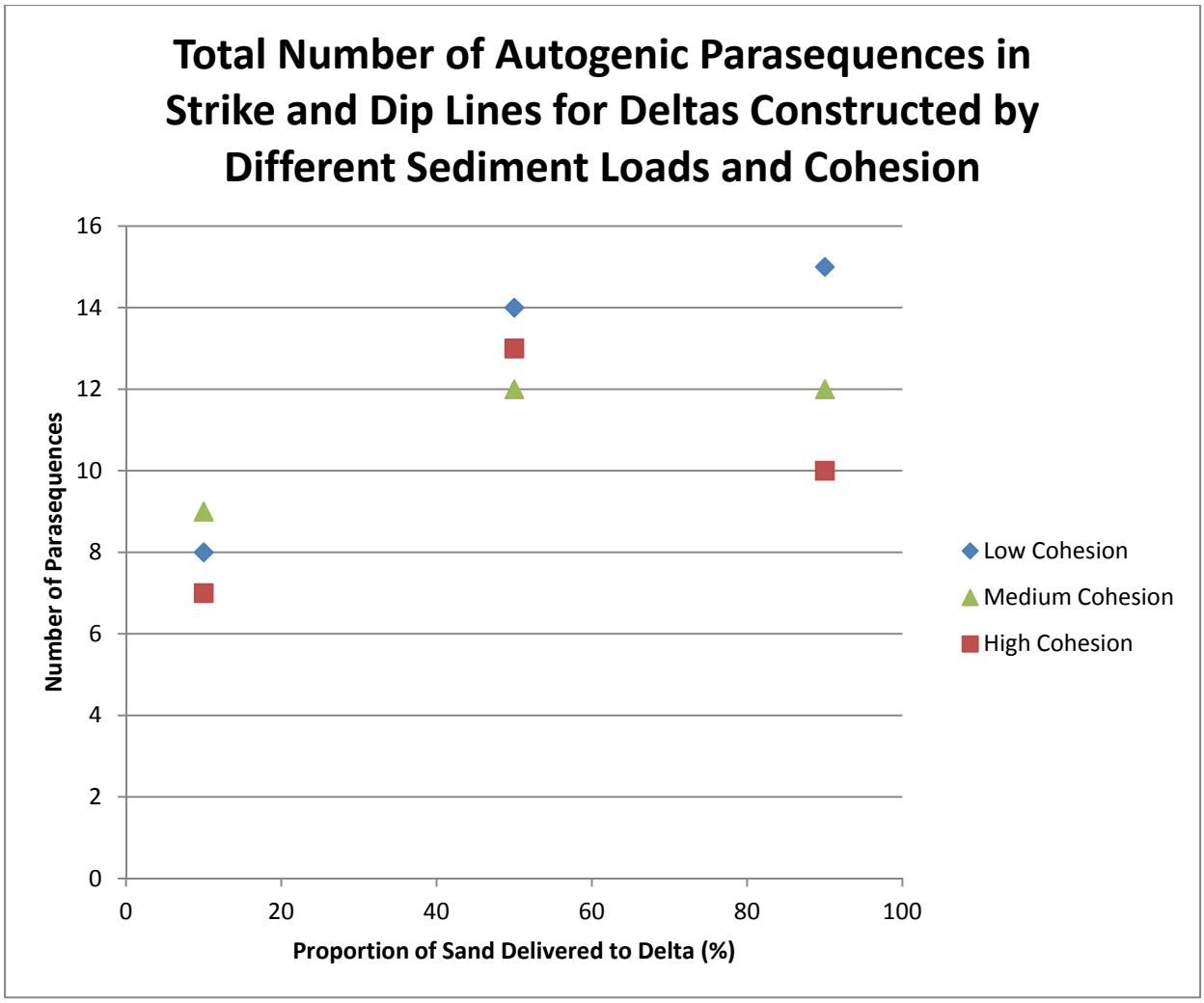

Figure 18. The number of autogenic parasequences increases with the proportion of sand delivered to the delta. Low-cohesion creates more parasequences in the sand-mixed and sand-dominated deltas. Note that error bars are absent because the number of parasequences is counted only once at the end of each delta simulation.

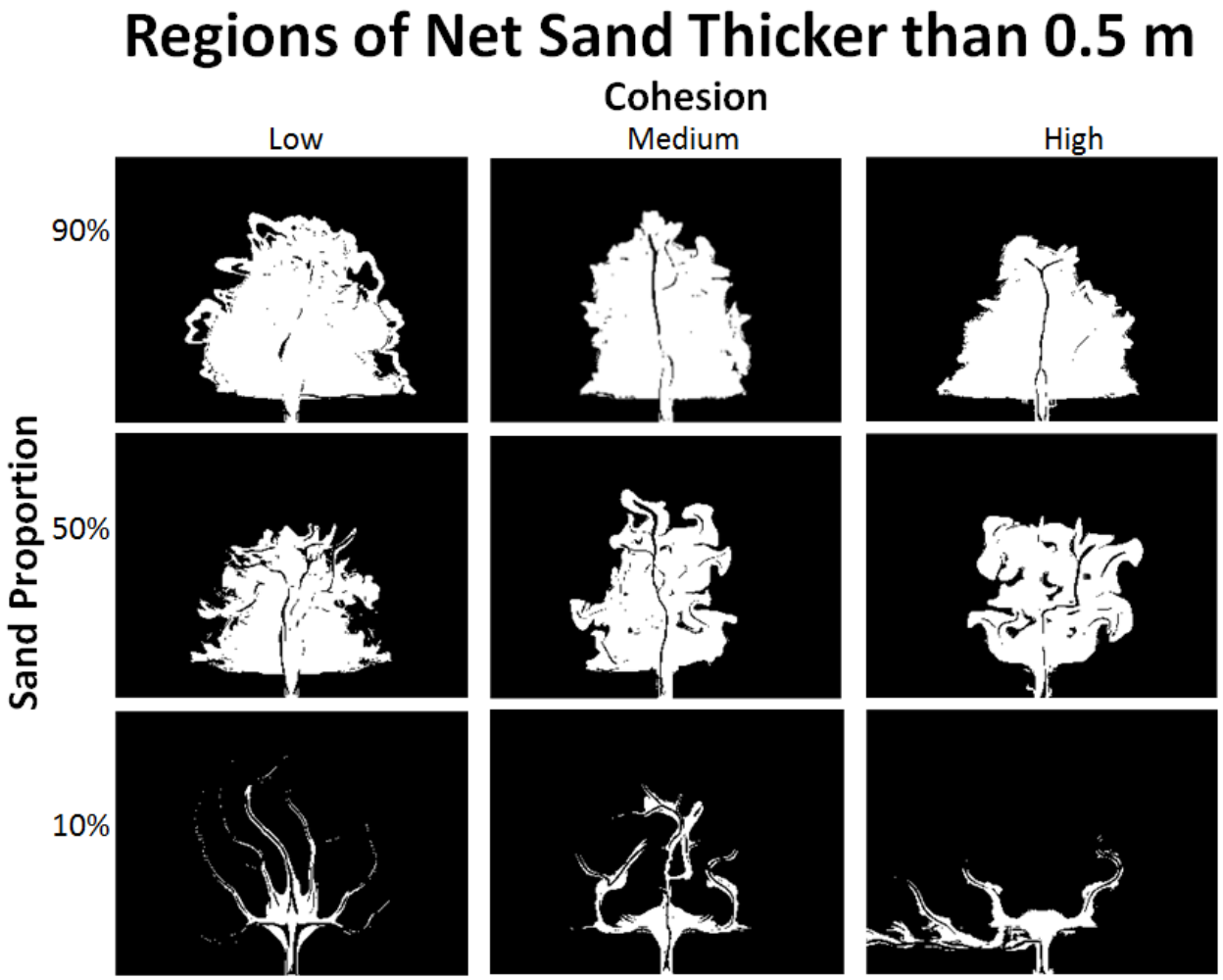

Figure 19. White areas outline regions of the delta where net sand thickness is greater than 0.5 m. Sand body shapes vary from large and continuous for the sand-dominated deltas to elongate and discontinuous for the mud-dominated deltas.

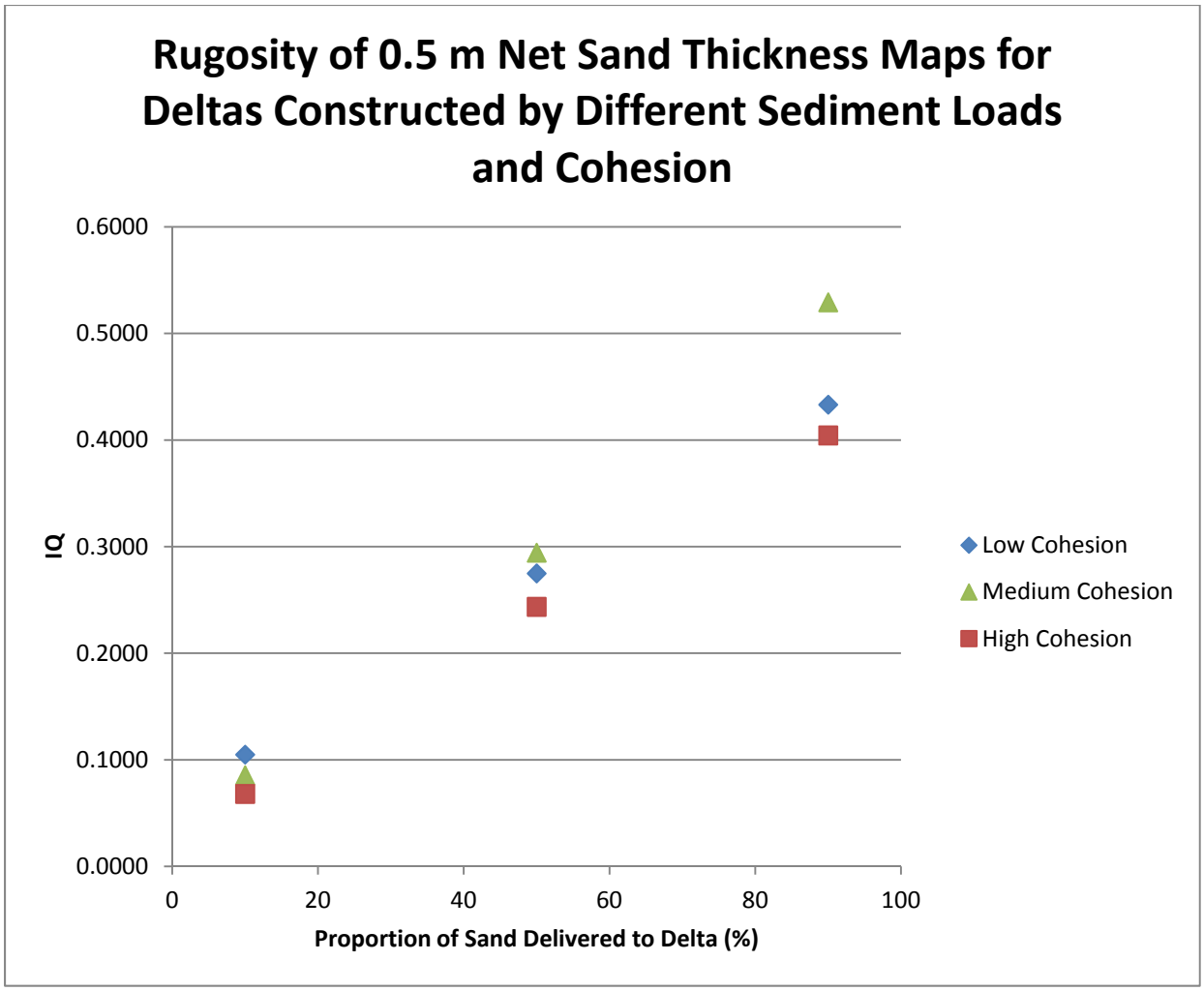

Figure 20. Sand bodies decrease in rugosity (higher IQ's) with increasing proportion of sand delivered to the delta. High-cohesion creates the most rugose sand bodies for each of the three delta types. Note the absence of error bars due to this measurement occurring only at one time after all sediments are deposited.

rugosity is the medium-cohesion, sand-dominated delta. Sand body rugosity between the three delta types shows statistically significant differences at 95% confidence.

Discussion

While Edmonds and Slingerland (2010) discovered an area in their parameter space that created ideal conditions for high numbers of distributaries (intermediate excess shear stress at the bed and intermediate sand proportion), we saw rather what appears to be a linear increase in the number of active distributaries with decreasing proportion of stiff mud delivered to the delta. This is likely because resistant mud stabilizes distributary levees, making them less likely to develop a crevasse. The idealized conditions of Edmonds and Slingerland (2010) experiments may be a function of their specific parameter space which differs from the parameter space used in this study.

The very different topset morphologies and stratigraphy of these nine numerically-modeled deltas can be understood in terms of delta growth processes. In high mud systems, the smaller number of distributaries delivers sediment less equitably around the delta perimeter, resulting in more rugose shorelines (Fig. 21). These results are consistent with the qualitative conclusion of Olariu et al. (2006) who determined that "the number of terminal distributaries controls… the overall shape of the shoreline." Stable distributaries produced by high-cohesion also give rise to the greatest average topset elevations, because as banks stabilize, fine-grained material continues to settle on them causing aggradation. These erosion-resistant levees are able to prograde and resist avulsion better than lower cohesion deltas, thereby increasing the rugosity of shorelines. This process is evident in the high-cohesion, mud-dominated delta and the high-cohesion, sand-dominated delta. Mississippi Delta distributaries erode into stiff prodelta muds, and this has been argued to prohibit lateral migration of distributaries, thereby creating a highly

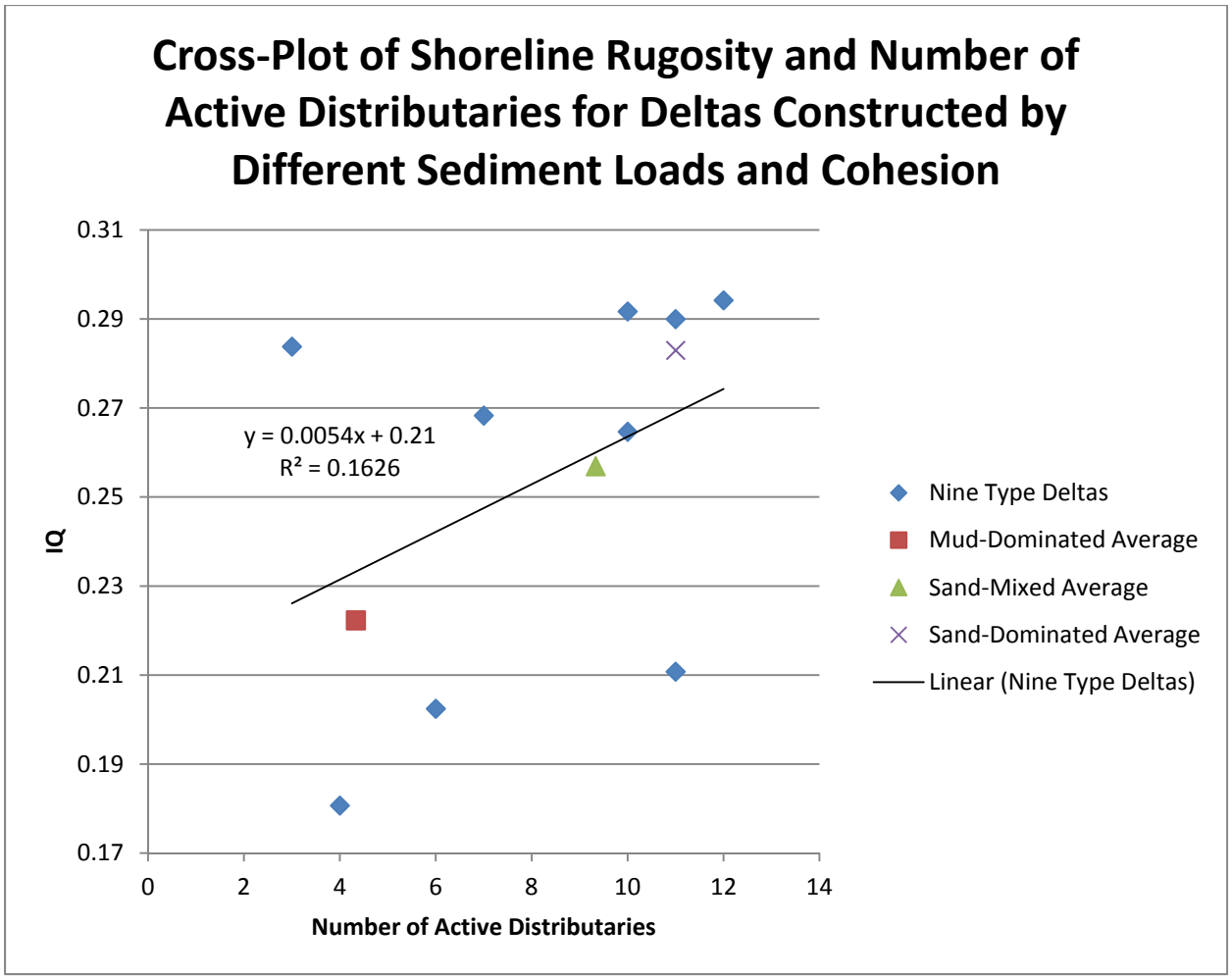

Figure 21. The cross-plot of shoreline rugosity and number of active distributaries shows a weak correlation ($R^2 = 0.1626$). Nevertheless, an increase in the number of active distributaries is generally an indicator of a smoother shoreline.

rugose shoreline (Coleman and Prior, 1982). In other modern deltas, the number of distributaries increases basinward, and as the number of terminal distributaries increases, the orientation angle of distributaries relative to the axial trunk stream increases (Olariu et al. 2006). This process allows an even sediment dispersal around the shoreline in the form of small mouth-bars and enables the delta to take a fan shape (Olariu et al., 2006).

Increased shoreline rugosity influences the active foreset. A cross-plot of delta shoreline rugosity and uniformity (Fig. 22) demonstrates that the delta shoreline shape and the shape of its foreset are moderately correlated ($R^2 = 0.6675$).

Distributaries are responsible for controlling the quantity, location, and timing of sediment deposition on the delta, so it should be no surprise that they set delta stratigraphy in these experiments devoid of waves and tides. As flows in active distributaries encounter open water beyond the shoreline, they expand, slow, and deposit sediments. Deposition typically occurs as a prograding delta-front mouth bar, the convexity of which determines the range of bar-front dip directions, and these in turn determine the uniformity of the delta-front dip azimuths. A large number of distributaries produces a low uniformity (Fig. 23). Numerous distributaries construct a foreset self-similarly whereas few distributaries construct the foreset irregularly.

It is somewhat counterintuitive to think that a delta with numerous active distributaries would develop many parasequences rather than continuously prograding as a single parasequence (Fig. 24). But the active distributaries are numerous because they evolve and heal frequently. Upon healing, a condensed horizon is formed offshore which is interpreted here as a flooding surface bounding a parasequence. Sand-dominated deltas that have numerous

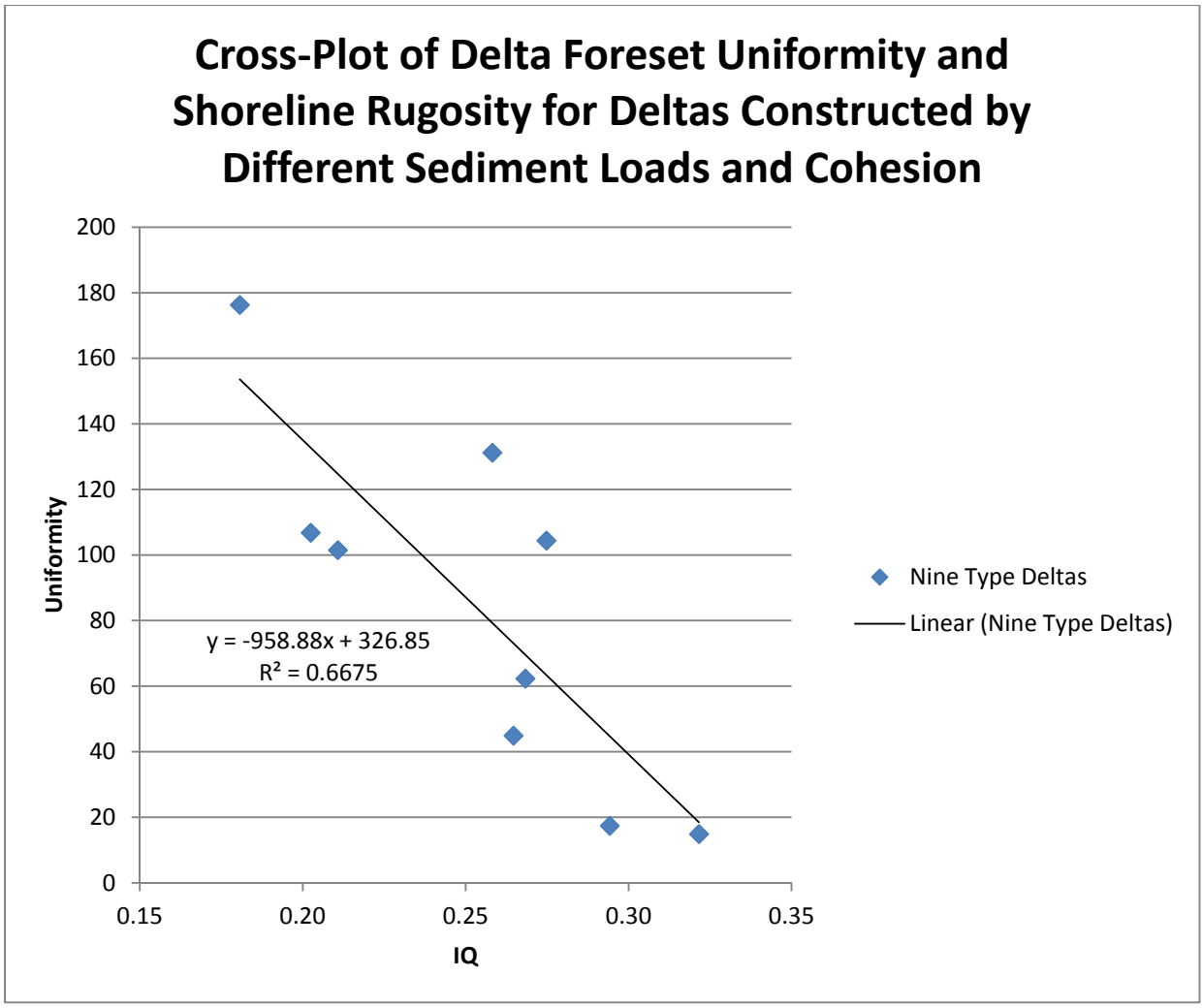

Figure 22. Foreset dip azimuth uniformity of a delta is negatively correlated with the rugosity of the shoreline (IQ). Rugosity controls the spread of dip directions of the delta foreset active at any one time. With continued progradation these foresets become stratigraphy.

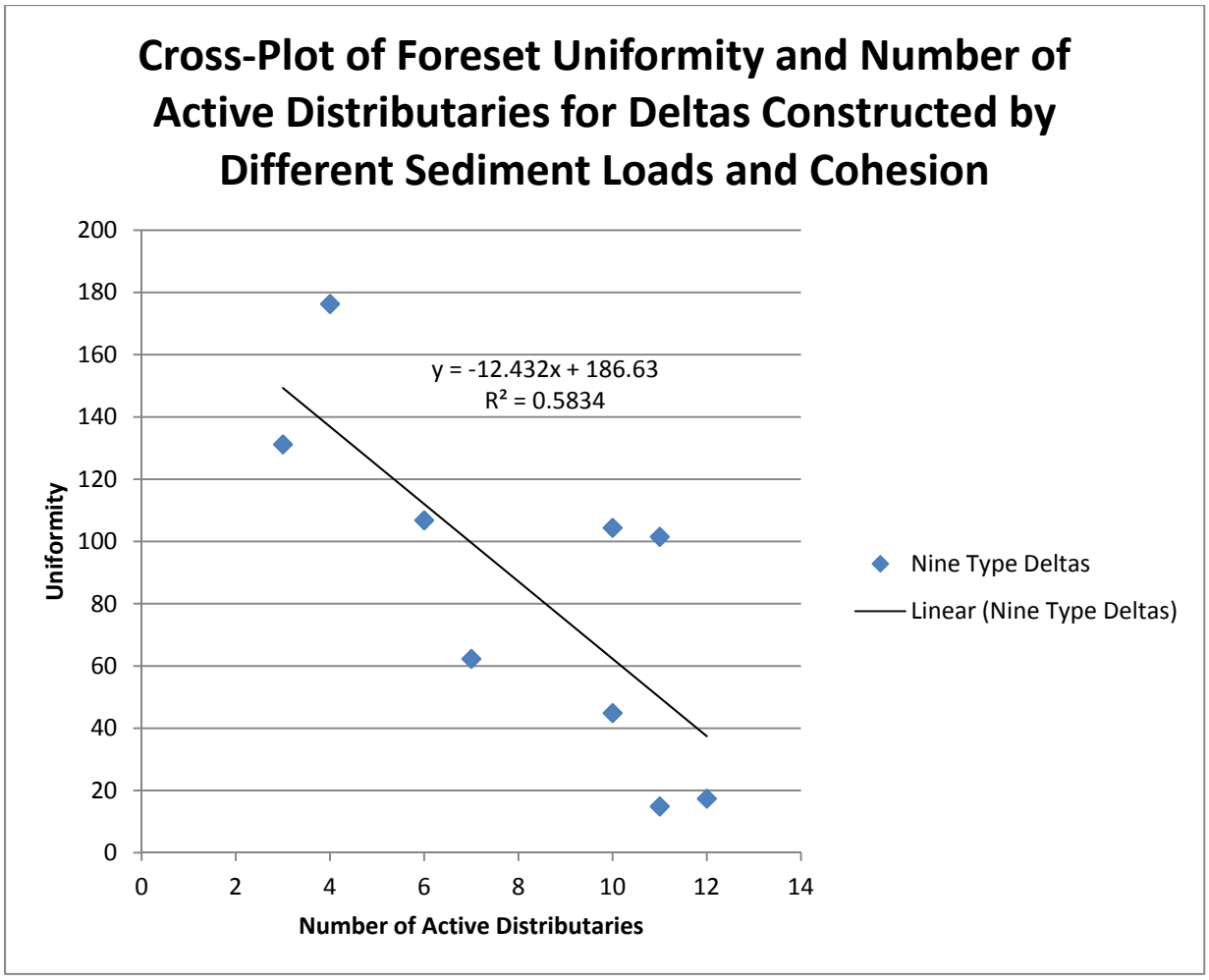

Figure 23. The number of active distributaries controls deposition of sediments along the shoreline and the uniformity of the foreset. The relationship between active distributaries and foreset uniformity is correlated to $R^2 = 0.5834$.

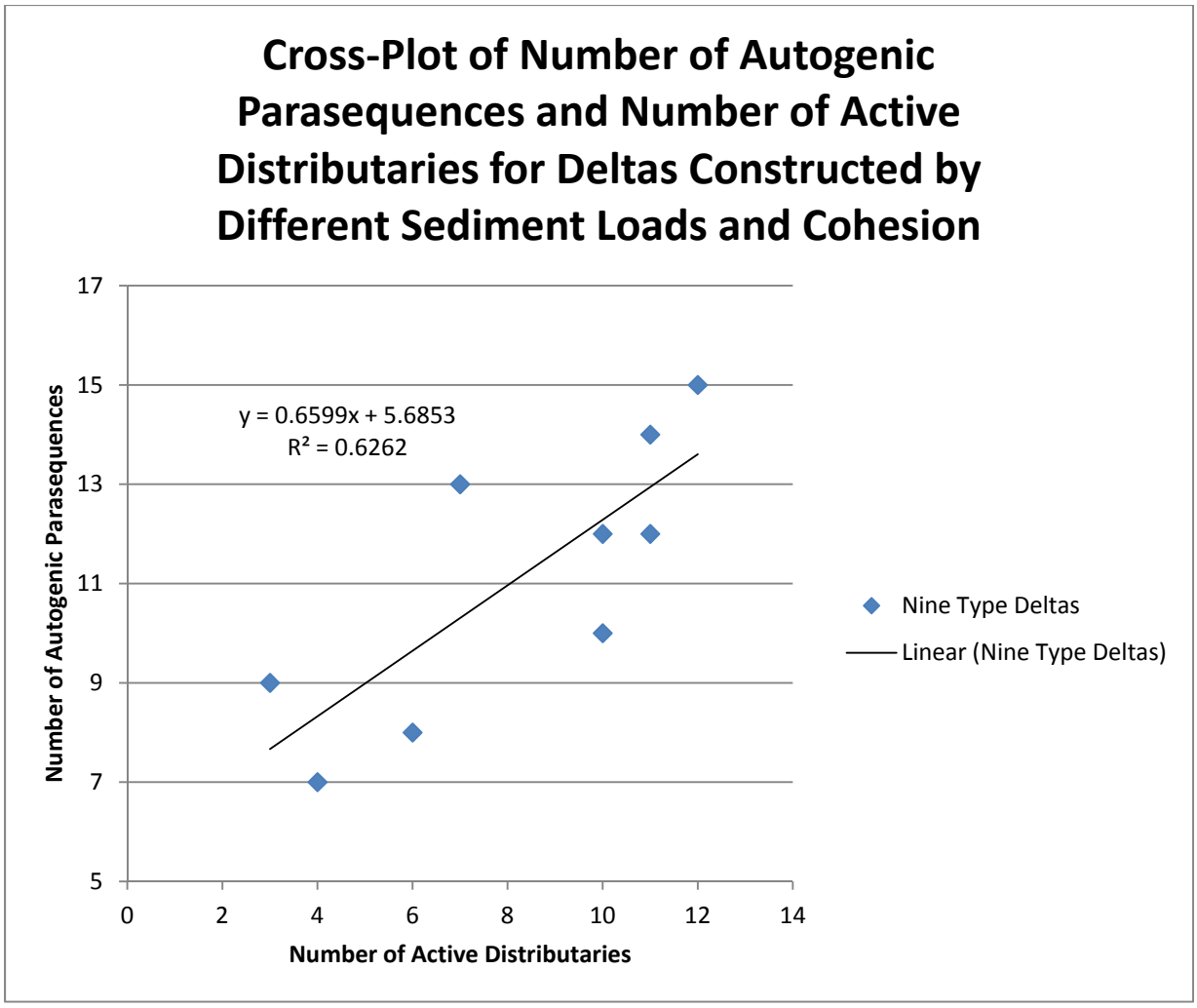

Figure 24. The number of active distributaries participates in setting the number of autogenic parasequences. The relationship is correlated to an $R^2 = 0.6262$.

distributaries develop numerous autogenic parasequences, but their condensed horizons lack fine-grained sediments and would not likely represent significant baffles to flow in a reservoir. Mud-dominated and sand-mixed deltas are able to accumulate significant mud deposits on the flooding surface. Therefore, while the sand-dominated deltas develop many parasequences, they do not significantly impede reservoir flow, and sand-mixed and mud- dominated deltas develop fewer parasequences which certainly have a greater influence on reservoir flow.

The process of distributary switching and abandonment also has a significant impact on the proportion of channel and foreset facies that are preserved in the stratigraphy. The proportion of channel facies preserved in cross-section increases as the number of active distributaries increases (Fig. 25). The number of distributaries is greatest for sand-dominated deltas and deltas having lower cohesion, and because these types of deltas have more mobile distributaries, they incise more of the previously deposited foreset as they deliver sediments to the active foreset. Sand-dominated deltas with a higher proportion of channel facies follow a more topset-dominated facies model and mud-dominated deltas with a higher proportion of foreset facies follow a more foreset-dominated facies model (Edmonds et al, 2011).

Clinoform dip magnitude and concavity are dependent upon the proportion of sand and mud being delivered to the foreset by the distributaries. This dependency can be understood as a balance between the proportions of coarse-grained bedload transport delivered to the clinoform rollover and finer-grained suspended load transported seaward in the expanding jet to settle out on the clinoform toe. Sand-dominated deltas controlled by bedload sedimentation should develop short steep clinoforms whereas mud-dominated deltas are controlled by suspended load sedimentation and should develop long, low-angle clinoforms. Variations in these proportions also should control clinoform concavity. The low-angle nature of mud-dominated delta

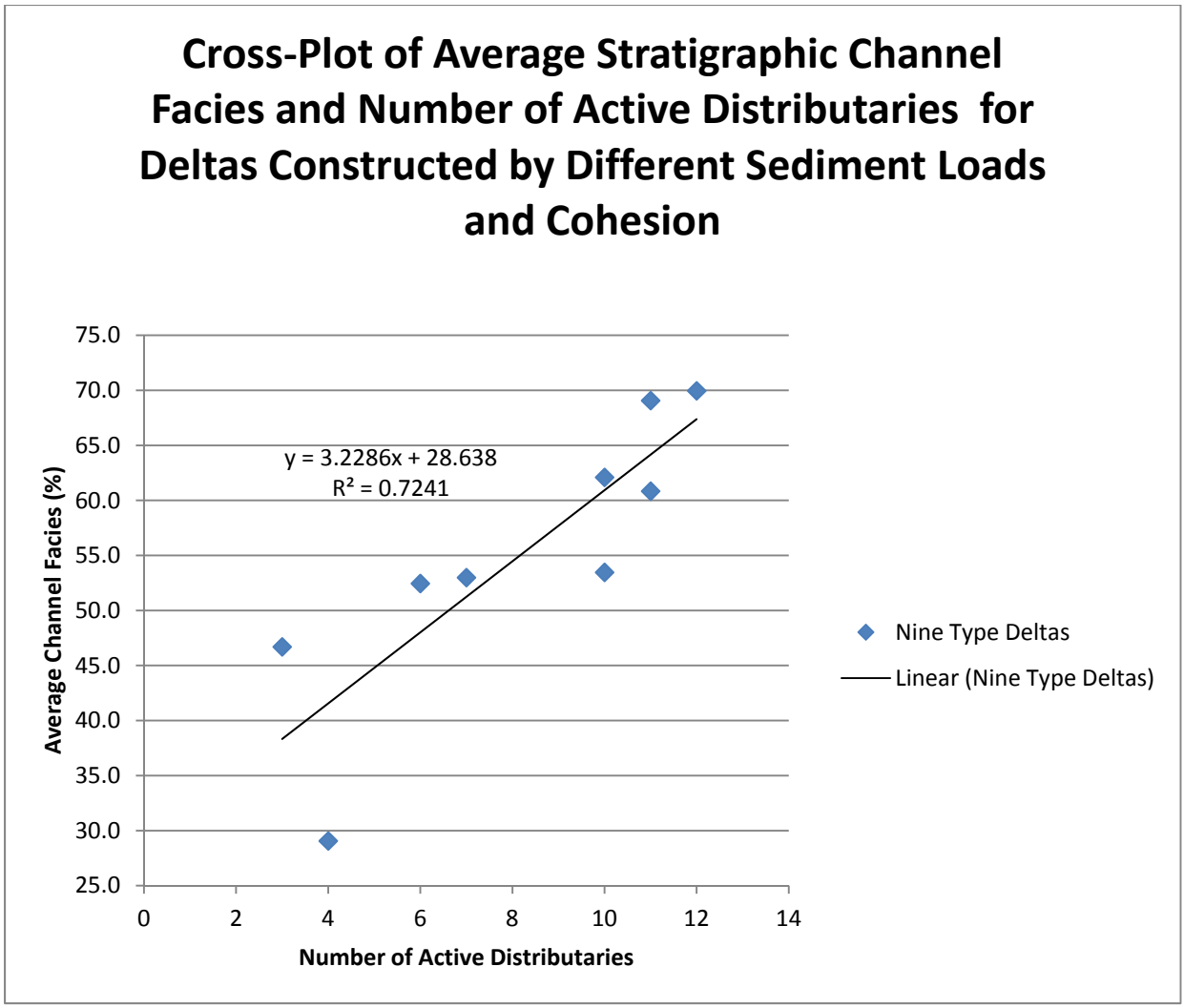

Figure 25. As the number of active distributaries increases, the proportion of channel facies also increases. The two variables are correlated with an $R^2 = 0.7241$.

clinoforms makes it difficult for concavity to become pronounced while the sand-dominated deltas with their steep clinoforms and fine-grained toes are more concave. The fining of bedload sediments down sand-dominated clinoforms also promotes concavity. Thus, sand-dominated deltas display concavities two orders of magnitude greater than the sand-mixed and sand-dominated deltas.

Sand-body geometry has been shown to be a function of the number of terminal distributaries (Olariu et al., 2006), and here we show that reservoir rugosity is a function of the number of active distributaries. Again, the stability of distributary banks and the frequency of distributary switching are determined by the proportion of sand and mud being carried by the distributary and the cohesion of the mud. Sand bodies deposited by mobile non-cohesive distributaries are expected to have larger, more connected sand deposits than those deposited by immobile cohesive distributaries, and this is what we observe. The number of active distributaries is strongly correlated to the amount of sand and mud in a system and the degree of cohesion of the mud, and we find that a low number of distributaries translates to highly rugose discontinuous deposits (Fig. 26). Rugosity of sand deposits is of particular interest to the oil and gas industry because highly rugose reservoirs are riskier prospects. Here, we see the risk of encountering a reservoir increasing significantly as the proportion of sand delivered to the delta decreases.

TESTING MODEL PREDICTIONS

Geologic Setting

The Goose River Delta---. The Goose River Delta is an unvegetated fan-shaped delta prograding into Goose Bay, a 30 m deep fjord arm in Labrador, Canada, called Lake Melville (Fig. 27; Fig. 28). Tides, buoyancy effects, and waves in Goose Bay are minimal, thereby

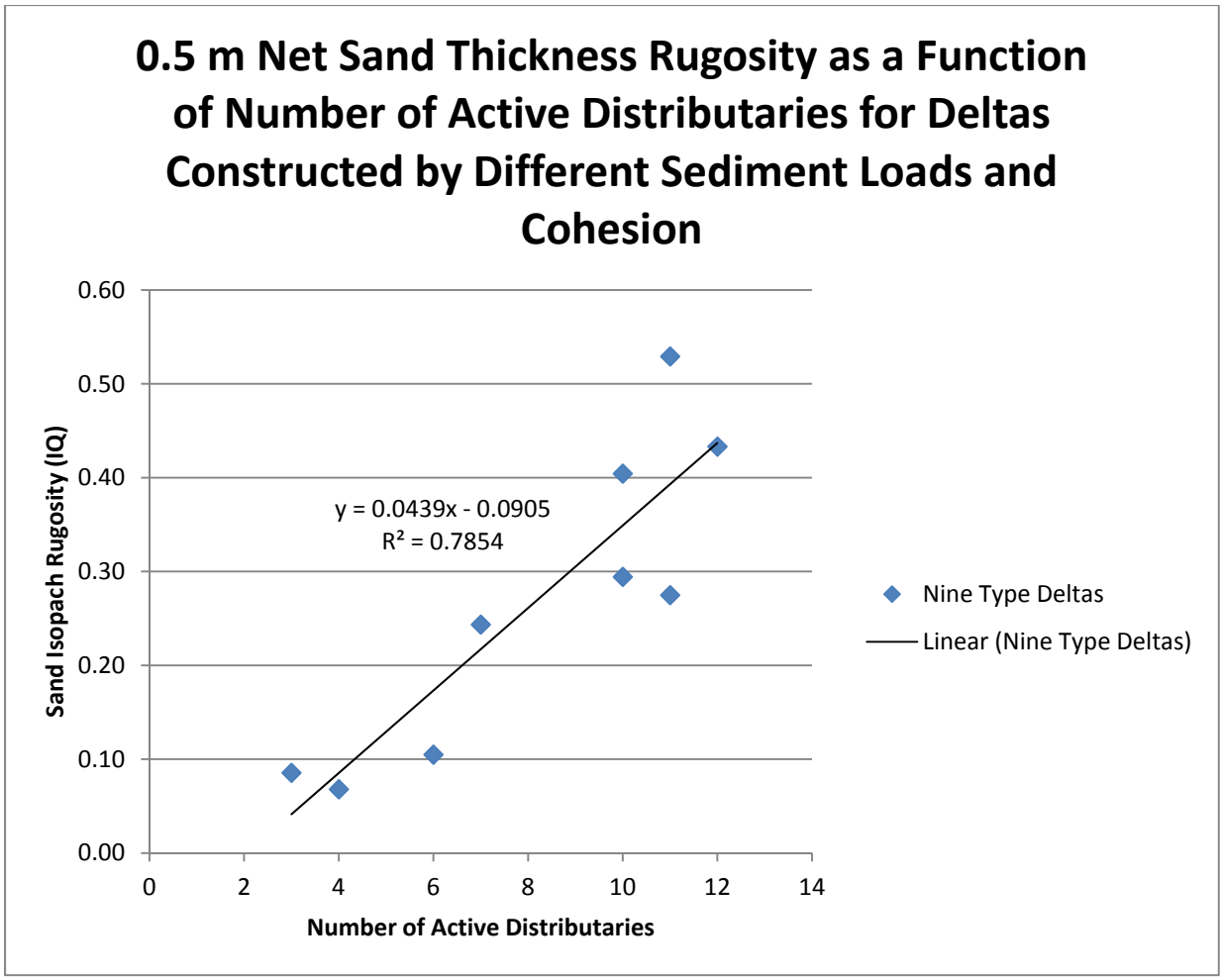

Figure 26. The number of active distributaries and the 0.5 m sand isopach rugosity are correlated to an $R^2 = 0.7854$.

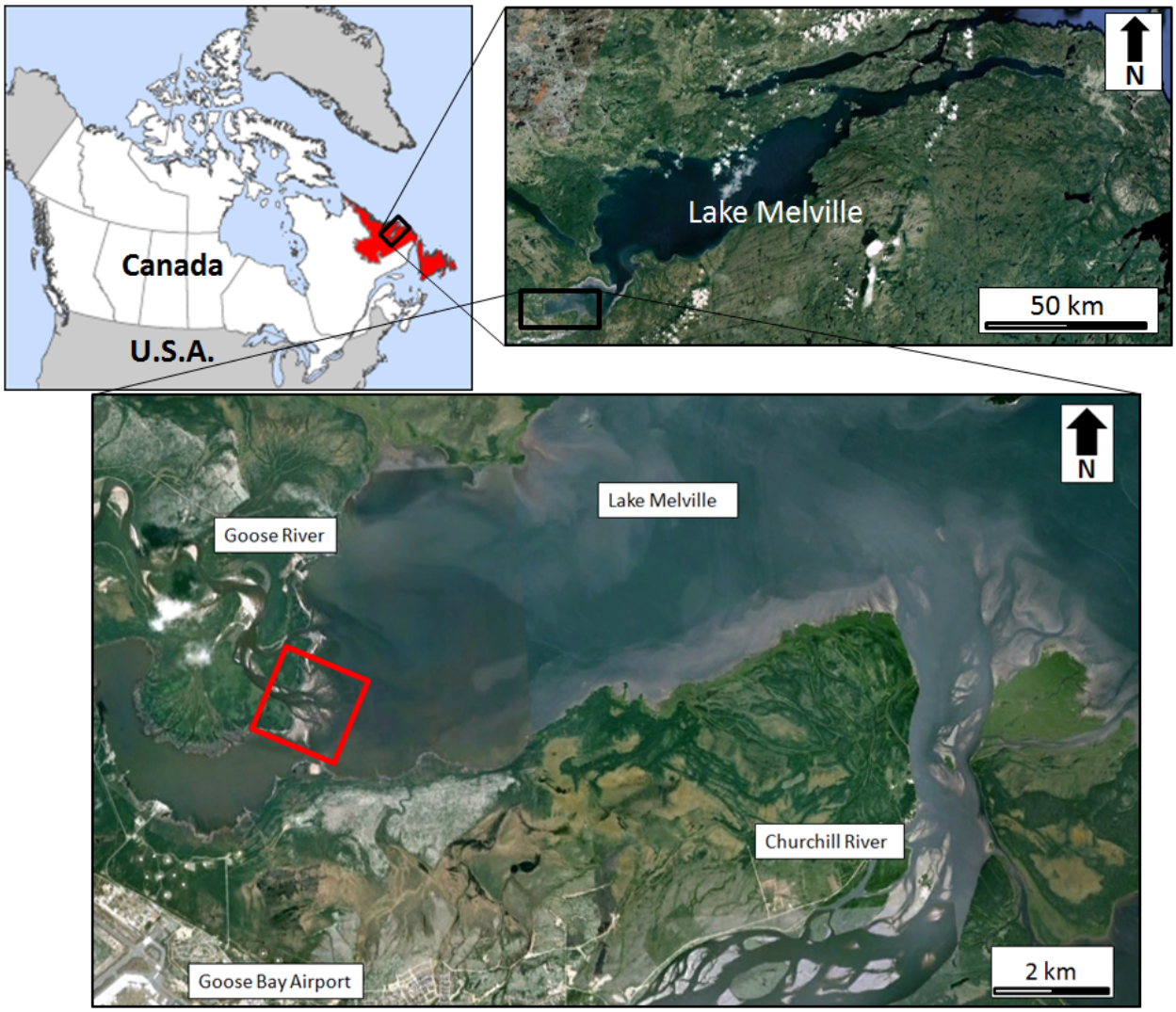

Figure 27. Lake Melville (upper right) is located in Labrador (upper left) of Canada. The active portion of the Goose River Delta (red box indicates area of Fig. 25) is a sandy, unvegetated lobe prograding east to south-east into Lake Melville ("Lake Melville, NL, Canada" Google Maps, 2007).

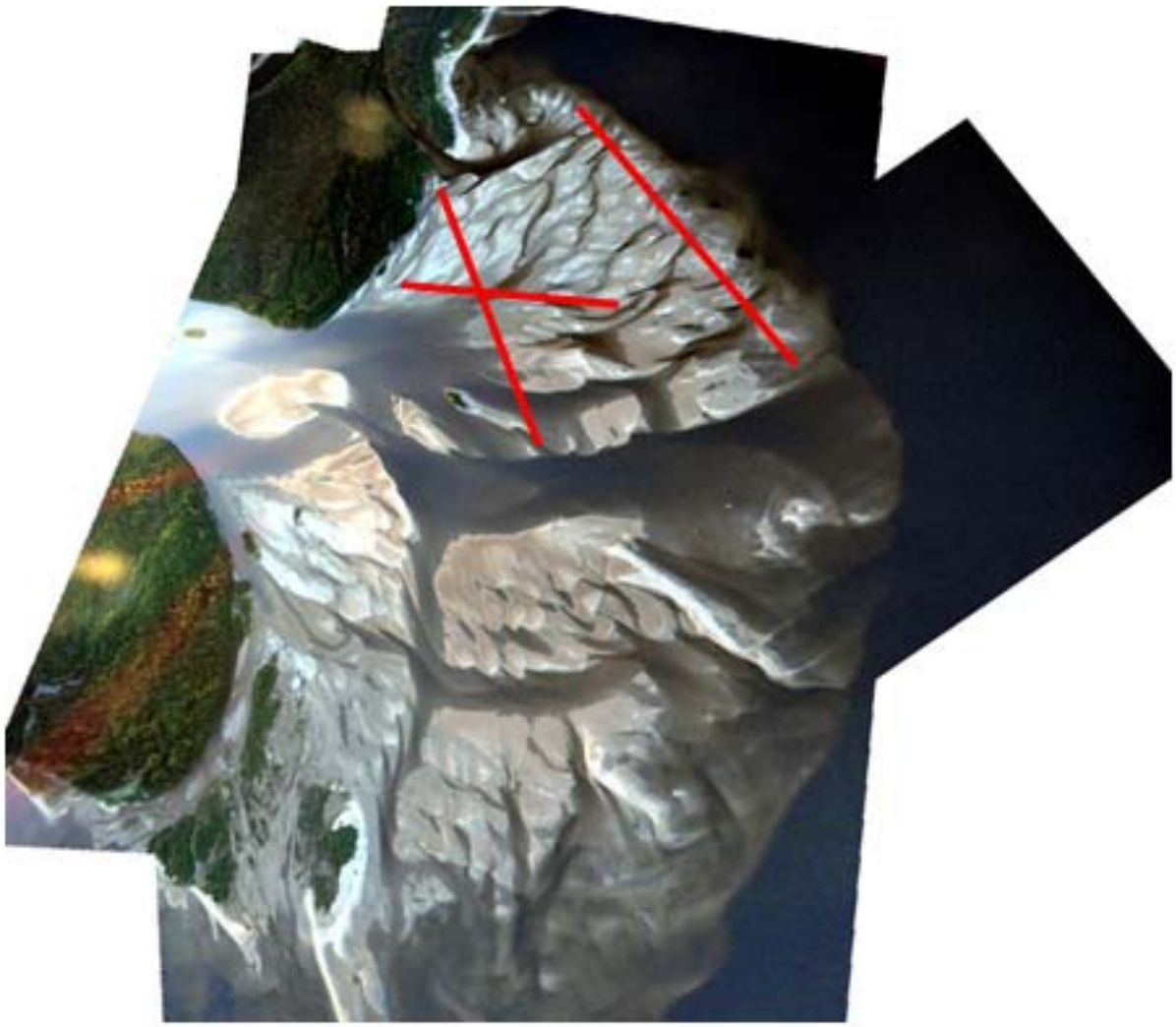

Figure 28. The Goose River Delta is a sandy, fan-shaped delta with very little vegetation on its topset. Photographs were taken August 4, 2012 at low flow and low tide. Red lines denote transects of topset elevations used to calculate roughness and average elevations (aerial photo constructed by Doug Edmonds from helicopter photos by Jim Best).

making the Goose River Delta a reasonable test case for the model predictions. Due to a sill near the mouth of Goose Bay, the bay is microtidal (0.5 m amplitude) (Vilks et al., 1987) and the surface waters average no more than 10 ppm salinity (Vilks and Mudie, 1983). Prevailing winds during ice-free conditions blow from the west and southwest such that the eastward-prograding Goose River Delta experiences only minor wave influence. However, the Goose River Delta, like other deglaciated fjord deposits, is experiencing a forced regression (Overeem and Syvitski, 2010). The Laurentide Ice Sheet retreated westward of the region approximately 8500 yr BP (Vilks and Mudie, 1983). Subsequent post-glacial rebound has subjected the Goose River to an average relative base level fall since that time equal to 6 mm yr^{-1} (Fitzhugh, 1972). Our model runs do not include this effect.

Most of the previous research in the greater Lake Melville area has focused on paleoceanography, paleoclimate, and postglacial sequence stratigraphy (Vilks and Mudie, 1983; Syvitski and Lee, 1997; Overeem and Syvitski, 2010). The stratigraphic studies (Syvitski and Lee, 1997; Overeem and Syvitski, 2010) developed a depositional model during and after glaciation, and illuminated the role of climate and environmental changes as controls on sedimentation style and rates. No studies have focused on the modern delta morphologies of Lake Melville.

The Goose River transports a dominantly coarse sand-sized mixture of quartz, feldspar, and heavy minerals derived from plutonic and metamorphic rocks (i.e. granite, granidiorite, gneiss) of the Canadian Shield (Wardle et al., 1997). The average grain size is 450 μm as determined from 17 topset sediment samples that were collected randomly on the delta topset at 20 cm depths.

Application of Methods

Because time-evolution of morphodynamic change is not observable in the Goose River Delta, we measured the number of active distributaries on the Goose River Delta from an aerial photograph. The photograph was taken from a helicopter during low flow at low tide. Distributaries were counted where they met the shoreline and directly connected to flow coming from the trunk stream. The shoreline rugosity of the Goose River Delta was obtained from our single-beam bathymetric data. We used the -1 m contour to define our shoreline because it is the shallowest reliable depth for marine echosounder data. This contour was not subject to the open angle method because unlike the numerical deltas, the contour did not enter any distributaries. Because we could not acquire a continuous strike line of elevations across the Goose River Delta, we averaged three strike lines. Topset roughness was calculated for the Goose River Delta from GPS elevation measurements along strike lines. Uniformity of the Goose River Delta was not calculated. Clinoform dip magnitudes and concavities were obtained by using the concavity method on 51 clinoforms present in an exposed section of a raised 500 year old lobe. Outcrops show prominent clinoforms and no vertical exaggeration is required. Channel and foreset facies of the Goose River Delta were not quantified due to the lack of channel facies representation in the cut-bank outcrops. The number of autogenic parasequences and reservoir rugosity were not measured for the Goose River Delta.

Results

The Goose River Delta consists of numerous distributaries feeding a uniform shoreline. On the southern active lobe, there are 14 active distributaries at the delta shoreline and at least five orders of bifurcation are observed. A shoreline rugosity of 0.47 was calculated from single-beam echosounder bathymetry data extracted along the -1 m contour. Topset roughness and elevations were computed from three GPS elevation transects across the northern portion of the delta (Fig.

28). Elevations are accurate to within a few centimeters. The average topset elevation of the Goose River Delta is 0.09 m (Fig. 29), the average topset roughness is 0.11 m (Fig. 30), and the maximum elevation is 0.54 m. Clinoform dip magnitudes and concavities were measured from a cut-bank of the Goose River in a delta lobe abandoned about 500 years ago (Fig. 31) (Taylor and Batterson, 2001). Clinoform concavity and clinoform dip magnitudes were calculated using the concavity method on 51 elevation points along these clinoforms. The average clinoform dip magnitude is 13.3° with a standard deviation of 5.8°. The average clinoform concavity of the Goose River Delta as measured from the same outcrop is 1.65×10^{-3} with a standard deviation of 1.34×10^{-3}.

Discussion

The Delft3D models predict that a low-cohesion, sand-dominated delta will have more active distributaries, a less rugose shoreline morphology, less topset complexity, and a foreset with smaller uniformity than a highly cohesive delta constructed by a mud-dominated sediment load. The morphology of the coarse-grained Goose River Delta is consistent with this prediction. The 14 distributaries and five orders of bifurcation observed are remarkably consistent with the 12 distributaries and five orders of bifurcation predicted for a low cohesion, sand-dominated delta. The higher rugosity of the Goose River Delta (0.47) than the low cohesion, sand-dominated numerical delta (0.29) is most likely a function of the depth at which the shoreline was defined for the Goose River Delta. The open angle method is used to objectively determine shoreline points around terminal distributaries, but the Goose River Delta terminal distributaries do not exceed 1 m in depth. Therefore, selecting the -1 m contour measurement dampens shoreline irregularities and causes a higher IQ. Unfortunately, it is not possible to select the -0.1 m

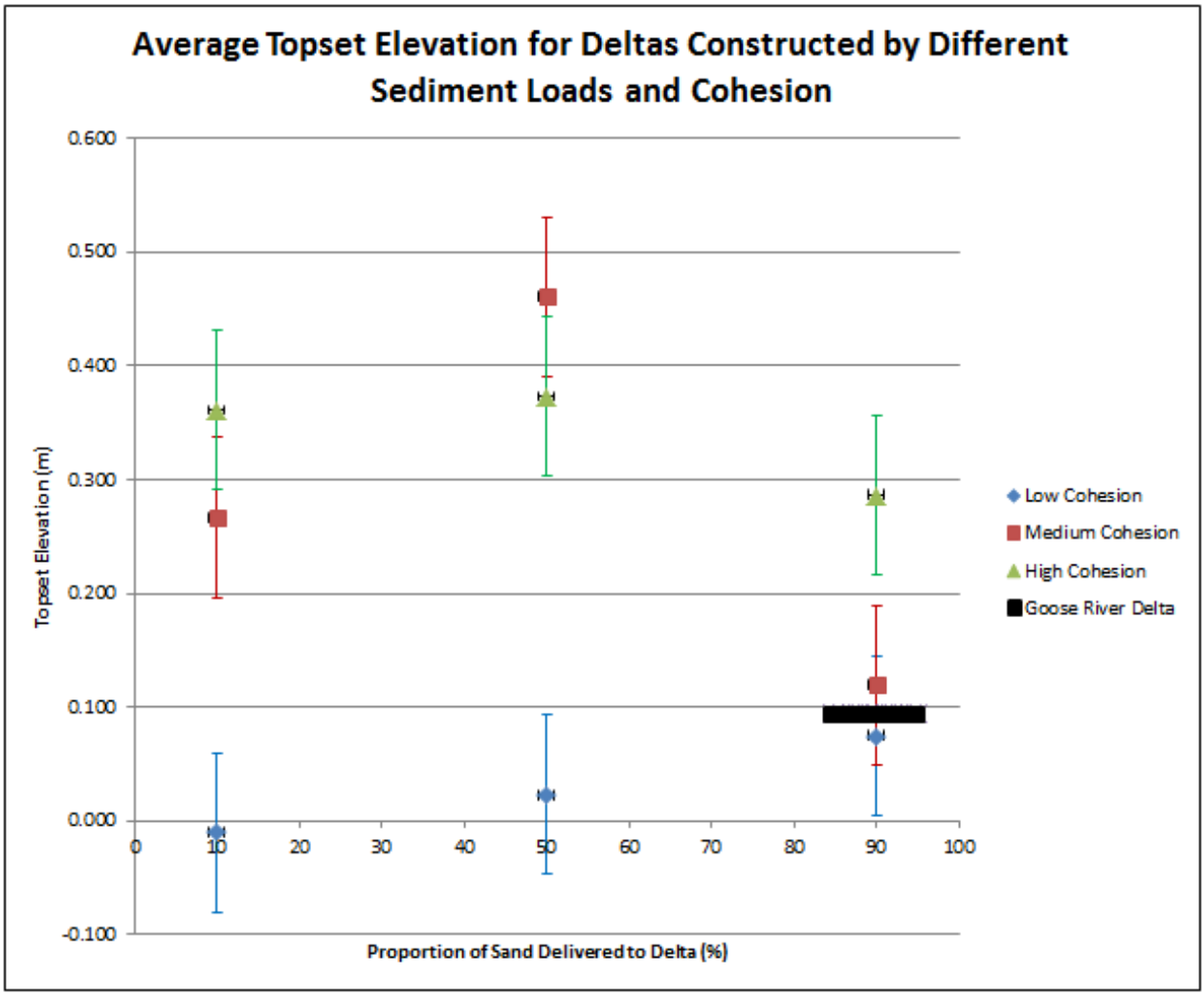

Figure 29. The Goose River Delta has an average topset elevation of 0.09 m. The error bar for proportion of sand delivered to the Goose River Delta spans 85-95% and the average topset elevation plots between the low-cohesion and medium-cohesion, sand-dominated numerical deltas.

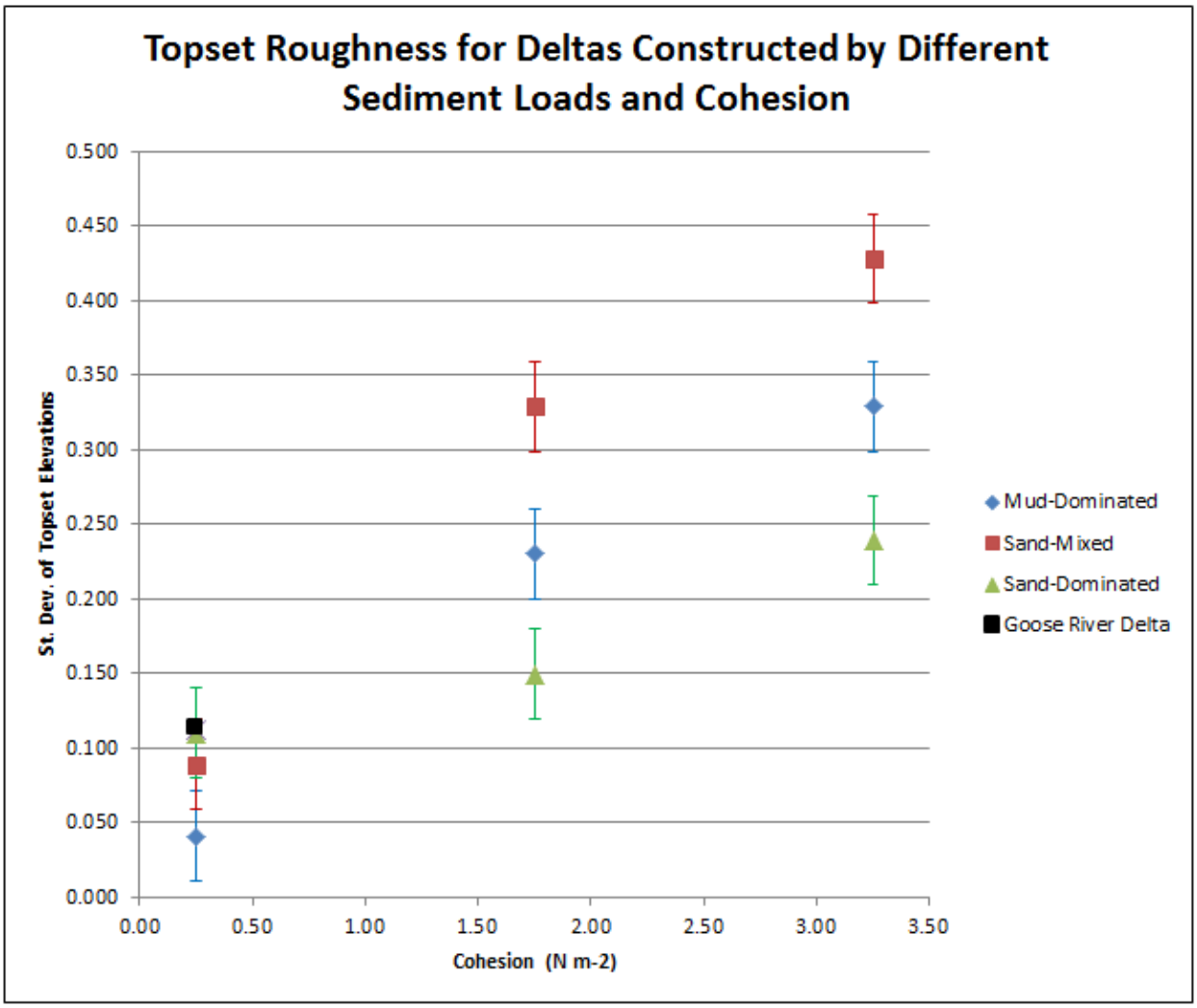

Figure 30. The Goose River Delta has a topset roughness of 0.112 and an estimated low-cohesion similar to the low-cohesion numerical deltas. The Goose River Delta topset roughness plots in a nearly identical location to the low-cohesion, sand-dominated numerical delta.

Figure 31. Clinoform dip magnitudes and concavities were measured from photographs of older deposits of the Goose River Delta. The outcrop is exposed along cut banks in the modern Goose River (N 53.3985° W 60.4035°). Clinoforms dip from left to right and the approximate rollover point is the orange color in the upper center of the photograph.

contour of the Goose River Delta for shoreline rugosity measurement due to the limitations of single-beam data acquisition. Nevertheless, the shoreline rugosity of the Goose River Delta is most similar to rugosity of the numerical sand-dominated deltas. The Goose River Delta topset roughness (0.112) is nearly identical to the roughness of the low-cohesion, sand-dominated numerical delta (0.110) (Fig. 30). Topsets in the numerical models become increasingly rough with decreasing sand and/or increasing cohesion, and as argued previously this is a function of stabilization and aggradation of levees by cohesive fine-grained sediments. The Goose River Delta is inarguably sand-dominated and unvegetated and as a result its levees do not aggrade. Foreset dip azimuth uniformity could not be quantified in the Goose River Delta.

The Goose River Delta allows us to test our hypothesis that a relatively non-cohesive delta constructed by a sand-dominated sediment load will have greater clinoform dip magnitudes, greater clinoform concavity, more channel facies, more autogenic parasequences, and lower rugosity sand bodies than a highly cohesive delta constructed by a mud-dominated sediment load. The Goose River Delta foreset is constructed by clinoforms with dips averaging 13° and a maximum dip of 28°. Direct comparison of the Goose River and numerical delta clinoform dips is not appropriate because the numerical deltas are topset-dominated deltas which typically have shallow dips (Edmonds et al., 2011). But the steep Goose River Delta clinoform is consistent with the steep clinoform of the sand-dominated numerical deltas. For comparison, the clinoform dip magnitudes of the fine-grained Atchafalaya Delta are around 1° (Neill and Allison, 2005) whereas the clinoform dips of the Goose River Delta are comparable to the 13° clinoform dips of the coarse-grained Pennsylvanian “Gilbert” Delta of New Mexico (Gani and Bhattacharya, 2005).

Clinoform concavity is more readily compared to the numerical models because it is not as dependent on basin water depth. The concavity of the Goose River Delta is most similar to the concavities of the sand-dominated deltas, although an order of magnitude greater (Fig. 32). This increase in concavity is likely due to the coarser grain size of the Goose River Delta which promotes bedload dumping at the clinoform rollover and steepening of the most proximal portion of the clinoform. Stratigraphic facies, number of parasequences, and sand body rugosity were not measured in the Goose River Delta.

In summary, we conclude that observations of the morphology and stratigraphy are consistent with the model predictions for a low-cohesion, sand-dominated delta. Although the exact magnitudes of Goose River Delta topset and stratigraphic attributes may differ from those predicted by the model, their trends are consistent.

APPLICATION OF MODEL PREDICTIONS

A common objective of paleo-environmental interpretation is to infer the three-dimensional rock properties of a deposit from limited data like 2D seismic or outcrop cross-sections. In oil and gas exploration this exercise is typically undertaken in order to generate a reservoir model and mitigate reservoir uncertainties arising from limited data. Our approach towards this end is to quantify clinoform dip magnitude, clinoform concavity, facies distributions, and the number of parasequences from outcrop cross-sections and use these measurements combined with the Delft3D predictions to hindcast the planform shoreline rugosity, topset roughness, and number of active distributaries of the paleo-delta. Our example is the Cretaceous Last Chance Delta of the Ferron Sandstone near Emery, UT.

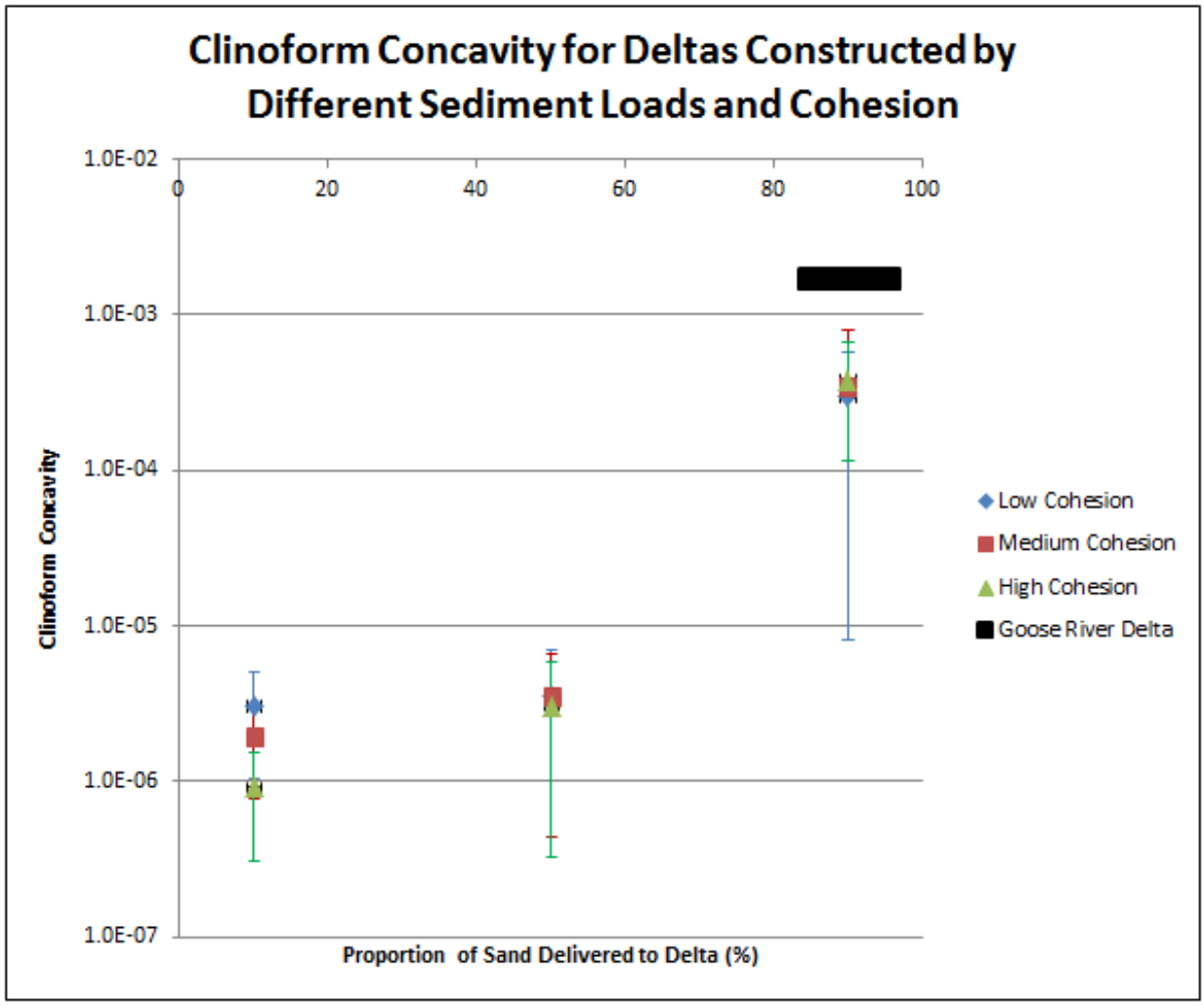

Figure 32. Goose River Delta clinoform concavity (the error bar for proportion of sand delivered to the Goose River Delta spans 85-95%) plots higher than any of the numerical deltas, but lies closest to the concavities of the sand-dominated deltas.

Geologic Setting

The Last Chance Delta--. The Upper Ferron Member of the (Turonian) Cretaceous Mancos Shale Formation was deposited by the Last Chance Delta; one of the most studied of all ancient deltas exposed in outcrop. The Upper Ferron (90.3 – 88.6 Ma), currently exposed in vertical cliffs of Castle Valley near the western flank of the San Rafael Swell (Fig. 33), is a fluvial-deltaic succession of strata deposited as part of the Southern Utah Deltaic Complex (Garrison and van den Bergh, 2004). Thrusting of the Sevier Orogeny created a foreland basin that was occupied by the Cretaceous Western Interior Seaway. The orogenic belt provided a large amount of clastic sediment to the basin (Sampson et al., 1999) and more than 20 known deltas prograded into Western Interior Seaway. Subsequent uplift during Basin and Range extension and an arid non-vegetated environment have left these deposits well exposed.

Numerous authors have studied the Last Chance Delta to better understand its coal deposits and more recently the Last Chance Delta has been used as a reservoir analog in research with application to the oil and gas industry (Katich, 1953; Hale and Van DeGraff, 1964; Cotter, 1976; Ryer, 1981; Gardner, 1992, 1995a, 1995b; Lowry and Jacobsen, 1993; Barton, 1994, 1997; Garrison et al., 1997; McMechan et al., 1997; Knox, 1997; Knox and Barton, 1999; Corbeanu et al., 2001; Novakovic et al., 2002; Moiola et al., 2004; Ryer and Anderson, 2004; Bhattacharya and Tye, 2004; Enge and Howell, 2010). Most research has been conducted on the seven parasequence sets exposed in cliff faces (Van Wagoner et al., 1990; Ryer and Anderson, 2004) with other studies incorporating core, wireline logs, and ground-penetrating radar (GPR) data (McMechan et al., 1997; Corbeanu et al., 2001; Zeng et al., 2004). Extensive work on facies descriptions and sediment-volume partitioning was conducted by Gardner (1992, 1995a, 1995b); later the Utah Geological Survey released Open File Report 412 (Anderson et al., 2003) which included photomosaics and measured sections for most of the Last Chance Delta outcrops.

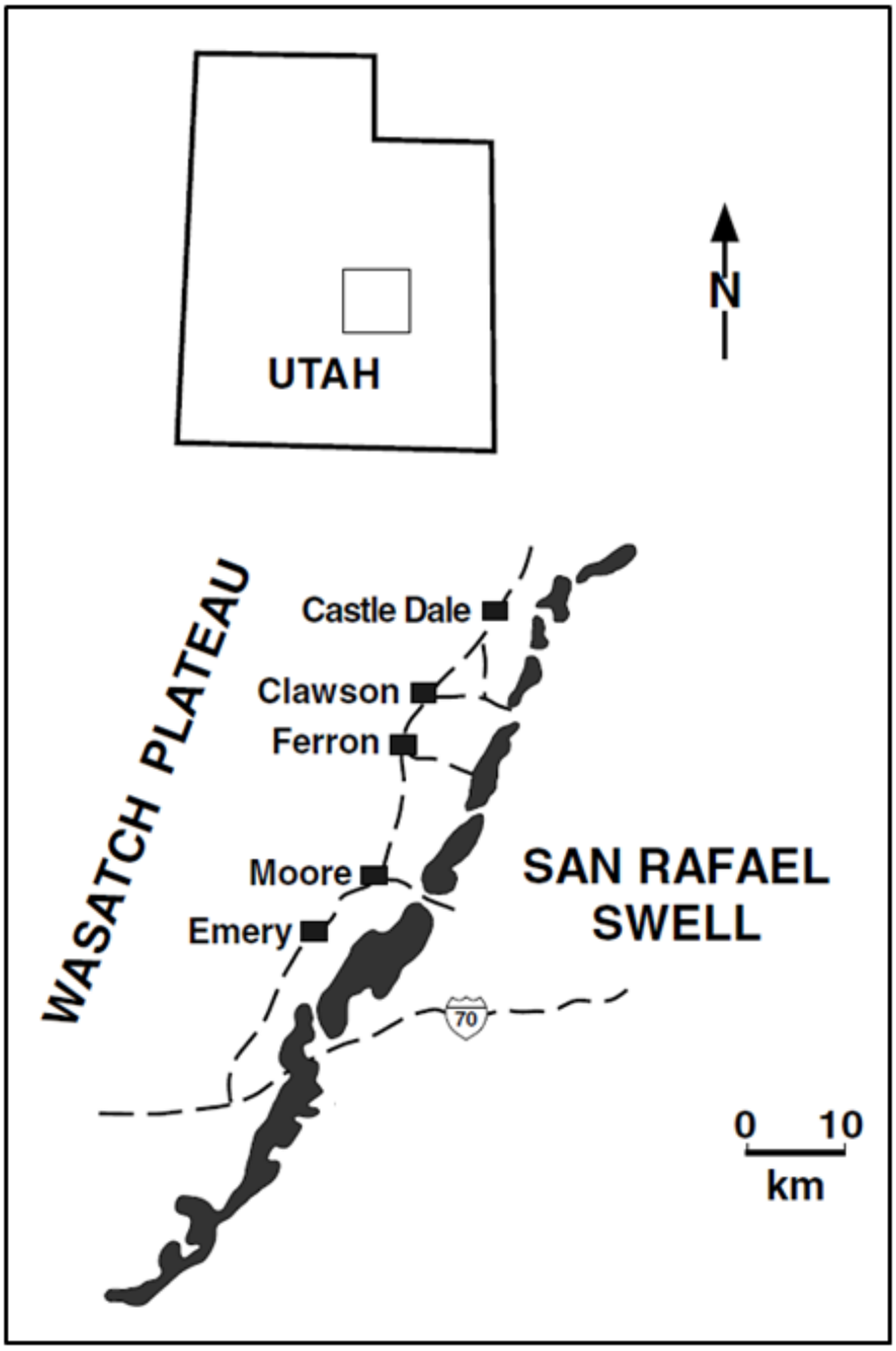

Figure 33. Outcrop belt of the Ferron Sandstone (black) in the Emery, UT area (modified from Zeng et al, 2004).

A handful of studies have been devoted to reconstructing the paleo-morphology and paleo-environment of the Last Chance Delta (Hale and Van DeGraff, 1964; Cotter, 1976; Thompson et al., 1986; Anderson and Ryer, 2004). The Last Chance Delta was first recognized as being sourced from the southwest by Katich (1953) and it was first mapped paleogeographically (Figure 34a) by Hale and Van de Graff (1964). It has been interpreted by some as a river-dominated lobate delta (Fig. 1; Fig 34b; Fig 34c) (Cotter, 1976; Thompson et al., 1986) and by others as a river-dominated bird's-foot delta (Fig. 34d; Fig. 34e; Fig. 34f) (Gardner, 1995a; Gardner 1995b; Anderson and Ryer, 2004). Many attribute its river-dominated nature to progradation roughly due north into an embayment that provided protection from waves and storms and may have had a reduced salinity (Cotter, 1976; Anderson and Ryer, 2004; Bhattacharya and Davies, 2004). Cotter (1976) described the paleo-shoreline as "a broad fan, smaller parts of which were subdelta lobes" (Fig 34b) and he estimated that the Ferron prograded into 12 m of water. Bhattacharya and Tye (2004) suggested that the Last Chance Delta "experienced only a few orders of bifurcation" and that its shoreline was "wave-influenced." Anderson and Ryer (2004) argued that there may have been as few as two orders of bifurcation in the Last Chance Delta and that the two lowermost parasequence sets (Kf-1 and Kf-2) of the Last Chance Delta were likely "formed within embayments" as a component of an "asymmetric wave-influenced delta" (Fig. 34f). The Mississippi Delta has been proposed as a modern analog to the Last Chance Delta (Cotter, 1975a; Moiola et al., 2004), but others think the Brazos, Ebro, and Rhone are better analogs (Bhattacharya and Tye, 2004). The trunk stream of the Last Chance Delta is estimated to have drained a 50,000 km^2 basin at a maximum discharge of 1,250 $m^3 s^{-1}$ (Bhattacharya and Tye, 2004). Tidal range at its mouth was likely micro-tidal (Ryer and Anderson, 2004) and wave climates were variable throughout the duration of deposition.

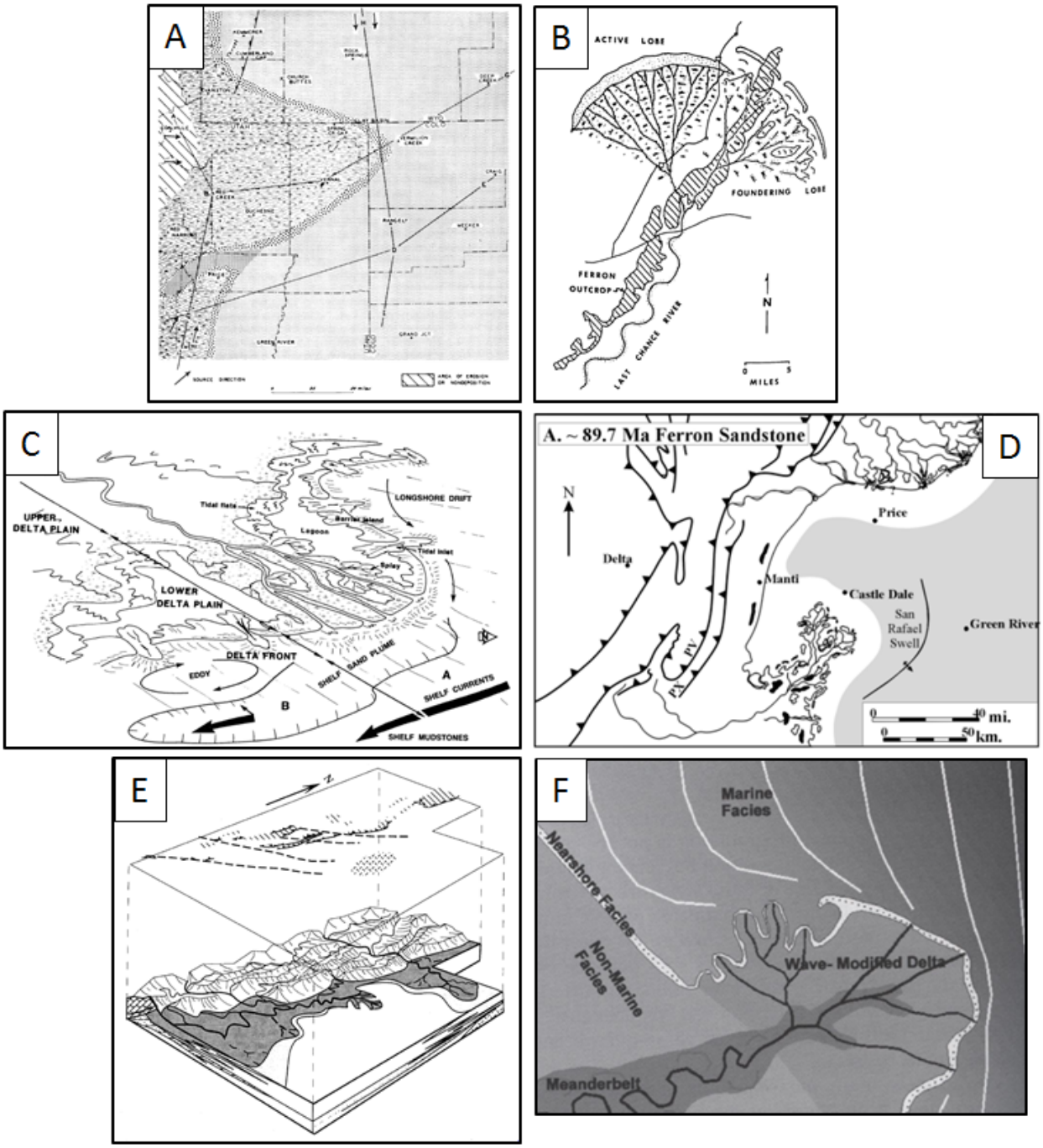

Figure 34. A) Hale and Van DeGraff (1964) first showed the Last Chance delta as being sourced from the southwest and their paleogeographic reconstruction shows a lobate feature. B) Cotter (1976) interpreted the Last Chance Delta as a lobate river-dominated delta having numerous distributaries and bifurcations. C) Thompson et al. (1986) interpreted the Last Chance Delta as being broadly lobate with interdistributary bays and lagoons. Only two orders of bifurcation are recognized. D and E) Gardner (1995a, 1995b) consistently interpreted the paleogeography of the Last Chance Delta as a bird's-foot type delta having a rugose shoreline. F) Anderson and Ryer (2004) interpreted the paleomorphology of the Last Chance Delta as having a fan-like eastern component and a rugose bird's-foot northwestern component.

In summary, despite excellent cross-sectional exposures, there are numerous conflicting views on the morphology of the Last Chance Delta. Here we use the stratigraphic variables defined earlier to compare the clinoform geometry of the Last Chance Delta to Delft3D predictions with the goal of hindcasting its topset attributes. We focus on the most river-dominated of the Last Chance Delta deposits; parasequence set Kf-1.

Application of Methods

Unfortunately, it is rarely possible to measure topset attributes of ancient deltas. We did not measure number of active distributaries because the number of distributaries present in outcrop may not necessarily be a reflection of the number of distributaries active at any one time. We did not measure shoreline rugosity or topset roughness because delta shoreline geometries must be explicitly known to quantify rugosity and the topset of the Last Chance Delta has been eroded. Uniformity of the Last Chance Delta was computed from true clinoform dip azimuth data calculated from 3D outcrop exposures. Eighty-eight clinoform dip magnitudes were measured using the two-point method and 33 clinoforms were measured using the concavity method to determine dip magnitude and concavity. Clinoforms of multiple parasequences were represented. Outcrops show prominent clinoforms and no vertical exaggeration is required. The proportions of channel and foreset facies were calculated from the Utah Geological Survey Open File Report 412 photomosaics (Anderson et al., 2003). Fifty photomosaics were selected by a random number generator from a list of roughly 150 photomosaics where Kf-1 is exposed in outcrop. This random list of photos filtered out any bias that might have occurred due to the relative proximal or distal position of any particular group of photos. On these photos, facies measurements were made for all parasequences within the first parasequence set (Kf-1). Channel facies were mapped where the Utah Geological Survey (Anderson et al., 2003)

identified channel bodies or distributaries belonging to Kf-1; we did not include interdistributary bay deposits or the "Sub-A coal zone" as part of our channel facies. Foreset facies were mapped where the Utah Geological Survey identified sand bodies that were either "wave-dominated nearshore marine", "wave-modified nearshore marine", or "fluvial-dominated nearshore marine," and they terminated where the sand bodies encountered channel, topset, or prodelta facies. Autogenic parasequences have been interpreted in the Last Chance Delta by others (Cotter et al., 1976; Anderson et al., 2003) and we used the Utah Geological Survey Open File Report 412 (Anderson et al., 2003) interpretations to count autogenic parasequences. Reservoir rugosity was not measured.

Observations

The estimated proportion of sand delivered to the Last Chance Delta was determined by measuring the relative proportions of sand and mud in vertical sections measured by the Utah State Geological Survey (Anderson et al., 2003). Proportion of sand was quantified by comparing the vertical thicknesses of sand deposits in Kf-1 to the total thickness of Kf-1. Measured sections are noticeably absent in the Limestone Cliffs, Indian Canyon, and Willow Springs areas, so we estimated the sand proportion in six measured sections in the Rock Canyon and Ivie Creek areas. The average sand proportion of these is 81%.

Using existing data from the Utah Geological Survey Open File Report 412 (Anderson et al., 2003), we measured clinoform geometries on photomosaics from the first parasequence set (Kf-1) of the Last Chance Delta. For each photomosaic a GPS position was collected at a location in the field from which a laser rangefinder was used to obtain horizontal and vertical distances, and azimuths of prominent bedding surfaces. Clinoform surfaces were measured where they were identifiable on both the outcrop and the photomosaic. Where this was not

possible, laser rangefinder data were gathered at evenly-spaced intervals along the photomosaic which permitted clinoform measurement after geo-referencing the photomosaics using the laser rangefinder data. Data were collected from thirty photomosaics and the images were geo-referenced by correcting azimuthal data from magnetic north to true north by adding 11.5 degrees to magnetic north. Next, point data on the photos were converted to spherical coordinates. From the geo-referenced photos, 88 apparent clinoform dip magnitudes were computed using the two-point method, 33 apparent clinoform dip magnitudes were computed using the concavity method, 33 clinoform concavities were measured, and 46 true clinoform dip azimuths were calculated. True clinoform dip azimuths were trigonometrically computed using roughly time-equivalent apparent clinoform dips (from the two-point method) and the strike of the cliff face of adjacent cliff faces. Using 50 images that were not geo-referenced, we calculated the proportion of channel and foreset facies using the techniques outlined earlier for the model data. The autogenic parasequences were counted from the interpretations of the Utah State Geological Survey following those authors' rigorous definition that there "must be proof of transgression and deepening of water" (Anderson et al., 2003).

Results

Apparent clinoform dip magnitudes of the Last Chance Delta range from near zero degrees to a maximum of 15.5°. Using the two-point method, the average apparent clinoform dip magnitude is 4.0° with a standard deviation of 4.0. Using the concavity method, the average apparent clinoform dip magnitude is 7.4° with a standard deviation of 2.3. True clinoform dip azimuth uniformity is 1.1 (Fig. 35). Average clinoform concavity is 1.3×10^{-4} and the standard deviation is 1.1×10^{-4} (Fig. 36). Last Chance Delta deposits that remain below the ravinement

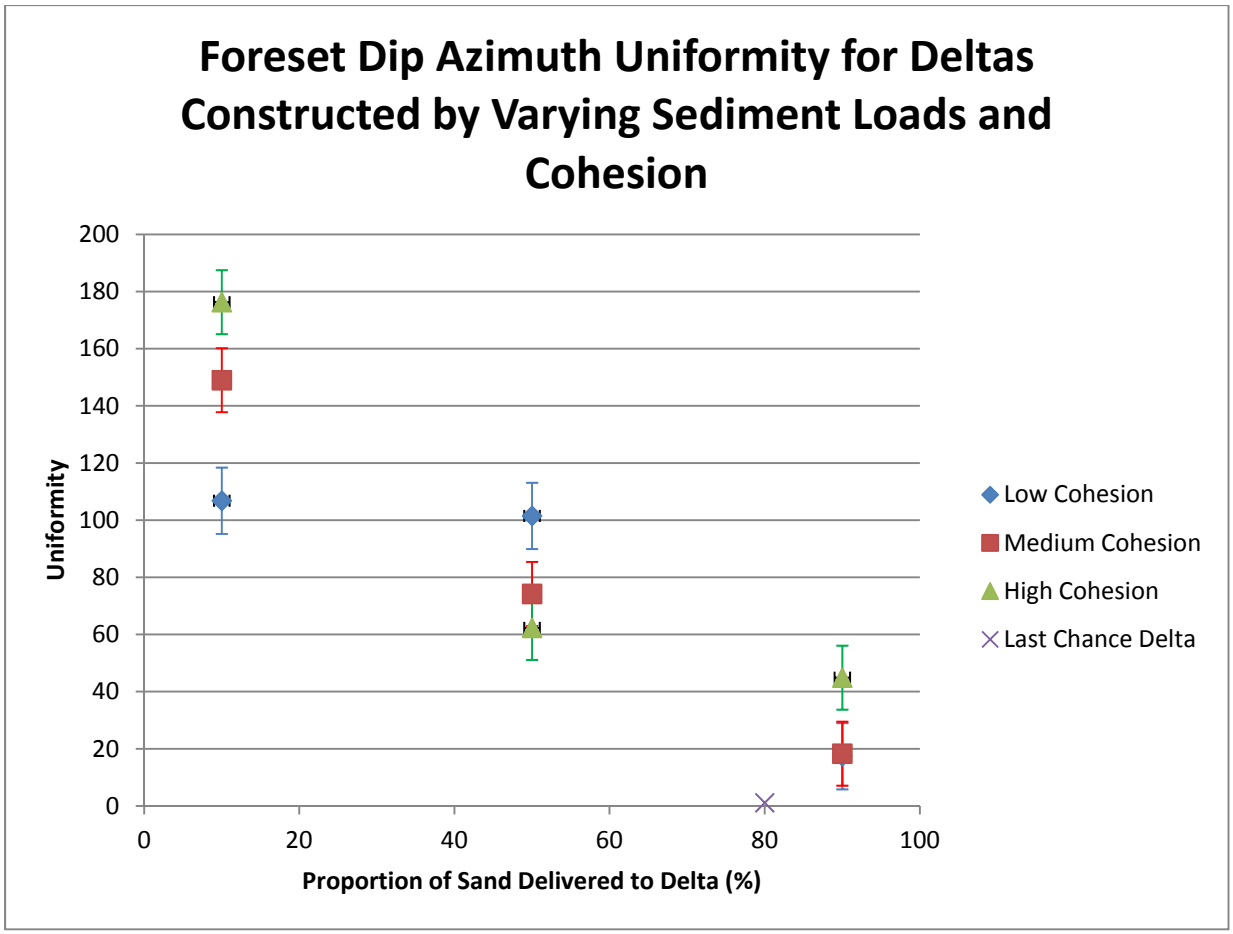

Figure 35. The Last Chance Delta foreset uniformity is 1.1 and plots near the sand-dominated foreset uniformity.

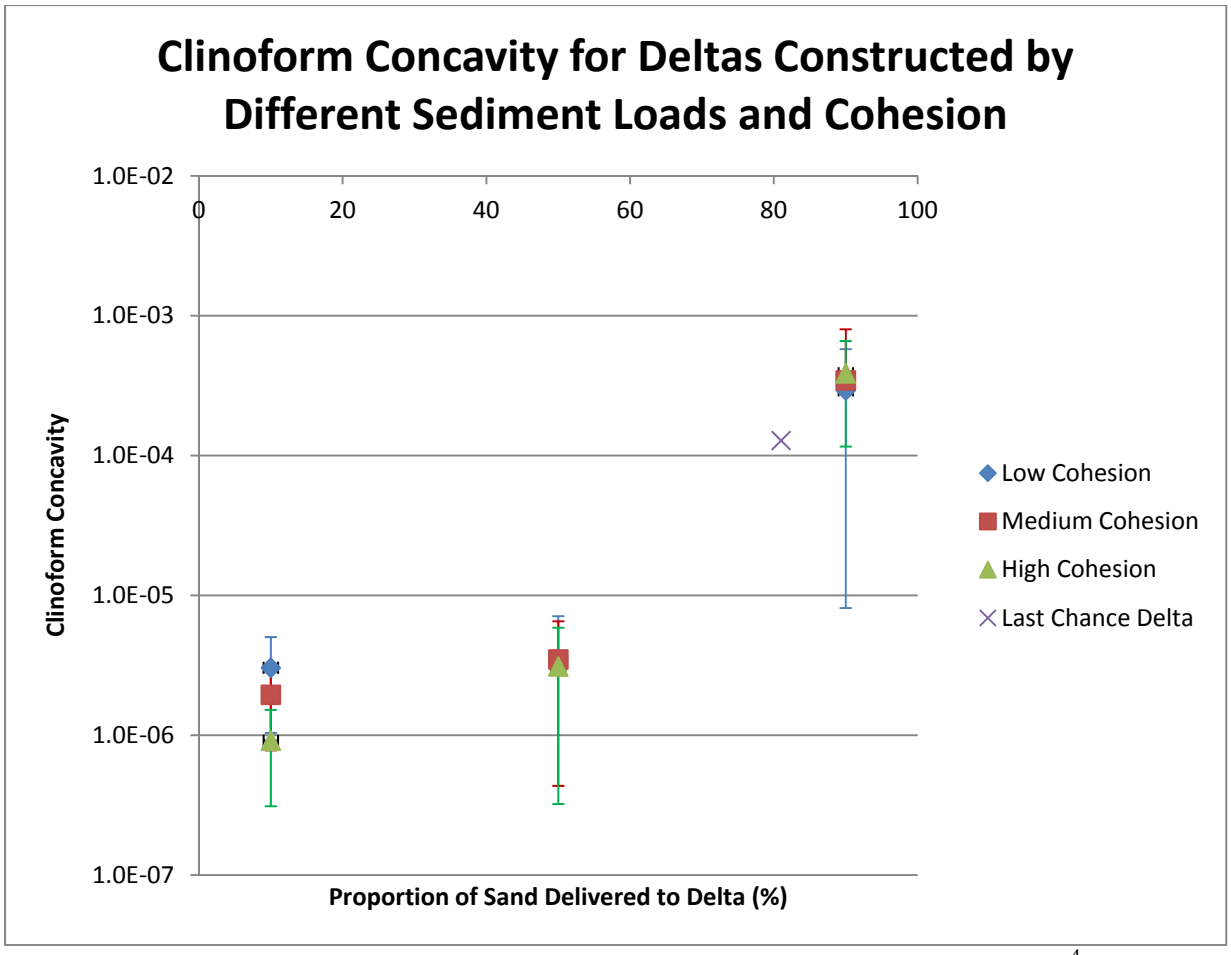

Figure 36. The Last Chance Delta has an average clinoform concavity of 1.3 x 10^{-4} and plots near the sand-dominated deltas.

unconformity are dominated by foreset facies where 88% of all deposits are of the foreset, whereas only 12% of deposits are channel facies (Fig. 37). The number of autogenic parasequences (Fig. 38) as interpreted by the Utah State Geological Survey in Kf-1 is 7 (Anderson et al., 2003).

Determining the Paleo-Morphology of the Last Chance Delta

We feel that our Delft3D model predications are readily applicable to the Last Chance Delta because grain size, proportion of sand delivered to the delta, and river discharge are comparable to values used to construct our numerical deltas (Anderson et al., 2003; Bhattacharya and Tye, 2004). Furthermore, Kf-1 represents the least wave influenced of the eight parasequence sets and tidal influence was negligible. Therefore we conjecture that the Last Chance Delta possessed topset distributary processes and morphologies similar to the sand-dominated delta type. The Last Chance Delta was most likely a fan-type delta with minor deviations from a uniform shoreline occurring concurrent with new mouth bar initiation. The delta probably was constructed by numerous distributaries with at least five orders of bifurcation. The topset was of intermediate roughness and contained small-scale interdistributary bays.

It may be argued that the Last Chance Delta can not be compared to our numerical deltas because they are topset dominated-deltas whereas the Last Chance Delta prograded into much deeper water. Even so, the Last Chance Delta has steep foresets and non-uniform foreset dip azimuths similar to the sand-dominated numerical deltas. Concavities measured from outcrops also plot on the sand-dominated end of the spectrum of the numerical models (Fig. 36). Cohesion does not systematically affect clinoform dip magnitude or concavity, so it is difficult to estimate a relative sediment cohesion for the Last Chance Delta from clinoform data. We do

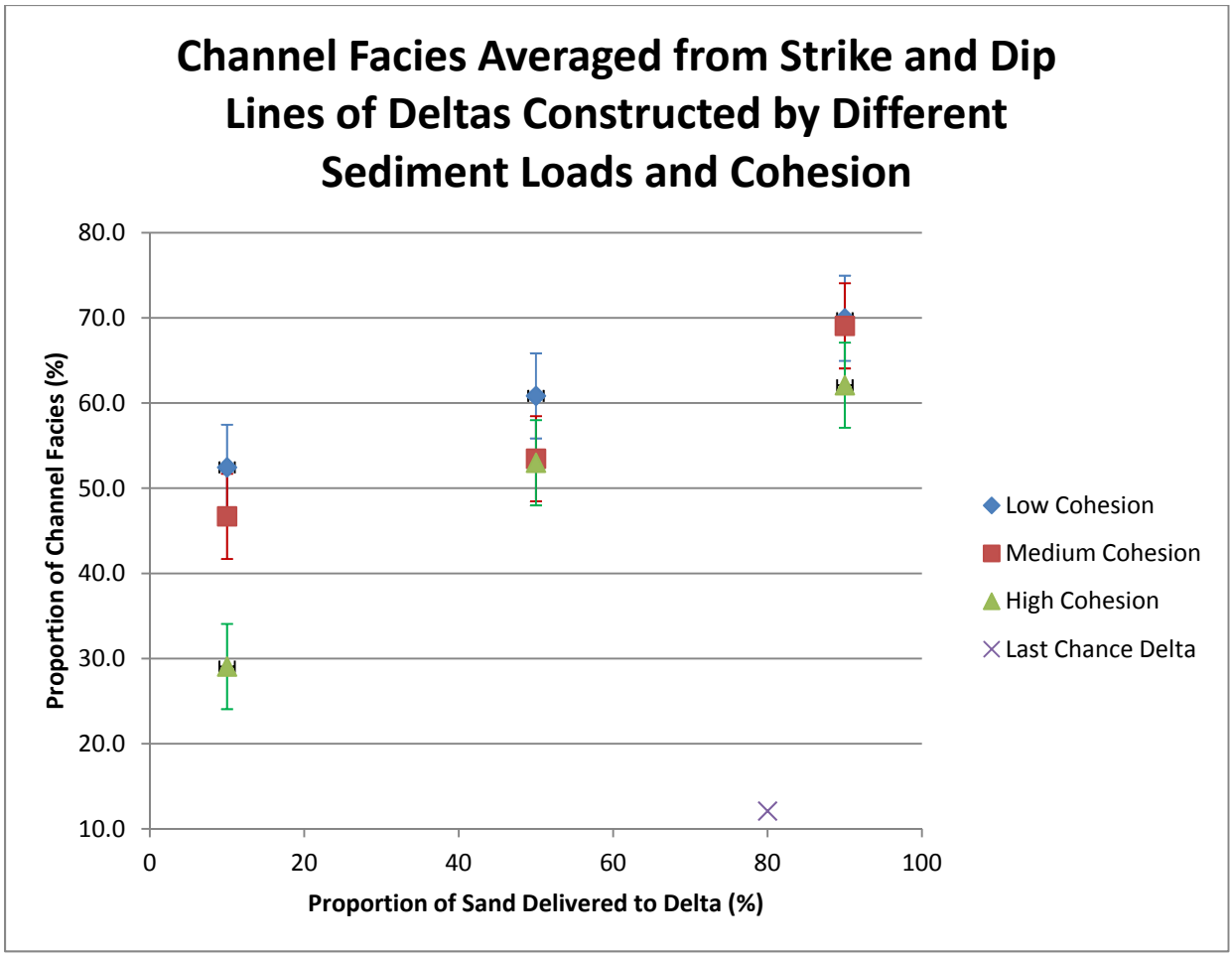

Figure 37. The Last Chance Delta stratigraphy is comprised of 12% channel facies. This does not plot near the values of any numerical deltas.

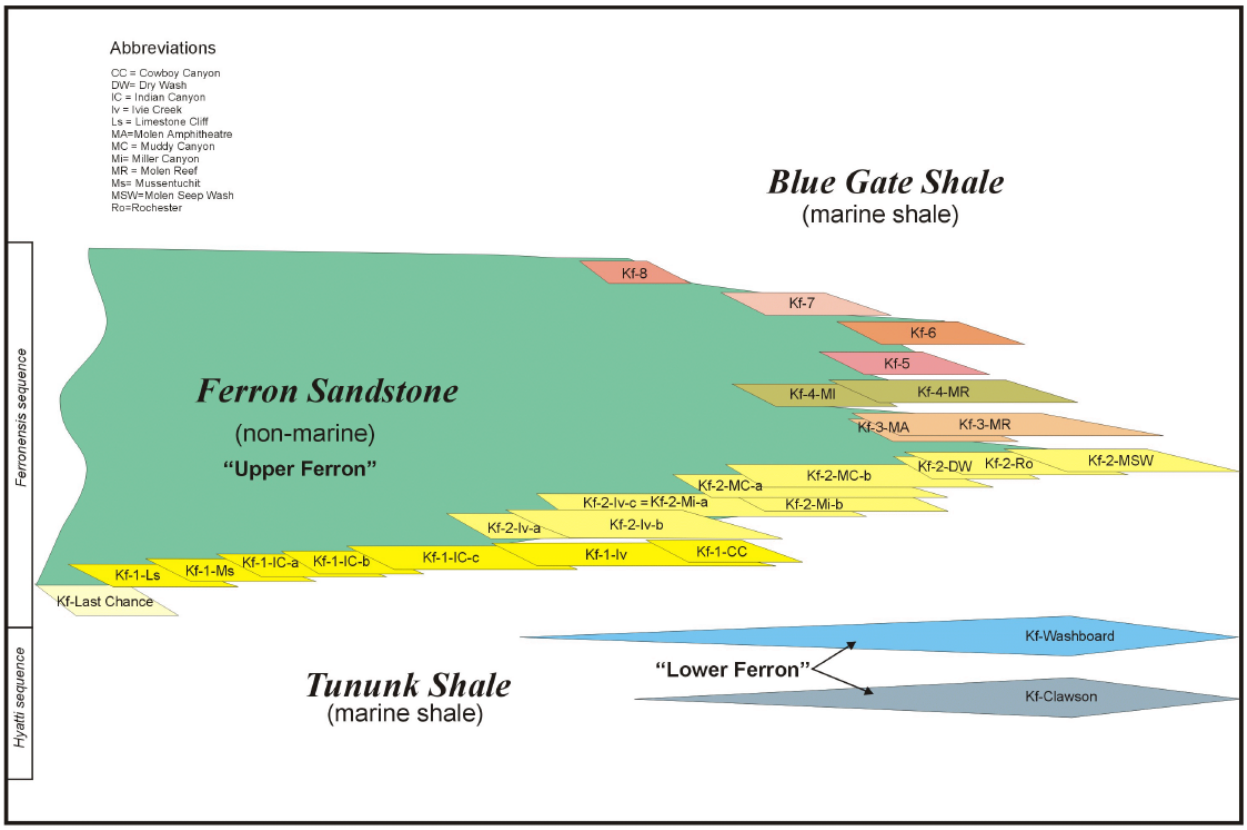

Figure 38. The first sand body deposited by the Last Chance Delta is Kf-Last Chance which is considered to be older than Kf-1. The first parasequence set (Kf-1) of the Last Chance Delta is comprised of 7 parasequences, starting with Kf-1-Ls and terminating with Kf-1-CC. Last Chance Delta deposition terminated with parasequence set Kf-8 (Anderson et al., 2003).

know that the delta formed in a humid, tropical to subtropical environment at paleolatitudes of 45-55^{o} N (Bhattacharya and MacEachern, 2009) and coal deposits are in excess of 1 m. These conditions are indicative of a highly vegetated topset that may have effectively increased its sediment cohesion.

To obtain our best estimate of the Last Chance Delta we simulated a delta with sediment of medium-cohesion, 80% sand, and the same parameters as the nine numerical deltas. Our findings are based on the assumption that the model basin geometry and depth are not appreciably different from the type of basin into which the Last Chance Delta prograded. The result (Fig. 39) is a low rugosity fan-delta with 12 distributaries and four orders of bifurcation. In modern deltas like the Atchafalaya and Wax lake Deltas, terminal distributaries are typically between 10 and 20 m in width and there is a strong correlation between number of active distributaries and orders of bifurcation (Overeem et al., 2003). Our grid resolution does not permit higher order bifurcations to occur because distributaries would be sub-grid scale, so it is reasonable to estimate one additional order of bifurcation and more distributaries than our model currently shows. Contrary to our estimate of high orders of bifurcation and numerous distributaries is the lack of preserved channel facies in the Last Chance Delta. We attribute the lack of preserved channel facies to erosion of the topset and conjecture that the Last Chance Delta was foreset-dominated because these types of deltas occur in deeper basins (Edmonds et al., 2011) and the Last Chance Delta likely prograded into a 12 m deep basin (Cotter, 1976).

Erosion of the topset has skewed the facies preservation towards the forest-dominated side of the spectrum. As the order of bifurcation increases, distributary channel depth decreases (Edmonds et al., 2011), and this makes high order distributaries more likely to have been eroded in the Last Chance Delta. Ravinement surfaces caused by transgressions commonly erode 5 – 10

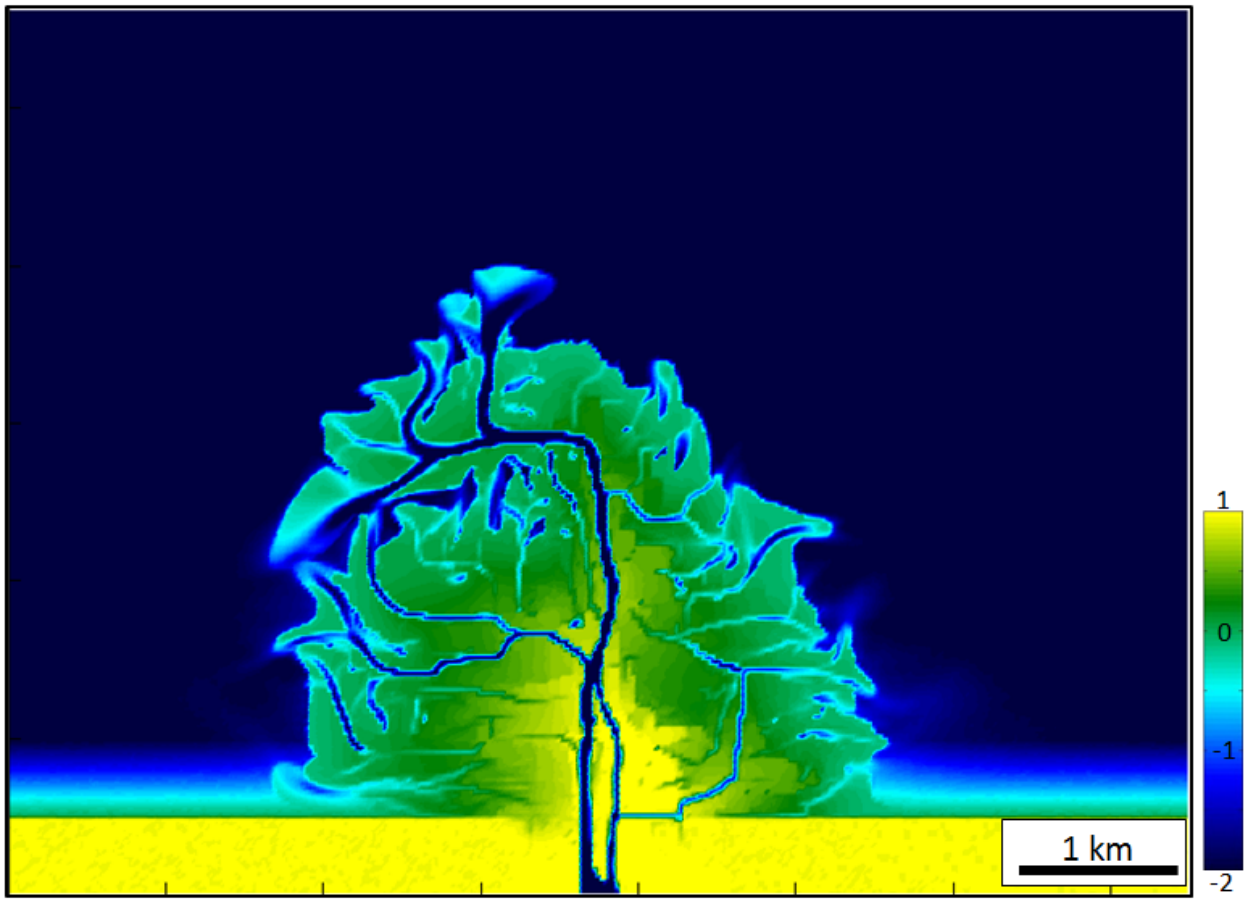

Figure 39. Model-predicted planform of the Last Chance Delta. Here we see a relatively uniform shoreline, numerous distributaries, and at least five orders of bifurcation.

m of topset sediments (Bhattacharya, 2006) and terminal distributaries are often less than 2 m deep (Olariu et al., 2006, Kroonenberg et al., 1997). Last Chance Delta distributaries that were unable to incise below the erosion threshold were not preserved. The two orders of bifurcations recognized by Bhattacharya and Tye (2004) and Anderson and Ryer (2004) likely represent only lower order, deeper channels. Possibly five or more orders of bifurcation may have existed, but they have been eroded due to their shallower depth of incision and subsequent erosion.

Earlier workers presented the idea that the first parasequence set of the Last Chance Delta developed an asymmetry due to wave-modification of the eastern portion of the delta (Anderson and Ryer, 2004) due to progradation beyond the protection of an embayment. In the Ivie Creek area (Fig. 40), our true dip azimuth calculations show Kf-1-Iv prograded generally north in the Scabby Canyon area and Kf-1-Iv[a] prograded generally west in the Ivie Creek area. Both do not show wave modification. From our true-dip azimuth calculations of Kf-1, we do not find any evidence of a parasequence prograding to the east. As Figure 38 illustrates, this may be because only the western half of the Last Chance Delta is preserved. Whether the embayment existed or not we are unable to interpret wave influence in the eastern portion of the delta. Our model predictions for the Last Chance Delta are consistent with Kf-1-Iv prograding to the north, Kf-1-Iv[a] prograding to the west, and the eastern portion of the delta having been eroded (Fig. 41).

DISCUSSION AND CONCLUSIONS

Re-classification of River-Dominated Deltas

Our first hypothesis was that a non-cohesive, sand-dominated delta will have more active distributaries, less rugose shoreline morphology, less topset complexity, and a foreset with smaller uniformity than a highly cohesive delta constructed by a mud-dominated sediment load. The results presented here do not serve to reject this hypothesis. While holding all other

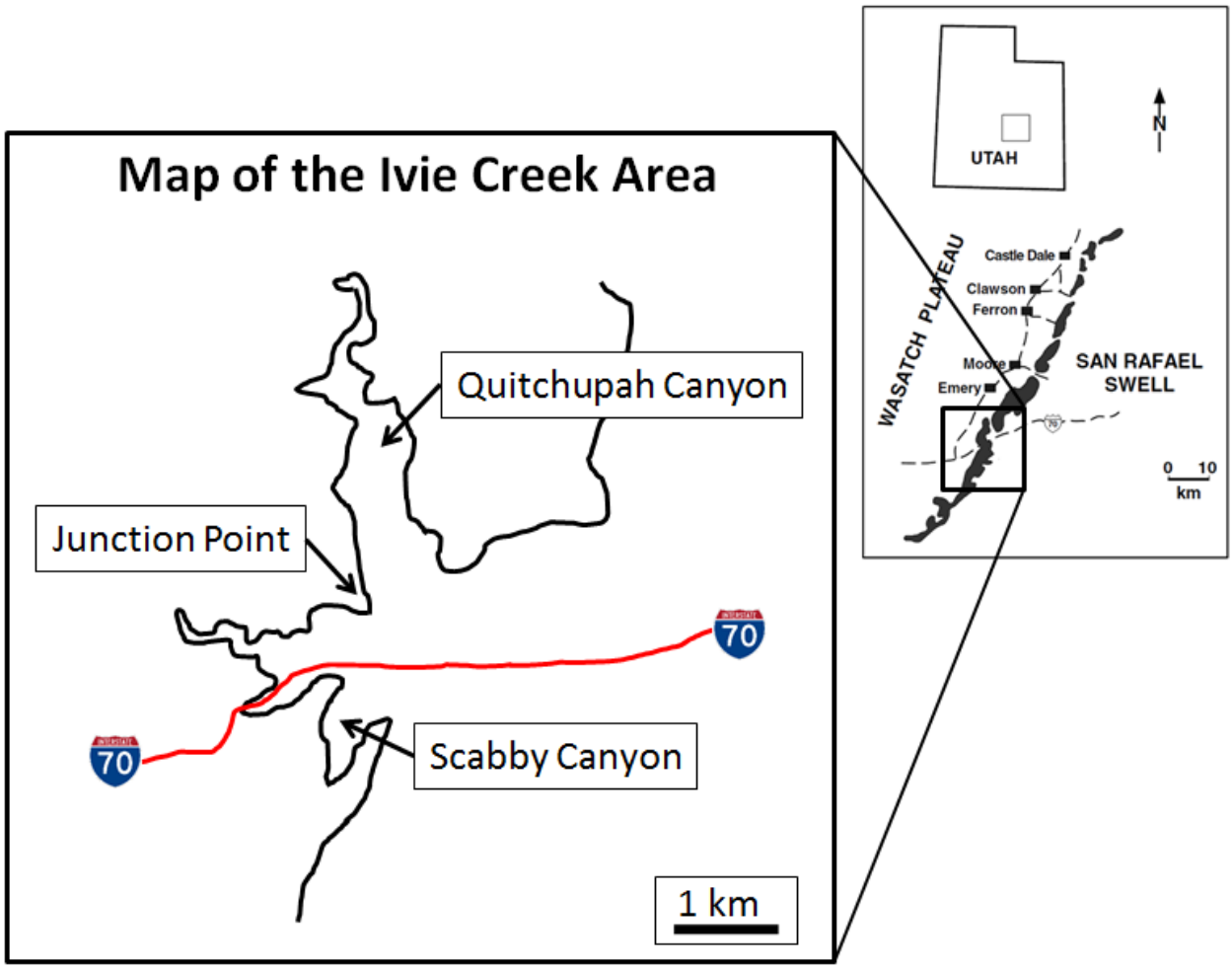

Figure 40. The Ivie Creek area consists of Quitchupah Canyon, Junction Point, and Scabby Canyon. The region is intersected by I-70. Outcrops of the Upper Ferron are indicated by the black lines (modified from Zeng et al, 2004).

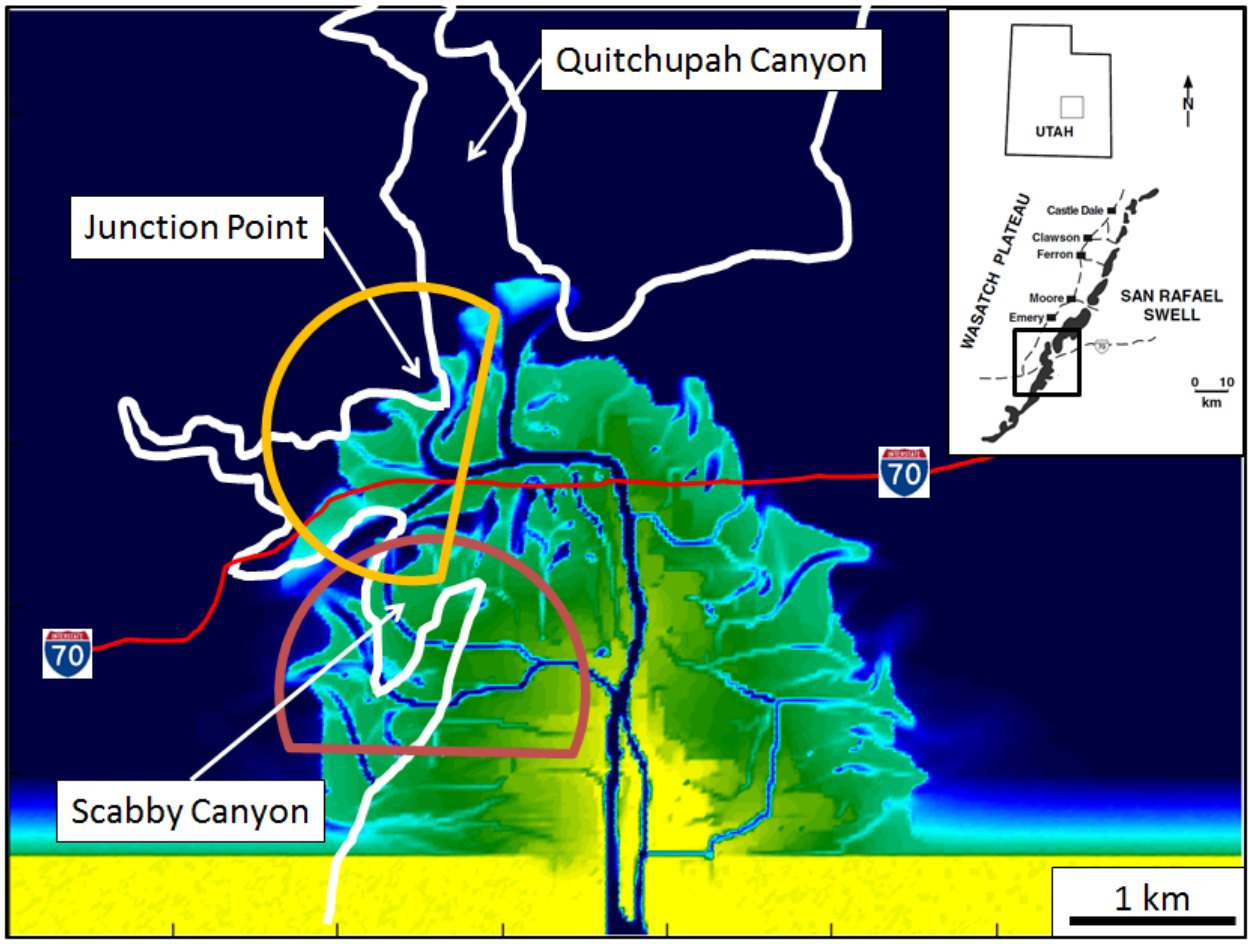

Figure 41. Numerically predicted planform of the Last Chance Delta with an overlay map of the Ivie Creek area consisting of outcrops of the Ferron Sandstone (white line), Interstate-70 (red line), parasequence Kf-1-Iv (maroon semi-circle), and parasequence Kf-1-Iv[a] (orange semi-circle). Model colors represent bed elevation points from low (blue) to high (yellow). Parasequence Kf-1-Iv[a] (orange semi-circle) progrades to the south in Scabby Canyon, almost due west at Junction Point, and northwest in the Quitchupah Canyon Area. Parasequence Kf-1-Iv progrades generally to the north in the Scabby Canyon Area and is onlapped by the younger Kf-1-Iv[a]. Scale bar is 1 km for both the numerical model and the outcrop belt. The numerical model builds lobes of similar scale and sequence.

variables constant and varying the proportion of sand and the sediment cohesion delivered to a numerical delta, we conclude that variations in the fluvial catchment control the distributary abundance, shoreline rugosity, topset roughness, and foreset uniformity. These in turn control sediment deposition and impact the stratigraphy of the delta through its clinoform dip magnitude, clinoform concavity, proportion of channel and foreset facies, number of parasequences, and reservoir rugosity.

Our second hypothesis was that a relatively non-cohesive delta constructed by a sand-dominated sediment load will have greater clinoform dip magnitudes, greater clinoform concavity, more channel facies, more autogenic parasequences, and better reservoir quality sand bodies than a highly cohesive delta constructed by a mud-dominated sediment load. This also cannot be rejected. Given these strong relationships, it is instinctive to re-classify river-dominated deltas based on their relative sand proportion and topset and stratigraphic attributes. Shoreline rugosity, number of distributaries, and foreset uniformity all show increasing or decreasing behavior proportional to the proportion of sand delivered to the delta (Fig. 42). Topset roughness is not included because it does not increase proportionally with sand proportion; it is more a function of sediment cohesion. Clinoform dip magnitude, clinoform concavity, and proportion of channel facies are used to classify river-dominated delta stratigraphy because they increase or decrease proportionally with sand proportion (Fig. 43). Number of parasequences is not used in this classification because the relationship with sand proportion behaves less reliably.

These two classification systems are particularly useful for lacustrine deltas having similar basin geometries. Lacustrine systems are not subject to tides, and in areas with minimal

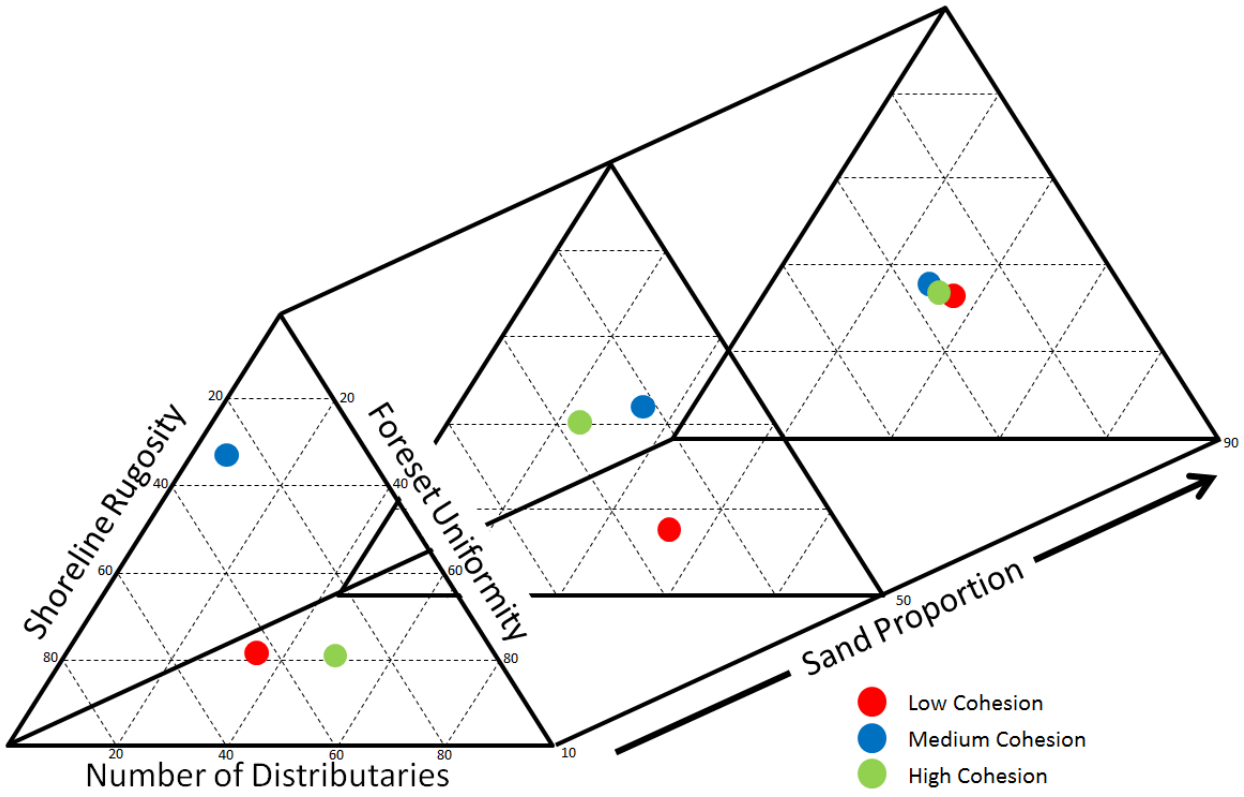

Figure 42. River-dominated delta topsets can be classified based on their sand proportion, number of active distributaries, shoreline rugosity, and foreset uniformity. Here, the nine numerical deltas are plotted. The values of each variable are non-dimensionalized and scaled to such that the minimum and maximum values of each variable respectively represent 10% and 90% of the range.

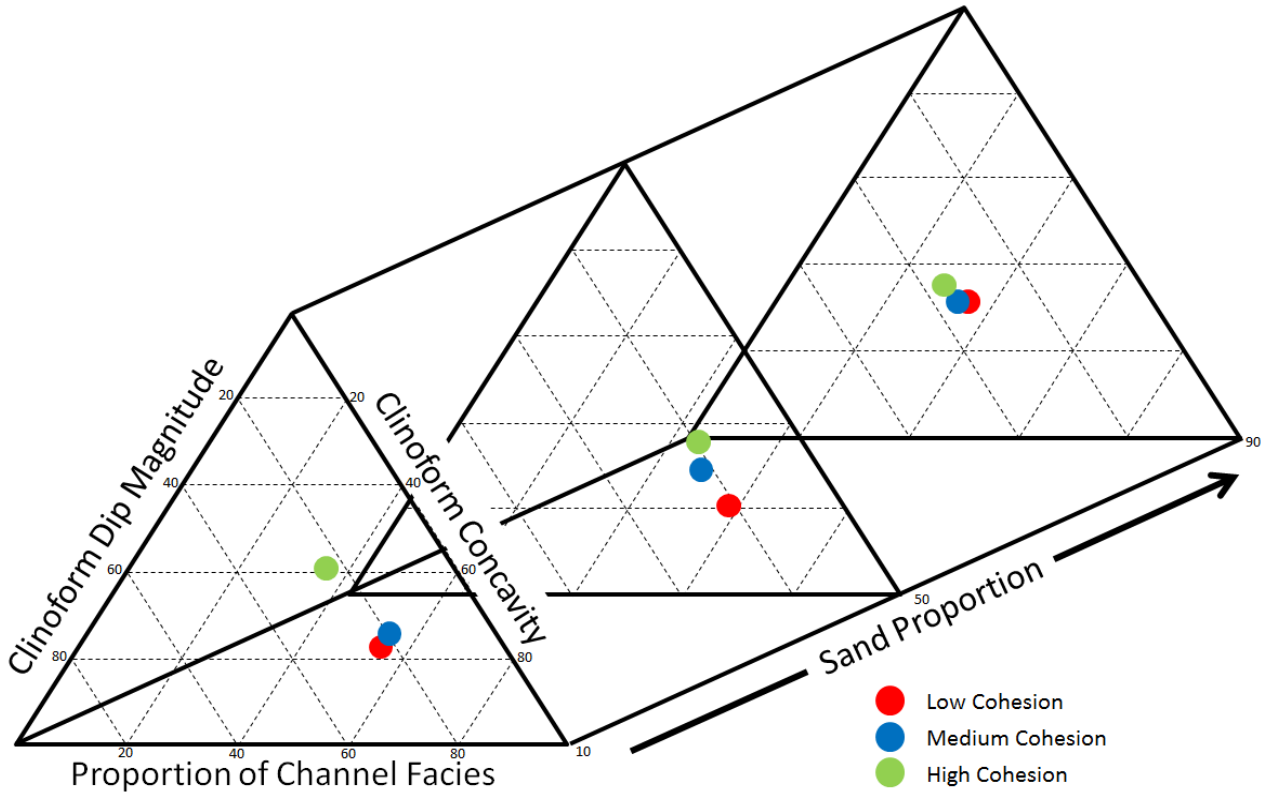

Figure 43. River-dominated delta stratigraphy can be classified based on their sand proportion, clinoform dip magnitude, clinoform concavity, and proportion of channel facies. Here, the nine numerical deltas are plotted. The values of each variable are non-dimensionalized and scaled to such that the minimum and maximum values of each variable respectively represent 10% and 90% of the range.

wave influence and consistent basin geometries, we believe that sediment properties will almost certainly be the first order control on delta topsets and stratigraphy, permitting application of these classification systems. The novelty of these classification systems is that they quantitatively link delta planform with delta stratigraphy and they can be used a) to predict delta morphology from the fluvial catchment, b) to predict the stratigraphy of modern deltas, and c) to interpret paleomorphology from stratigraphy. In this study, we have demonstrated the application of this predictive model to the Cretaceous Last Chance Delta; application of this predictive model to other ancient systems will allow consistent and realistic paleo-interpretations.

REFERENCES

Anderson, P.B., McClure, K., Chidsey Jr., T.C., Ryer, T.A., Morris, T.H., Dewey Jr., J.A., Adams, R.D. (2003). "Interpreted regional photomosaics and cross-section, Cretaceous Ferron sandstone, east-central Utah." Utah Geological Survey, Open File Report 412.

Anderson, P.B. and Ryer, T.A. (2004). "Regional stratigraphy of the Ferron Sandstone." AAPG Studies in Geology, 50, 211 – 226.

Barton, M. D. (1994). "Outcrop Characterization of Architecture and Permeability Structure in Fluvial-Deltaic Sandstones, Cretaceous Ferron Sandstone, Utah." Dissertation, University of Texas at Austin, Austin, TX, United States (USA), 277.

Barton, M. D. (1997). "Application of cretaceous interior seaway outcrop investigations to fluvial-deltaic reservoir characterization; part I, predicting reservoir heterogeneity in delta front sandstones, Ferron gas field, central Utah." Papers Presented at the Gulf Coast Section, Society of Economic Paleontologists and Mineralogists Foundation Annual Bob F. Perkins Research Conference, 18, 33-40.

Bhattacharya, J.P., (2006). "Deltas." In: Walker, R.G., and Posamentier, H., (eds.) "Facies Models Revisited." SEPM Special Publication, v. 84, 237-292.

Bhattacharya, J.P., and Davies, R.K. (2004). "Sedimentology and structure of growth faults at the base of the Ferron Member along Muddy Creek, Utah." *in* Chidsey, T.C., Adams, R.D., and Morris, T.H., eds., "Regional to Wellbore Analog for Fluvial-Deltaic Reservoir Modeling: the Ferron Sandstone of Utah." American Association of Petroleum Geologists, Studies in Geology, no. 50, 279 – 304.

Bhattacharya, J.P., and MacEachern, J.A. (2009). "Hyperpycnal rivers and prodeltaic shelves in the Cretaceous Seaway of North America." Journal of Sedimentary Research, v. 79, 184 – 209.

Bhattacharya, J. P., & Tye, R. S. (2004). "Searching for modern Ferron analogs and application to subsurface interpretation." AAPG Studies in Geology, 50, 39 – 57.

Bhattacharya, J.P, and Walker, R.G. (1991b). "Facies and facies successions in river- and wave-dominated depositional systems of the Upper Cretaceous Dunvegan Formation, northwestern Alberta." Bulletin of Canadian Petroleum Geology, v. 39, 165–191.

Coleman, J.M., and Prior, D.B. (1982). "Deltaic environments." *in* Scholle, P.A., and Spearing, D.R., eds., "Sandstone Depositional Environments." American Association of Petroleum Geologists, Memoir 31, 139 – 178.

Coleman, J.M., and Wright, L.D. (1975). "Modern river deltas: variability of processes and sand bodies." *in* Broussard, M.L., ed., "Deltas, Models for Exploration: Houston." Houston Geological Society, 99–149.

Corbeanu, R. M., Soegaard, K., Szerbiak, R. B., Thurmond, J. B., McMechan, G. A., Wang, D., Menitove, A. (2001). "Detailed internal architecture of a fluvial channel sandstone determined from outcrop, cores, and 3-D ground-penetrating radar; example from the middle cretaceous Ferron sandstone, east-central Utah." AAPG Bulletin, 85(9), 1583-1608.

Cotter, E. (1976). "The role of deltas in the evolution of the Ferron Sandstone and its coals." Brigham Young University, Geology Studies, v. 22, part 3, 15-41.

Driscoll, N.W., Karner, G.D., (1999). "Three-dimensional quantitative modeling of clinoform development." Mar. Geol. 154 (1–4), 383–398.

Edmonds, D. A., Shaw, J. B., & Mohrig, D. (2011). "Topset-dominated deltas: A new model for river delta stratigraphy." Geology, 39(12), 1175-1178.

Edmonds, D.A. and Slingerland, R.L (2010). "Significant effect of sediment cohesion on delta morphology." Nature Geoscience 3(2), 105-109.

Enge, H. D., & Howell, J. A. (2010). "Impact of deltaic clinothems on reservoir performance; dynamic studies of reservoir analogs from the Ferron sandstone member and panther tongue, Utah." AAPG Bulletin, 94(2), 139-161.

Fielding, C.R., Trueman, J., and Alexander, J. (2005a). "Sedimentology of the modern and Holocene Burdekin River delta of North Queensland, Australia—Controlled by river output, not by waves and tides." *in* Giosan, L., and Bhattacharya, J.P., eds., "River Deltas—Concepts, Models, and Examples." SEPM, Special Publication 83, 467–496.

Fielding, C.R., Trueman, J., and Alexander, J. (2005b). "Sharp-based mouth bar sands from the Burdekin River Delta of northeastern Australia: extending the spectrum of mouth bar facies, geometry, and stacking patterns." Journal of Sedimentary Research, v. 75, 55–66.

Fitzhugh, W.W. (1972). "Environmental archeology and cultural systems in Hamilton Inlet, Labrador." Smithsonian Contributions to Anthropology, 16. 99 pp.

Galloway, W. E. (1975). "Process framework for describing the morphologic and stratigraphic evolution of deltaic depositional systems. Deltas: Models for Exploration." M. L. Broussard. Houston, TX, Houston Geological Society**:** 87-98.

Gani, M.H., and Bhattacharya, J.P. (2005). "Bedding correlation vs. facies correlation in deltas: lessons for Quaternary stratigraphy." *in* Giosan, L., and Bhattacharya, J.P., eds., "River Deltas—Concepts, Models, and Examples." SEPM, Special Publication 83, 31- 47.

Gardner, M.H. (1992). "Sequence stratigraphy of the Ferron Sandstone (Turonian) of east-central Utah." Ph.D. Dissertation, Colorado School of Mines, Golden, 406 p.

Gardner, M.H. (1995b). "The stratigraphic hierarchy and tectonic history of the mid-Cretaceous foreland basin of central Utah." in Dorobek, S.L., and Ross, G.M., eds., "Stratigraphic Evolution of Foreland Basins." SEPM, Special Publication 52, 283–303.

Gardner, M. H., Willis, B. J., & Barton, M. D. (1995a). "Accommodation controls on fluvial-deltaic reservoir architecture." AAPG Bulletin, 79(8), 1213-1213.
Garrison, James R.,, Jr., van den Bergh, ,T.C.V., Barker, C. E., & Tabet, D. E. (1997). "Depositional sequence stratigraphy and architecture of the cretaceous Ferron sandstone; implications for coal and coalbed methane resources; a field excursion." Geology Studies, 42, Part 2, 155-202.

Giosan, L., Donnelly, J.P., Vespremeanu, E.I., and Buonaiuto, F.S., 2005, River delta morphodynamics: Examples from the Danube delta, in Giosan, L., and Bhattacharya, J.P., eds., River deltas—Concepts, models, and examples: SEPM (Society for Sedimentary Geology) Special Publication 83, p. 87–132.

Hale, L.A., and Van DeGraff, R.F. (1964). "Cretaceous stratigraphy and facies patterns – northeastern Utah and adjacent areas." Intermountain Association of Petroleum Geologists, 13th Annual Field Conference Guidebook, 115 – 138.

Jones, T.A. (2006). "MATLAB functions to analyze directional (azimuthal) data – I: Single-sample inference." Computers & Geosciences 36: 520-525.

Katich, P.J., Jr. (1953). "Source direction of Ferron Sandstone in Utah." American Association of Petroleum Geologists Bulletin, v. 83, 1649-1670.

Knox, P. R. (1997). "Application of outcrop analogs to fluvial-deltaic reservoirs II; example from Gulf of Mexico reservoirs, Frio Formation, south Texas." Papers Presented at the Gulf Coast Section, Society of Economic Paleontologists and Mineralogists Foundation Annual Bob F. Perkins Research Conference, 18, 127-138.

Knox, P. R., & Barton, M. D. (1999). "Predicting interwell heterogeneity in fluvial-deltaic reservoirs; effects of progressive architecture variation through a depositional cycle from outcrop and subsurface observations." AAPG Memoir, 71, 57-72.

Kostic, S. and Parker, G. (2003a). "Submitted Progradational sand-mud deltas in lakes and reservoirs Part 1. Theory and numerical modeling." Journal of Hydraulic Research, 41(2).

Kostic, S. and Parker, G. (2003b). "Submitted Progradational sand-mud deltas in lakes and reservoirs Part 2. Experiment and numerical simulation." Journal of Hydraulic Research, 41(2).

Kroonenberg, S.B. Ruskakov, G.V., and Svitoch, A.A, (1997). "The wandering of the Volga Delta: a response to rapid Caspian sea-level change." Sedimentary Geology, v. 107, 189-209.

Kuehl, S. A., Nittrouer, C. A., and DeMaster, D. J. (1986). "Nature of sediment accumulation on the Amazon continental shelf." Cont. Shelf Res., v. 6, 209 – 225.

Lambiase, J.J., Damit, A.R., Simmons M.D., Abdoerrias, R., and Hussin, A. (2003). "A depositional model and the stratigraphic development of modern and ancient tide dominated deltas in NW Borneo." *in* Sidi, F.H., Nummedal, D., Imbert, P., Darman, H., and Posamentier, H.W., eds., "Tropical Deltas of Southeast Asia—Sedimentology, Stratigraphy, and Petroleum Geology." SEPM, Special Publication 76, 109–123.

"Lake Melville, NL, Canada." Map. *Google Maps.* Google, 7 June, 2003. Web. 10 October, 2012.

Lesser, G., Roelvink, J., Van Kester, J., & Stelling, G. (2004). "Development and validation of a three-dimensional morphological model." Coast. Eng. 51, 883-915.

Lowry, P., & Jacobsen, T. (1993). "Sedimentological and reservoir characteristics of a fluvial-dominated delta-front sequence; Ferron sandstone member (Turonian), east-central Utah, USA." Geological Society Special Publications, 69, 81-103.

McMechan, G. A., Gaynor, G. C., & Szerbiak, R. B. (1997). "Use of ground-penetrating radar for 3-D sedimentological characterization of clastic reservoir analogs." Geophysics, 62(3), 786-796.

McPherson, J.G., Shanmugan, G., and Moiola, R.J., (1987). "Fan deltas and braid deltas: Varieties of coarse-grained deltas." Geological Society of America Bulletin, v. 99, 331-340.

Mitchum, R.M., Vail, P.R., and Sangree, J.B., (1977). "Seismic stratigraphy and global changes of sea level, Part 6: Stratigraphic interpretation of seismic reflection patterns in depositional sequences." *in* "Seismic stratigraphy—Application to hydrocarbon exploration." American Association of Petroleum Geologists Memoir 26, 117-133.

Moiola, R. J., Welton, J. E., Wagner, J. B., Fearn, L. B., Farrell, M. E., Enrico, R. J., & Echols, R. J. (2004). "Integrated analysis of the upper Ferron deltaic complex, southern castle valley, Utah." AAPG Studies in Geology, 50, 79-91.

Niedoroda, A.W., Reed, C.W., Das, H., Fagherazzi, S., Donoghue, J.F., and Cattaneo, A. (2005). "Analyses of a large-scale depositional clinoformal wedge along the Italian Adriatic coast." Marine Geology, v. 222 – 223, 179 – 192.

Nittrouer, C.A., Curtin, T.B., DeMaster, D.J., (1986). "Concentration and flux of suspended sediment on the Amazon continental shelf." Cont. Shelf Res. 6 (1–2), 151–174.

Nittrouer, C.A., Kuehl, S.A., Sternberg, R.W., Figueiredo, A.G., Faria. L.E.C., (1995). "An introduction to the geological significance of sediment transport and accumulation on the Amazon continental shelf." Mar. Geol. 125, 177 – 192.

Novakovic, D., White, C. D., Corbeanu, R. M., Hammon, William S., I.,II, Bhattacharya, J. P., & McMechan, G. A. (2002). "Hydraulic effects of shales in fluvial-deltaic deposits; ground-penetrating radar, outcrop observations, geostatistics, and three-dimensional flow modeling for the Ferron Sandstone, Utah." Mathematical Geology, 34(7), 857-893.

Olariu, C., and Bhattacharya, J.P. (2006). "Terminal distributary channels and delta front architecture of river-dominated delta systems." Journal of Sedimentary Research, v. 76, no. 2, 212 – 233.

Orton, G. J. and H. G. Reading (1993). "Variability of deltaic processes in terms of sediment supply, with particular emphasis on grain size." Sedimentology 40: 475-512.

Overeem, I., Kroonenberg, S.B., Veldkamp, A., Groenensteijn, K., Rusakov, G.V., and Svitoch, A.A. (2003). "Small-scale stratigraphy in a large ramp delta: recent and Holocene sedimentation in the Volga delta, Caspian Sea." Sedimentary Geology, v. 159, 133-157.

Overeem, I., and Syvitski, J.P.M. (2010). "Experimental exploration of the stratigraphy of fjords fed by glaciofluvial systems." Geological Society, London, Special Publications, v. 344, 125 – 142.

Paola, C., Mullin, J., Ellis, C., Mohrig, D. C. Swenson, J. B. Parker, G. Hickson, T. Heller, P. L. Pratson, L. Syvitski, J. Sheets, B. and Strong, N. (2001). "Experimental stratigraphy." GSA Today, v. 11, 4 – 9.

Postma, G. (1990). "Depositional architecture and facies of river and fan deltas: a synthesis." Special Publications International Association of Sedimentologists 10: 13-27.

Pratson, L.F., Swenson, J., Kettner, A.J., Fedele, J.J., Postma, G., Niedoroda, A.W., Friedrichs, C.T., Syvitski, J.P.M., Paola, C., Steckler, M.S., Hutton, E.W.H., (2004). "Modeling continental shelf formation in the Adriatic Sea and elsewhere." Oceanography 17 (4), 118–131.

Rodriguez, A.B., Hamilton, M.D., and Anderson, J.B. (2000). "Facies and evolution of the modern Brazos Delta, Texas: wave versus flood influence." Journal of Sedimentary Research, v. 70, 283–295.

Ryer, T. A. (1981). "Deltaic coals of Ferron sandstone member of Mancos shale; predictive model for cretaceous coal-bearing strata of western interior." AAPG Bulletin, 65(11), 2323-2340.

Ryer, T. A., & Anderson, P. B. (2004). "Facies of the Ferron sandstone, east-central Utah." AAPG Studies in Geology, 50, 59-78.

Sampson, G.J., Howell, J.A., Flint, S.S. (1999). "A sedimentological and sequence stratigraphic reinterpretation of the Upper Cretaceous Prairie Canyon Member ('Mancos B') and associated strata, Book Cliffs area, Utah, USA." Journal of Sedimentary Research; v. 69, no. 2, 414-433.

Shaw, J.B., Wolinsky, M.A., Paola, C. and Voller, V.R. (2008). "An image-based method for shoreline mapping on complex coasts." Geophys. Res. Lett., 35, L12405.

Syvitski, J. P. M. (2006). "The morphodynamics of deltas and their distributary channels." River, Coastal, and Estuarine Morphodynamics: RCEM 2005, Urbana, Illinois, USA, Taylor & Francis.

Syvitski, J. P. M. (2008). "Deltas at risk." Sustainable Science, v. 3, 23 – 32.

Syvitski, J.P.M. and Lee, H.J. (1997). "Postglacial sequence stratigraphy of Lake Melville, Labrador." Marine Geology 143, 55 – 79.

Syvitski, J. P. M. & Saito, Y. (2007) "Morphodynamics of deltas under the influence of humans." Glob. Planet. Change 57, 261–282.

Taylor, D.M. and Batterson, M.J. (2001). "Carbon-14 date list for Newfoundland and Labrador." Newfoundland Department of Mines and Energy, Geological Survey, Open File NFLD/2190, version 2.

Thompson, S.L., Ossian, C.R., and Scott, A.J. (1986). "Lithofacies, inferred processes, and log response characteristics of shelf and shoreface sandstones, Ferron Sandstone, central Utah." *in* T.F. Moslow and E.G. Rhodes, eds., "Modern and ancient shelf clastics – a core workshop." S.E.P.M. Core Workshop, Vol. 9, 325 – 361.

Vilks, G., Deonarine, B., and Winters, G. (1987). "Late Quaternary marine geology of Lake Melville, Labrador." Geol. Surv. Can. Pap. 87 – 22, 50 pp.

Vilks, G. and Mudie P.J. (1983). "Evidence for postglacial paleoceanographic and paleoclimatic changes in Lake Melville, Labrador, Canada." Arctic and Alpine Research, Vol. 15, No. 3, 307 – 320.

Wardle, R.J., Gower, C.F., Ryan, B., Ninn, G.A.G., James, D.T., and Kerr, A. (1997). "Geological Map of Labrador; 1:1 million scale." Government of Newfoundland and Labrador, Department of Mines and Energy, Geological Survey, Map 97-07.

Zeng, X., McMechan, G.A., Bhattacharya, J.P., Aiken, C.L.V., Xu, X., Hammon III, W.S., and Corbeanu, R.M. (2004). "3D imaging of a reservoir analogue in point bar deposits in the Ferron Sandstone, Utah, using ground-penetrating radar." Geophysical Prospecting, 52, 151 – 163.

APPENDIX A

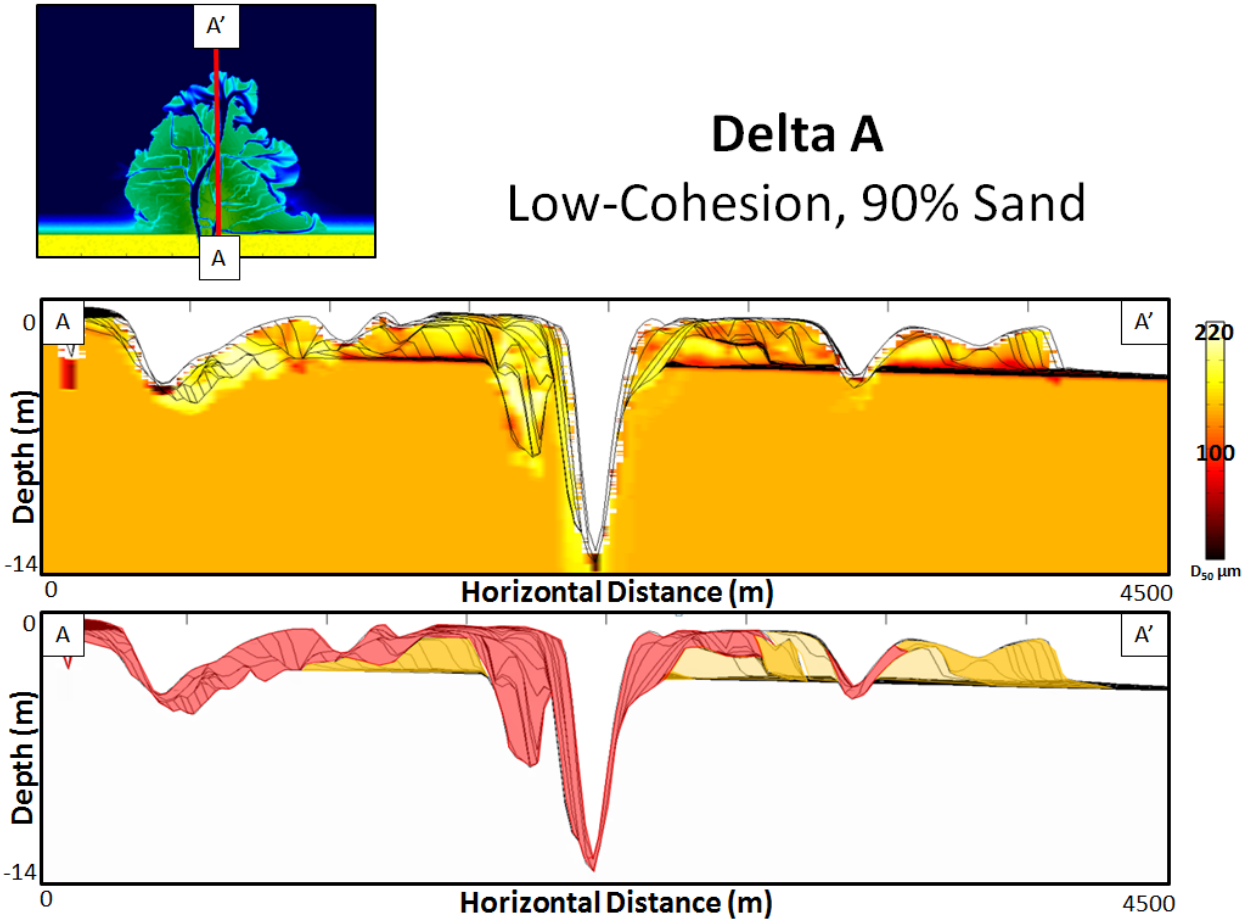
A'
A
Delta A
Low-Cohesion, 90% Sand
A
A'
0
Depth (m)
-14
0
Horizontal Distance (m)
4500
220
100
D50 µm
A
A'
0
Depth (m)
-14
0
Horizontal Distance (m)
4500

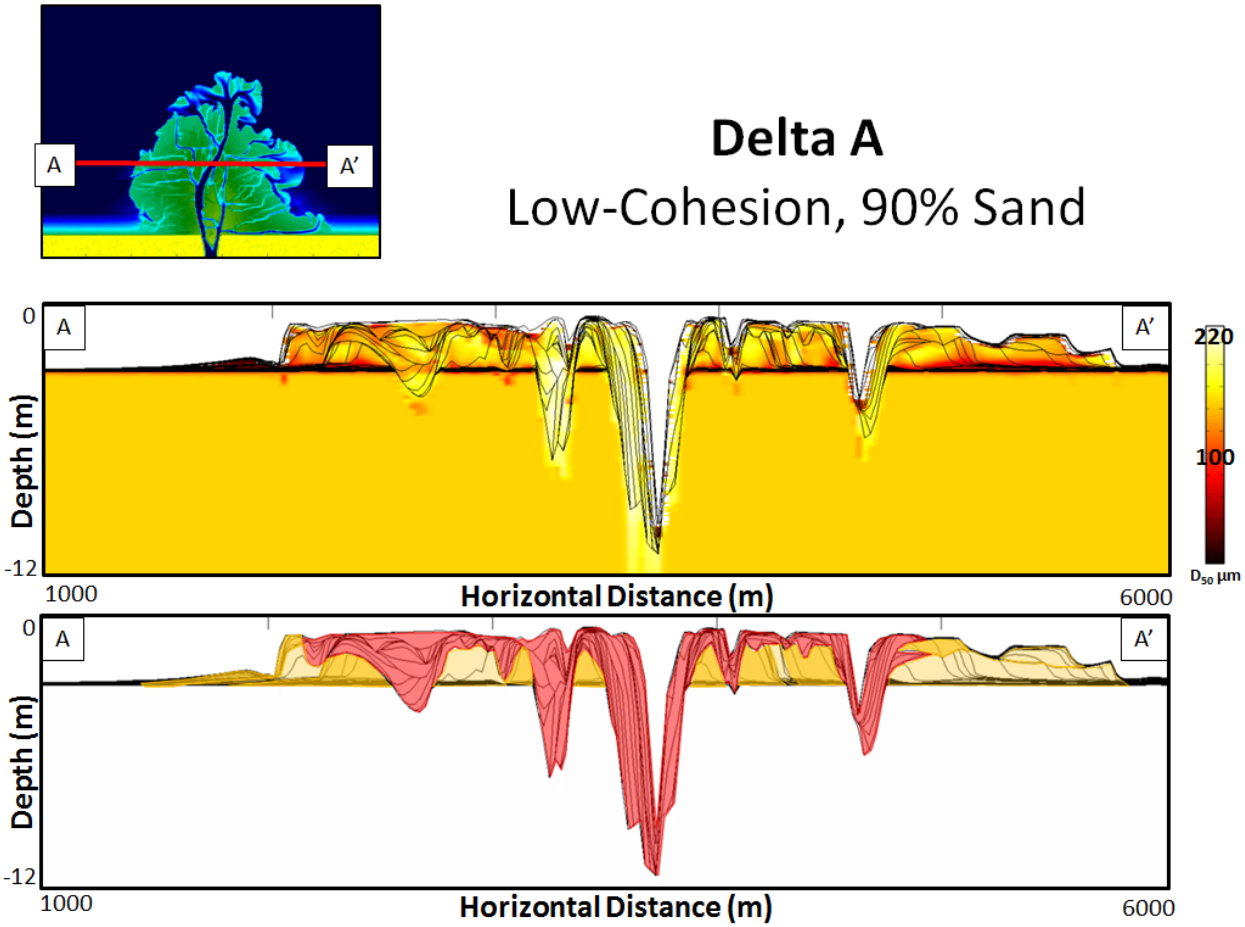
A
A'
Delta A
Low-Cohesion, 90% Sand
0
-12
Depth (m)
A
A'
1000
Horizontal Distance (m)
6000
220
100
D50 µm
0
-12
Depth (m)
A
A'
1000
Horizontal Distance (m)
6000

APPENDIX B

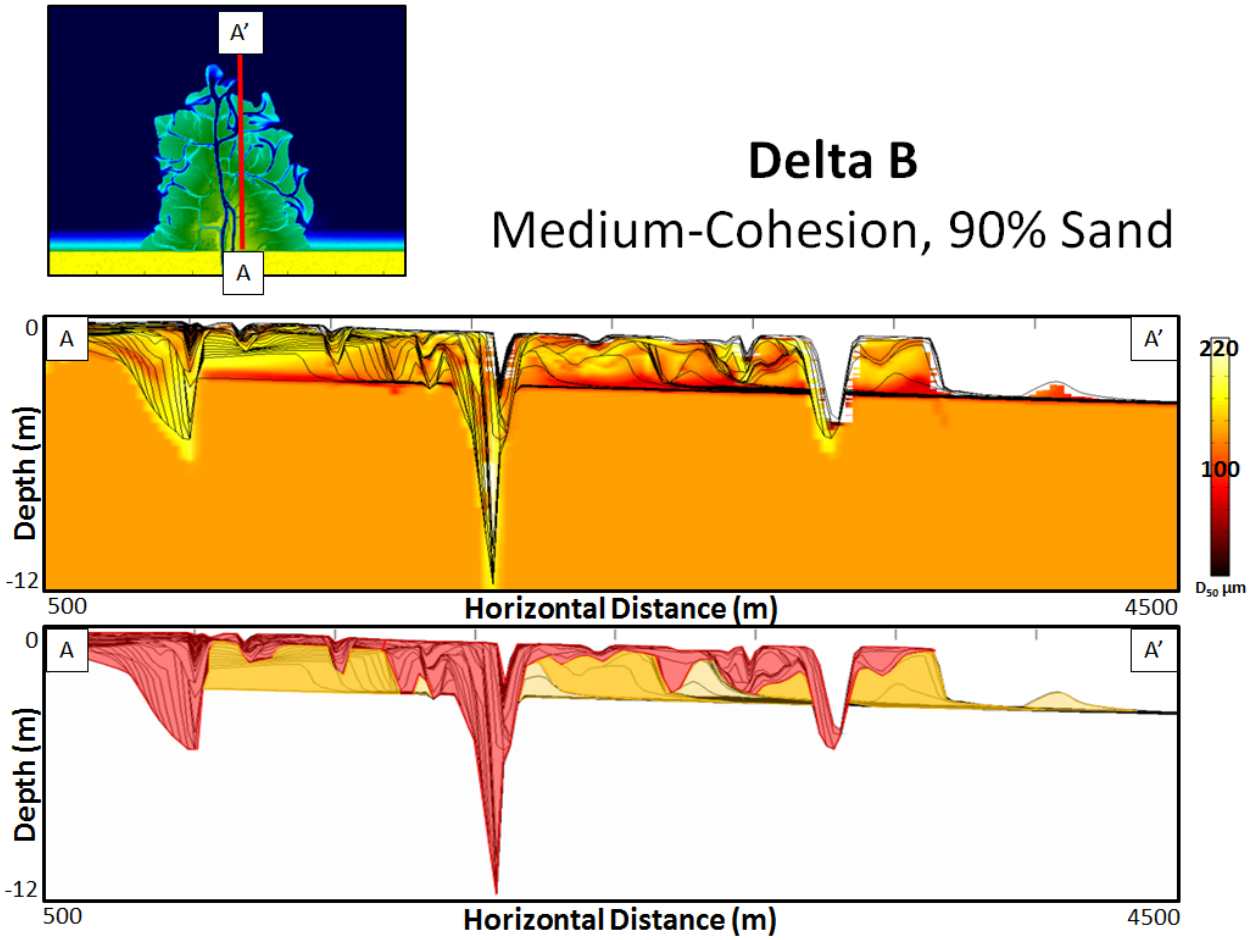
A'
A
Delta B
Medium-Cohesion, 90% Sand
A
A'
0
-12
Depth (m)
500
Horizontal Distance (m)
4500
220
100
D_{50} µm
A
A'
0
-12
Depth (m)
500
Horizontal Distance (m)
4500

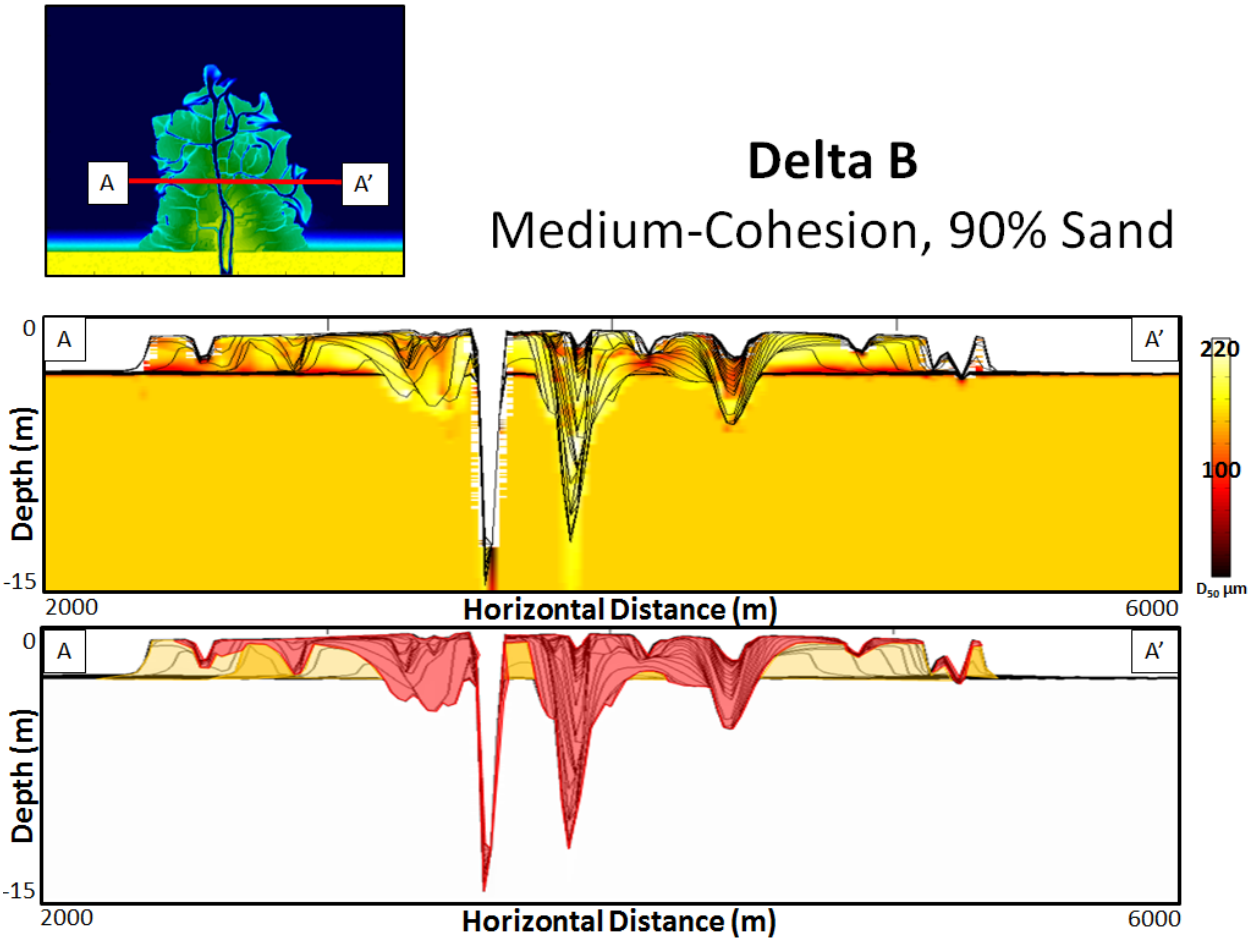
A
A'
Delta B
Medium-Cohesion, 90% Sand
0
-15
Depth (m)
2000
Horizontal Distance (m)
6000
220
100
D50 µm

APPENDIX C

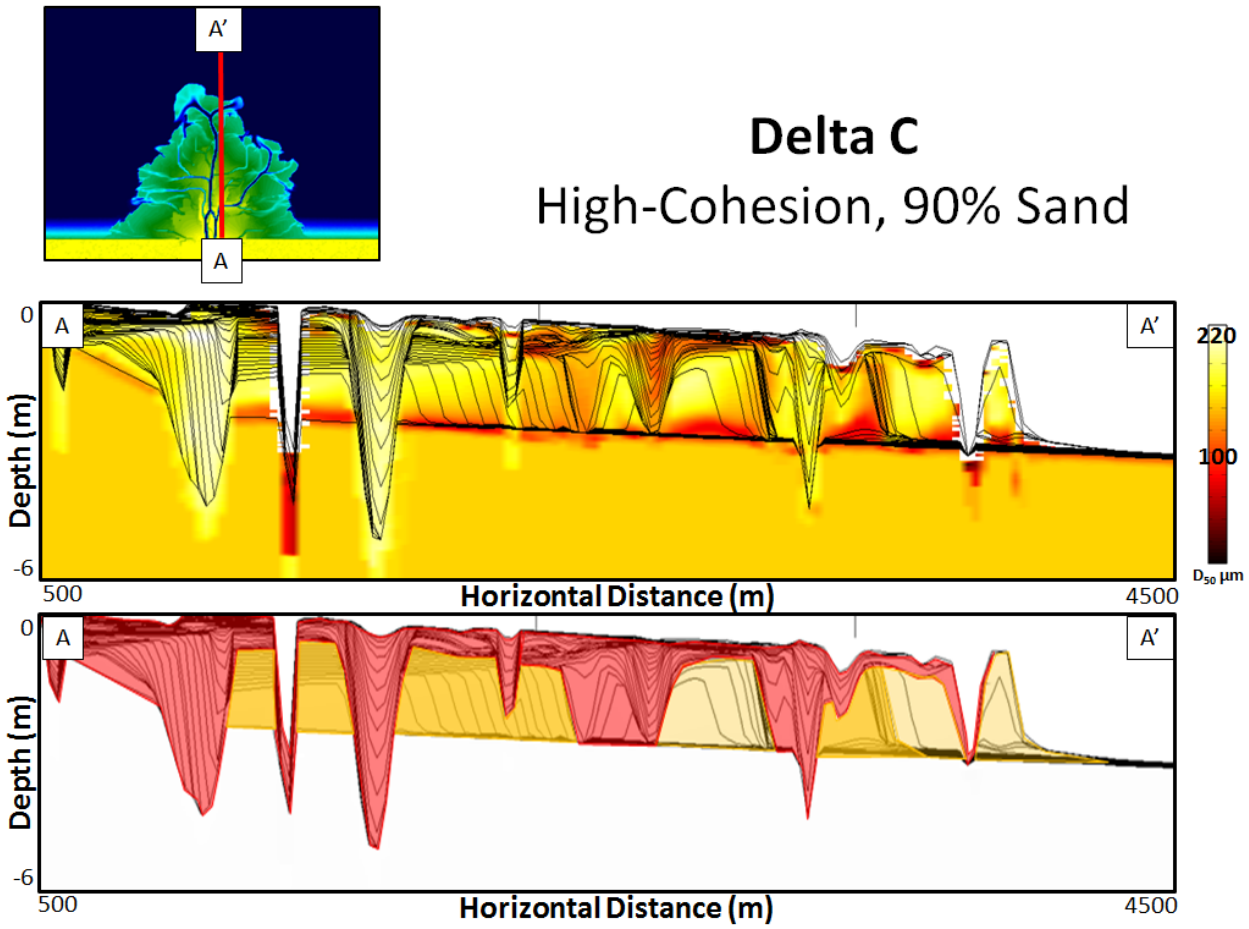
A'
A
Delta C
High-Cohesion, 90% Sand
A
A'
0
-6
Depth (m)
500
Horizontal Distance (m)
4500
220
100
D50 µm
A
A'
0
-6
Depth (m)
500
Horizontal Distance (m)
4500

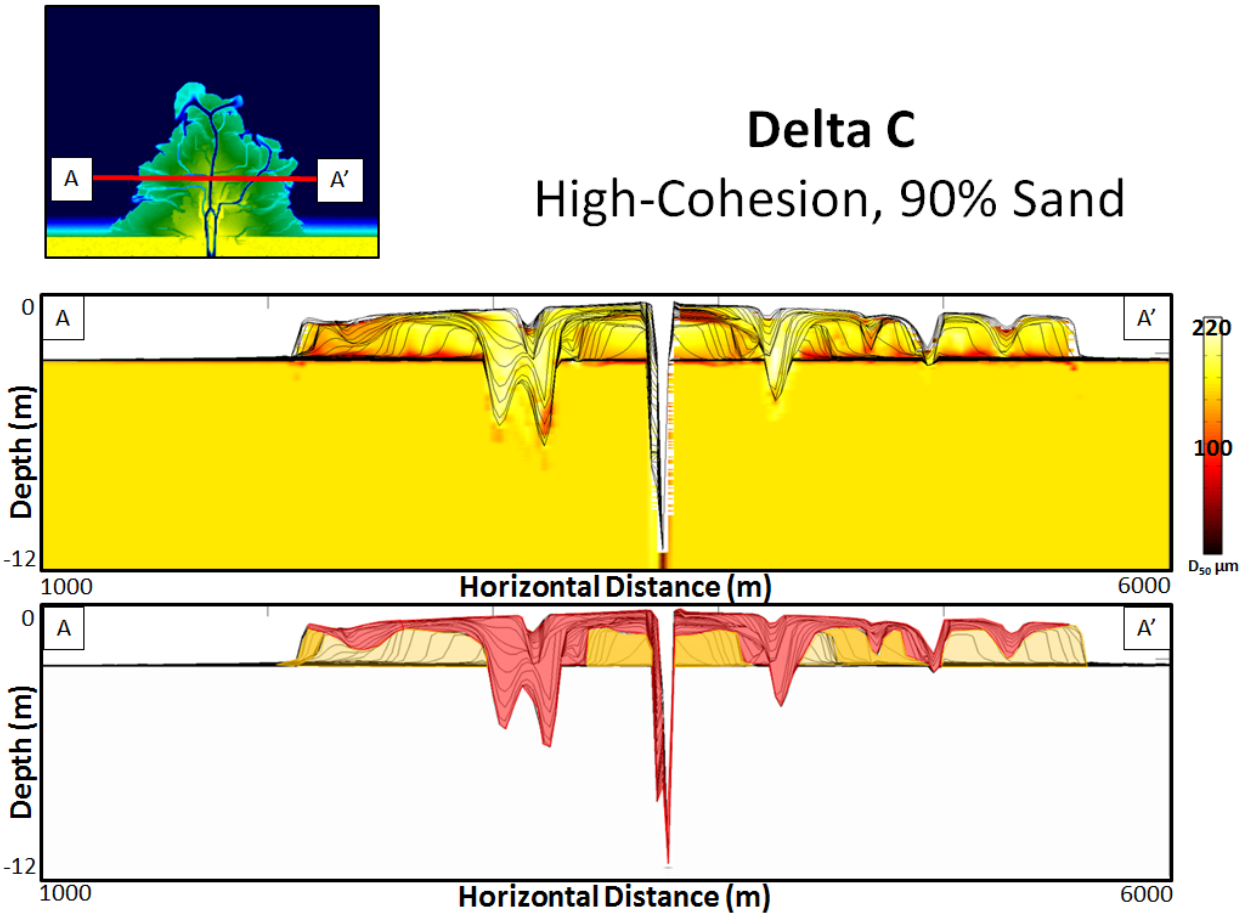
A
A'
Delta C
High-Cohesion, 90% Sand
0
-12
Depth (m)
A
A'
1000
Horizontal Distance (m)
6000
220
100
D50 µm
0
-12
Depth (m)
A
A'
1000
Horizontal Distance (m)
6000

APPENDIX D

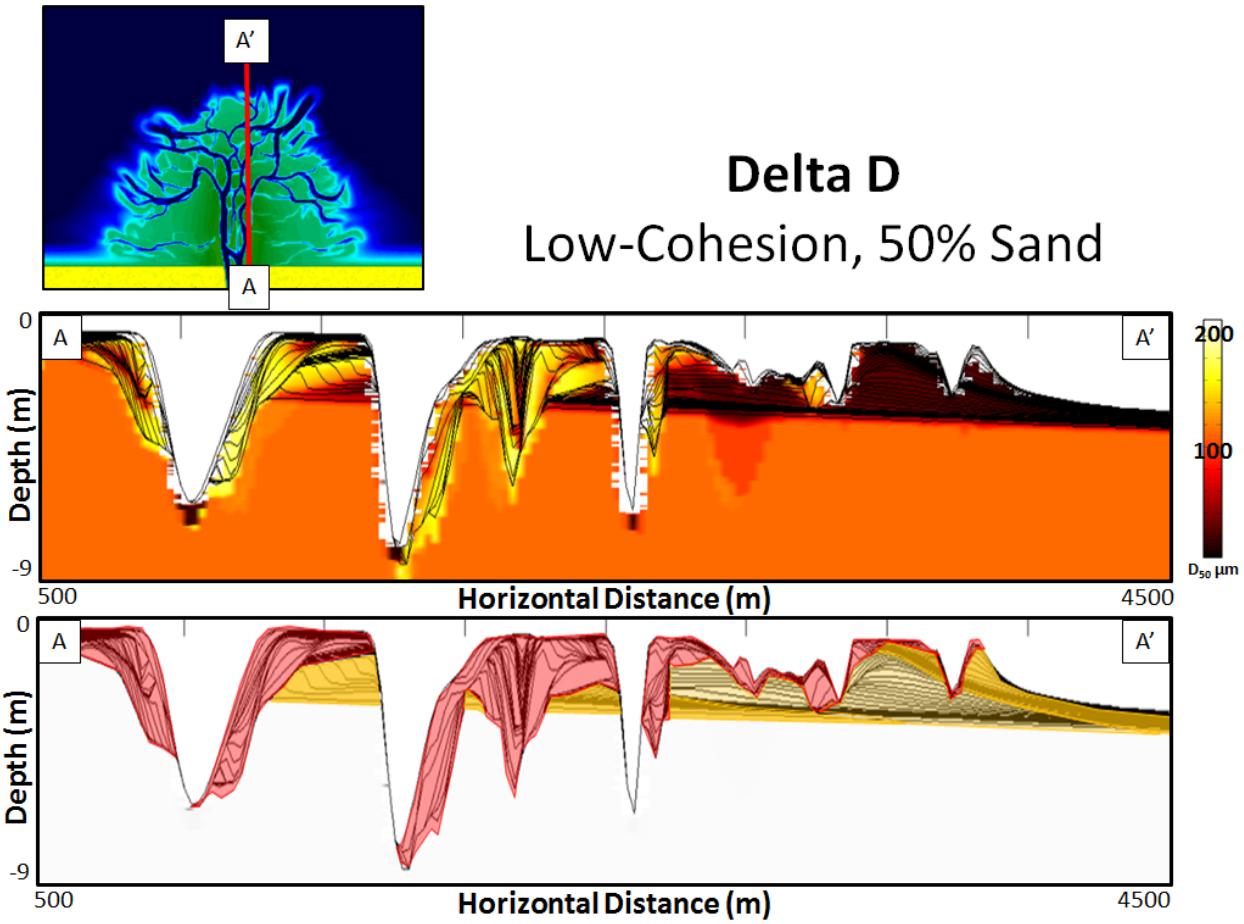
A'
A
Delta D
Low-Cohesion, 50% Sand
0
A
A'
Depth (m)
-9
500
Horizontal Distance (m)
4500
200
100
D50 µm
0
A
A'
Depth (m)
-9
500
Horizontal Distance (m)
4500

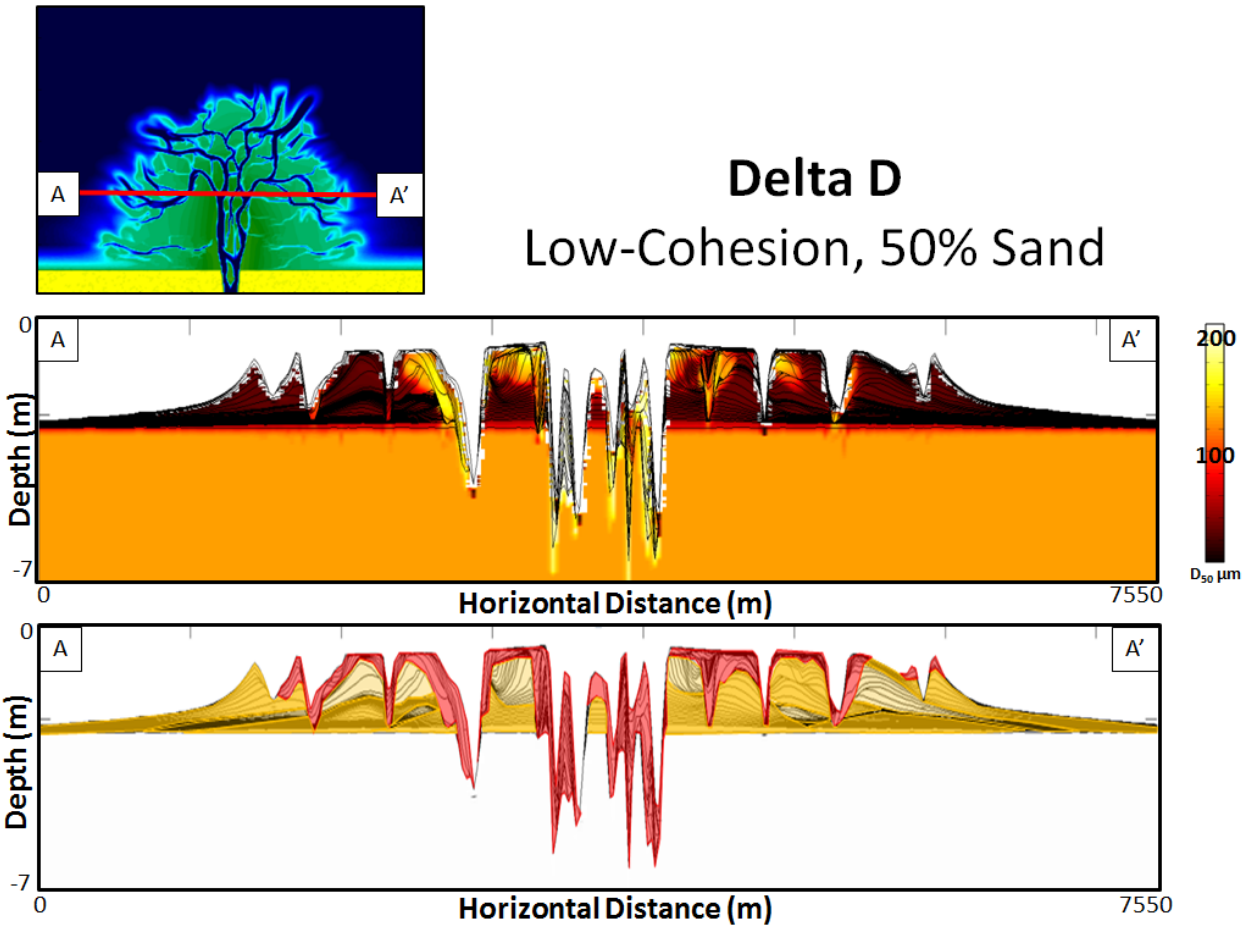
A
A'
Delta D
Low-Cohesion, 50% Sand
0
A
A'
Depth (m)
-7
0
Horizontal Distance (m)
7550
200
100
D50 µm
0
A
A'
Depth (m)
-7
0
Horizontal Distance (m)
7550

APPENDIX E

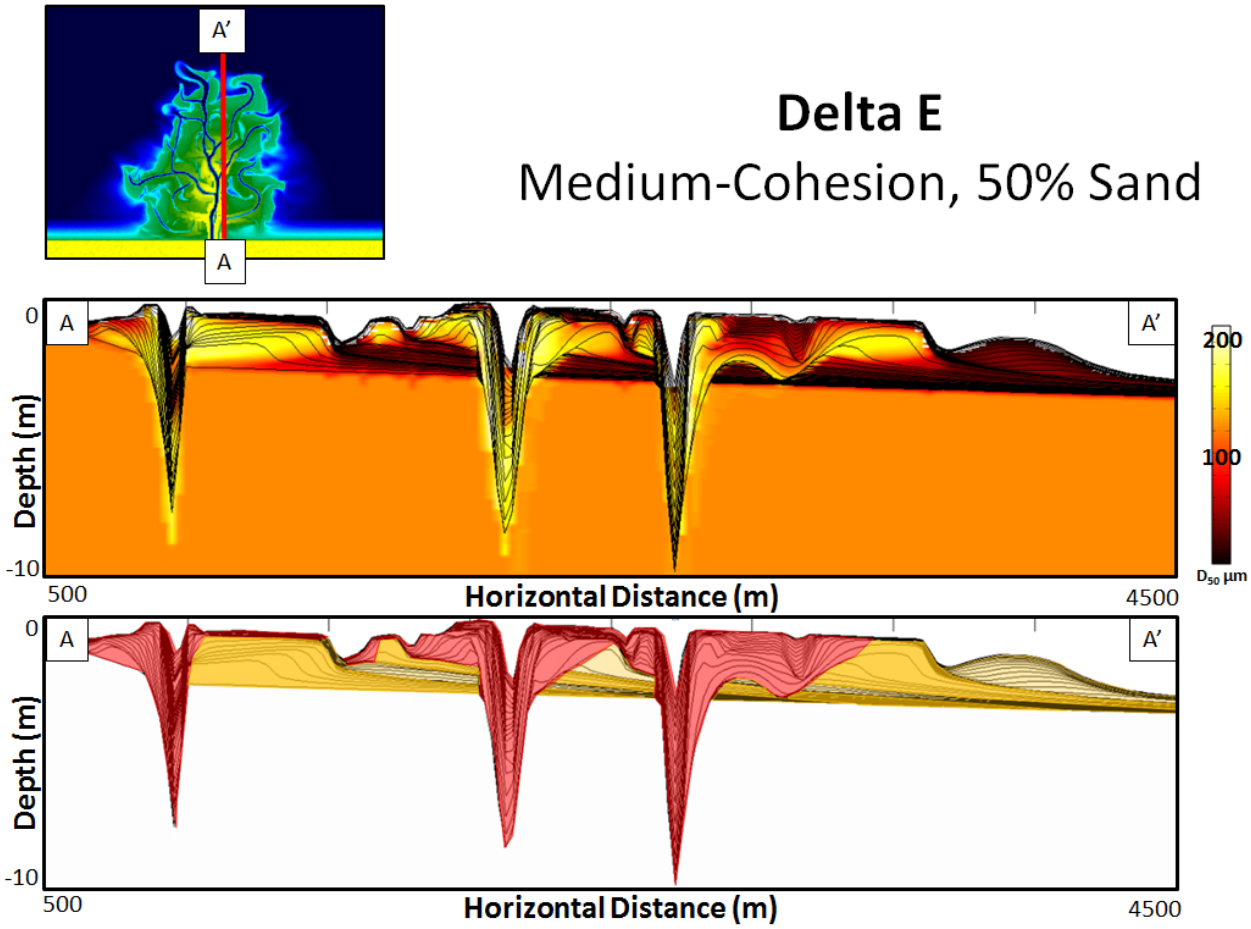
A'
A
Delta E
Medium-Cohesion, 50% Sand
A
A'
0
-10
Depth (m)
500
Horizontal Distance (m)
4500
200
100
D50 µm
A
A'
0
-10
Depth (m)
500
Horizontal Distance (m)
4500

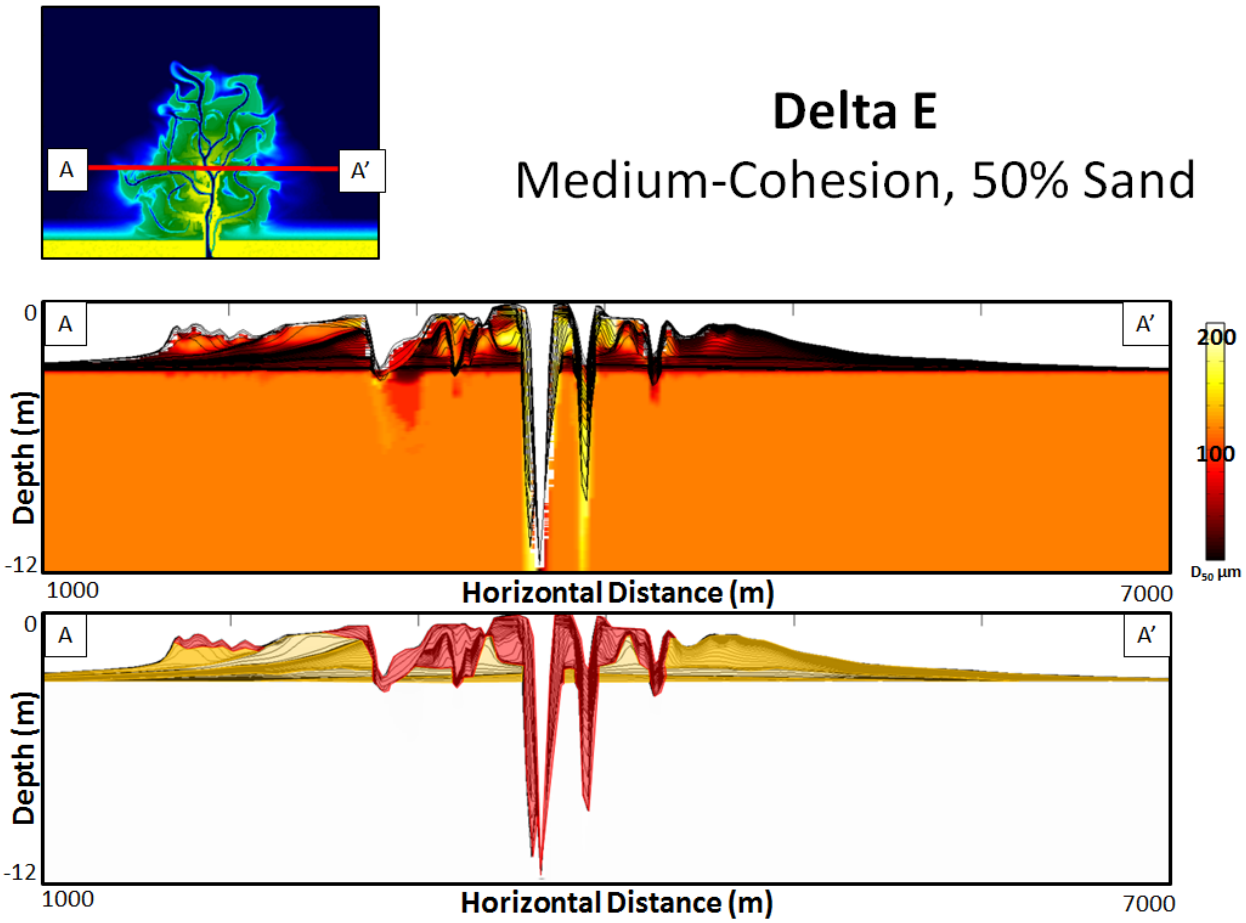
A
A'
Delta E
Medium-Cohesion, 50% Sand
0
-12
Depth (m)
A
A'
1000
Horizontal Distance (m)
7000
200
100
D50 µm
0
-12
Depth (m)
A
A'
1000
Horizontal Distance (m)
7000

APPENDIX F

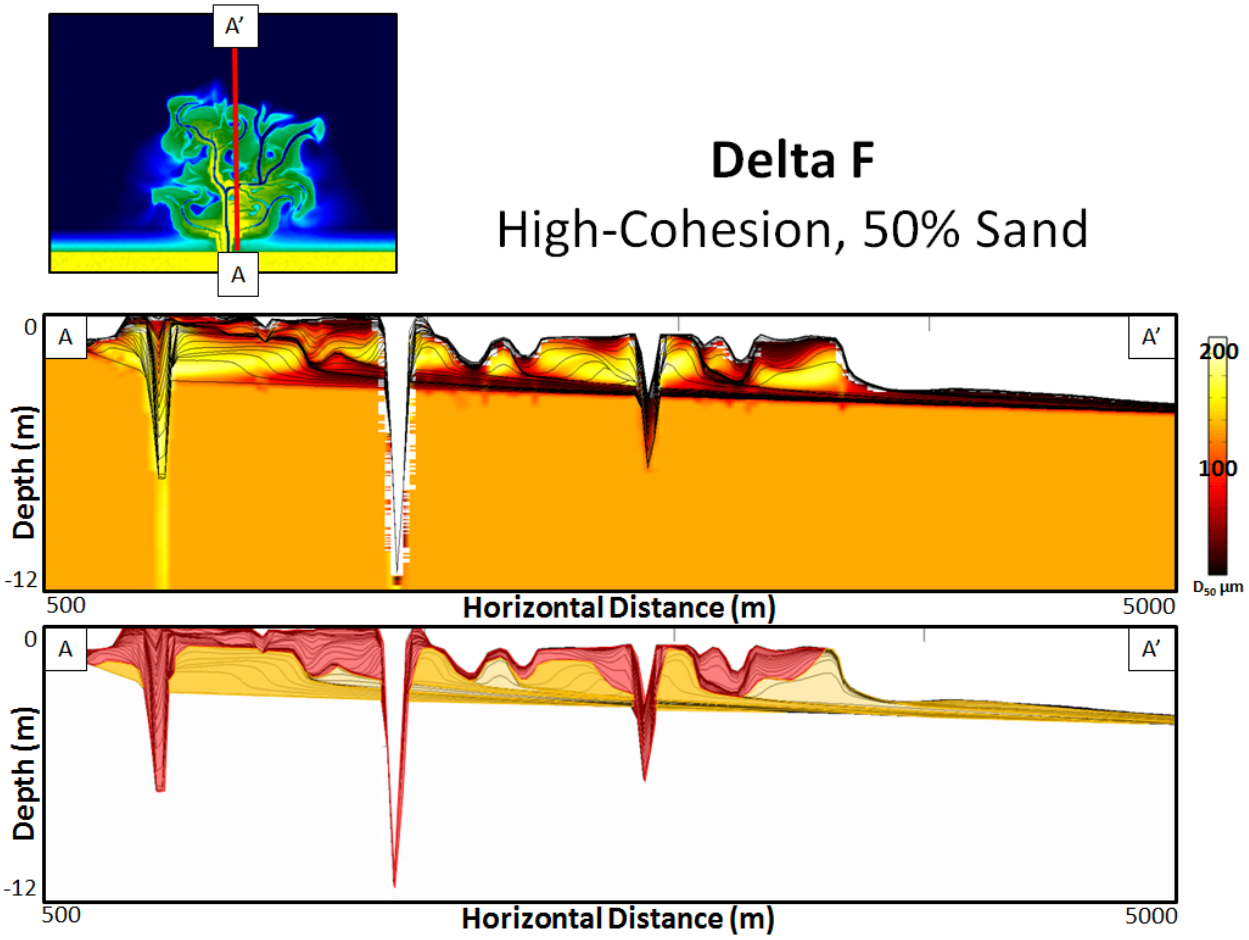
A'
A
Delta F
High-Cohesion, 50% Sand
A
A'
0
-12
Depth (m)
500
Horizontal Distance (m)
5000
200
100
D50 µm
A
A'
0
-12
Depth (m)
500
Horizontal Distance (m)
5000

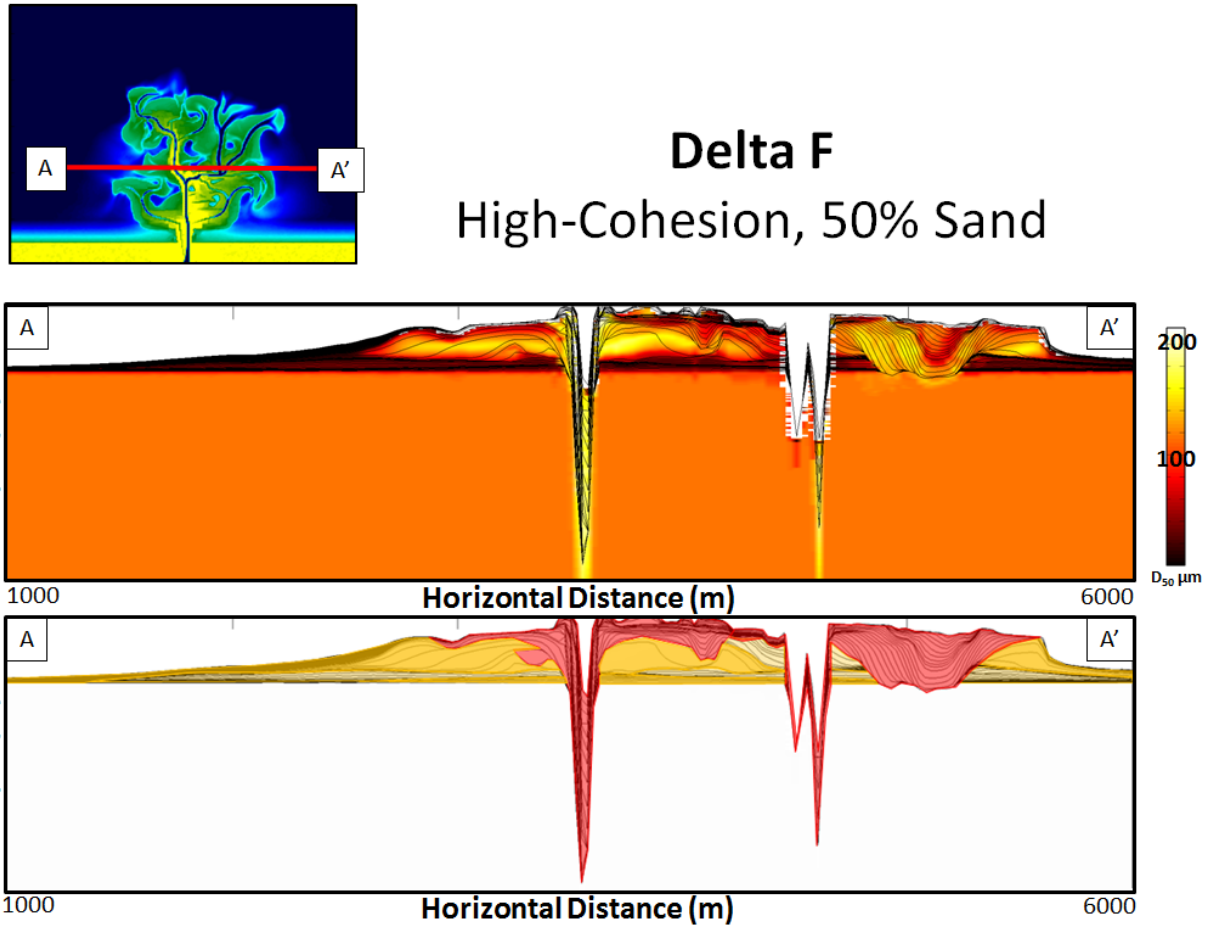
A
A'
Delta F
High-Cohesion, 50% Sand
0
A
A'
Depth (m)
-13
1000
Horizontal Distance (m)
6000
200
100
D50 µm
0
A
A'
Depth (m)
-13
1000
Horizontal Distance (m)
6000

APPENDIX G

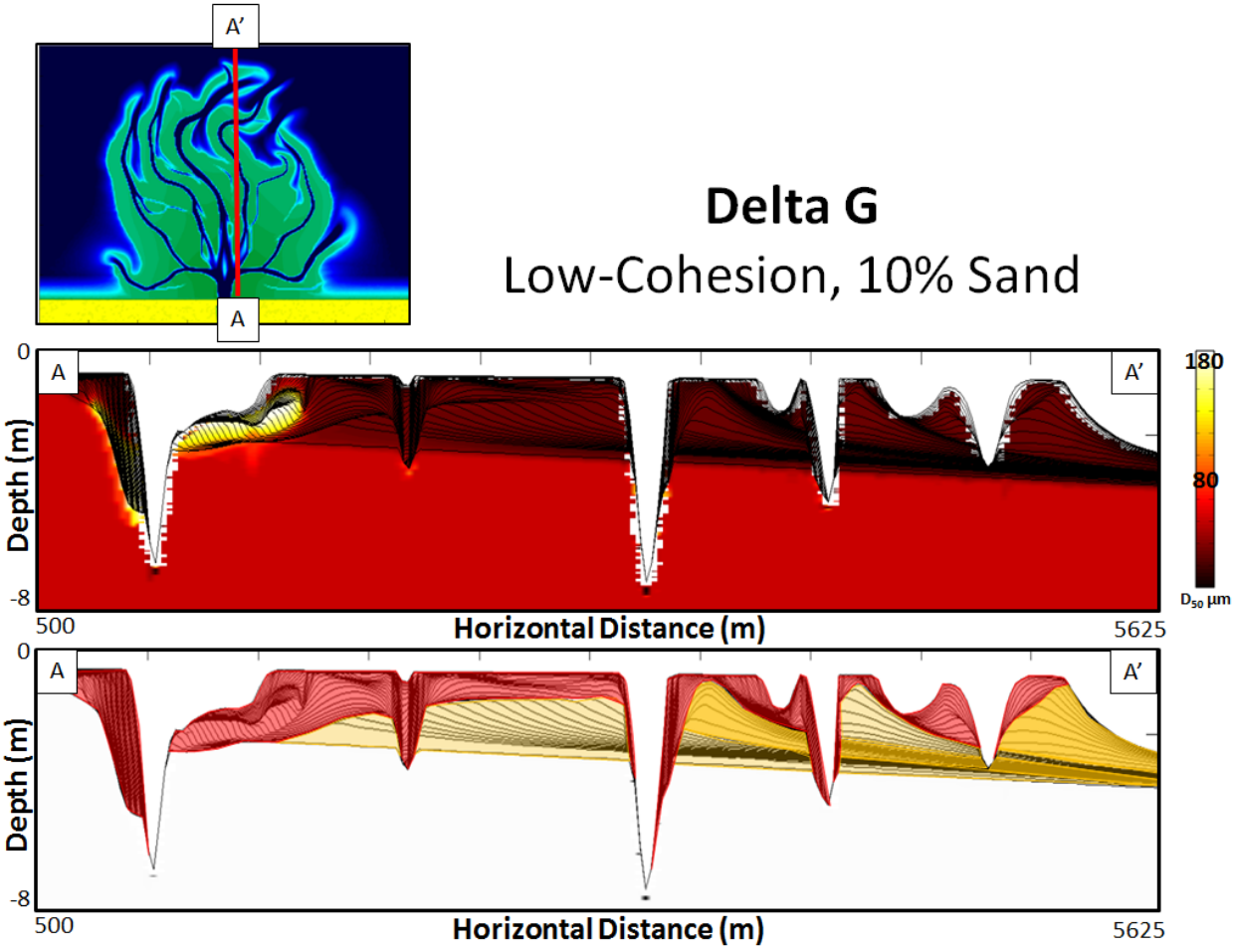
A'
A
Delta G
Low-Cohesion, 10% Sand
A
A'
0
-8
Depth (m)
500
Horizontal Distance (m)
5625
180
80
D50 µm
A
A'
0
-8
Depth (m)
500
Horizontal Distance (m)
5625

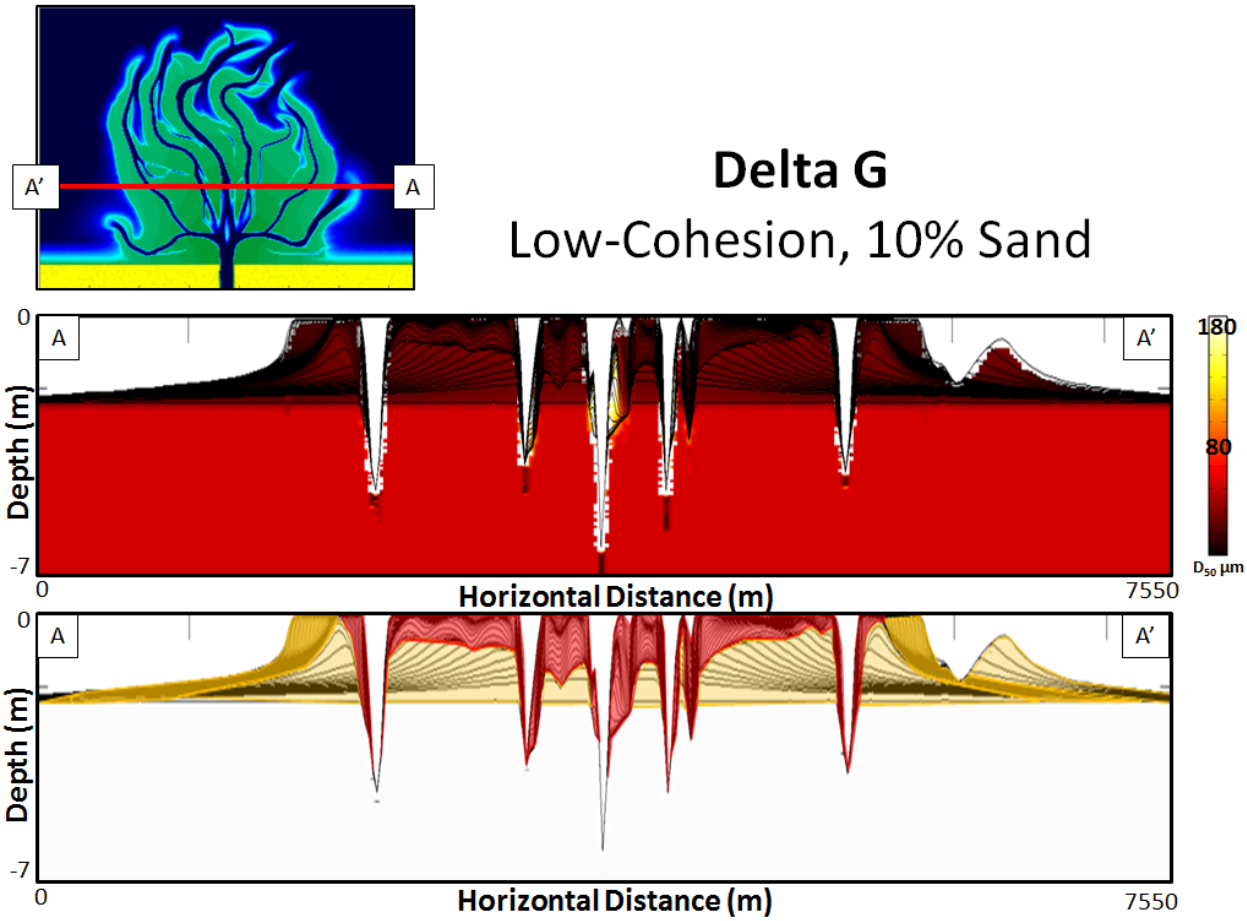
A'
A
Delta G
Low-Cohesion, 10% Sand
0
A
A'
Depth (m)
-7
0
Horizontal Distance (m)
7550
180
80
D_{50} µm
0
A
A'
Depth (m)
-7
0
Horizontal Distance (m)
7550

APPENDIX H

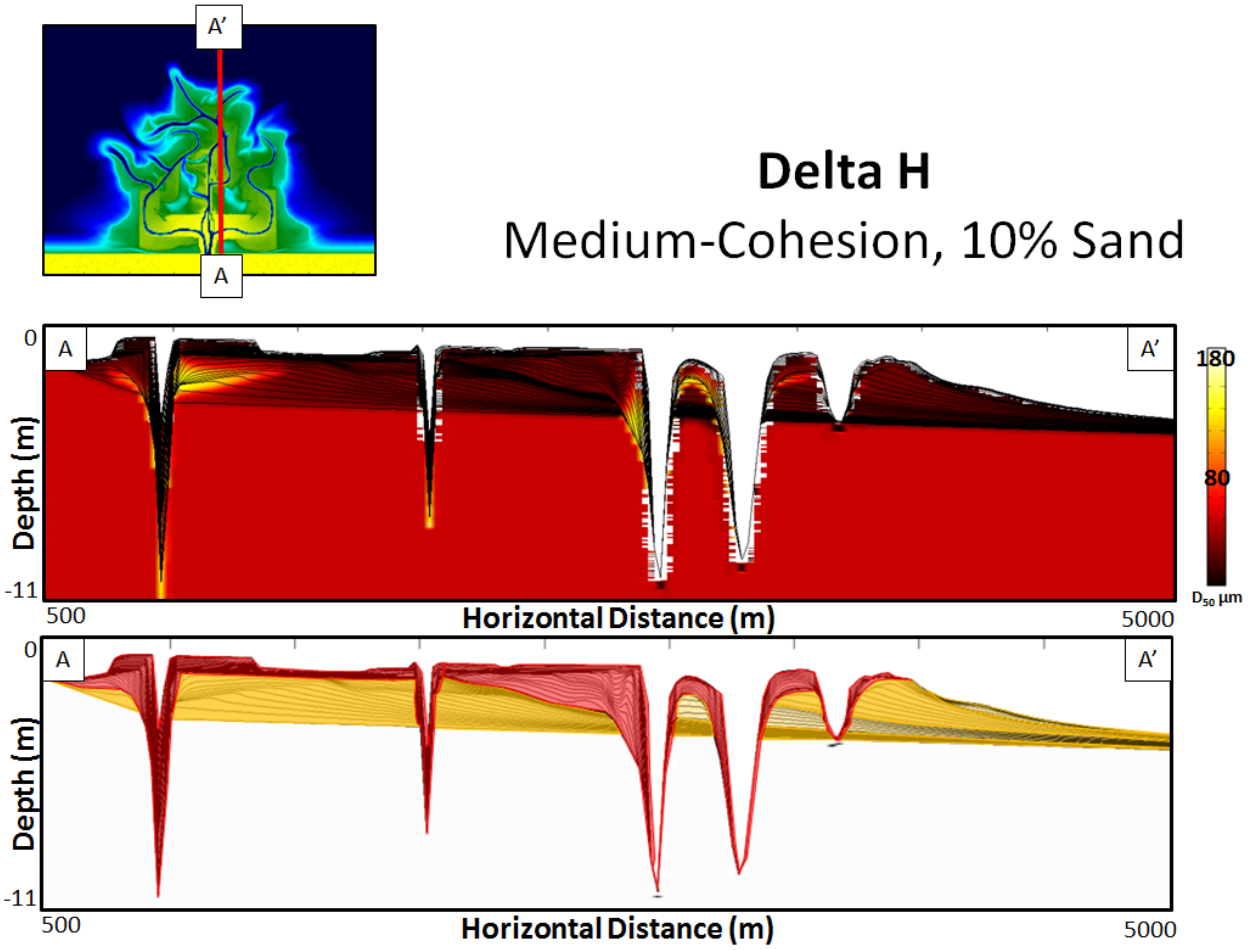
A'
A
Delta H
Medium-Cohesion, 10% Sand
A
A'
0
-11
Depth (m)
500
Horizontal Distance (m)
5000
180
80
D50 µm
A
A'
0
-11
Depth (m)
500
Horizontal Distance (m)
5000

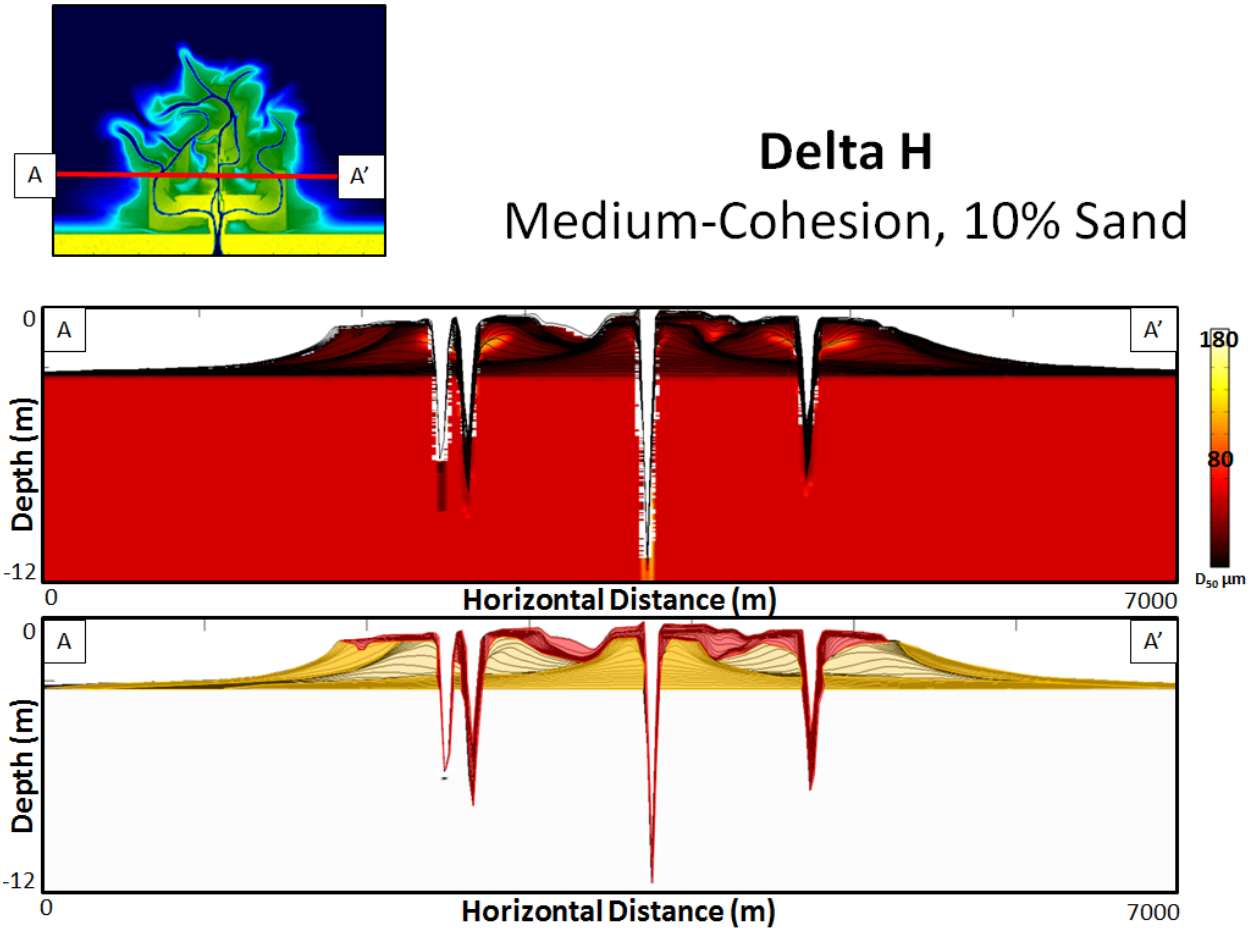
A
A'
Delta H
Medium-Cohesion, 10% Sand
0
-12
Depth (m)
A
A'
0
Horizontal Distance (m)
7000
180
80
D50 µm
0
-12
Depth (m)
A
A'
0
Horizontal Distance (m)
7000

APPENDIX I

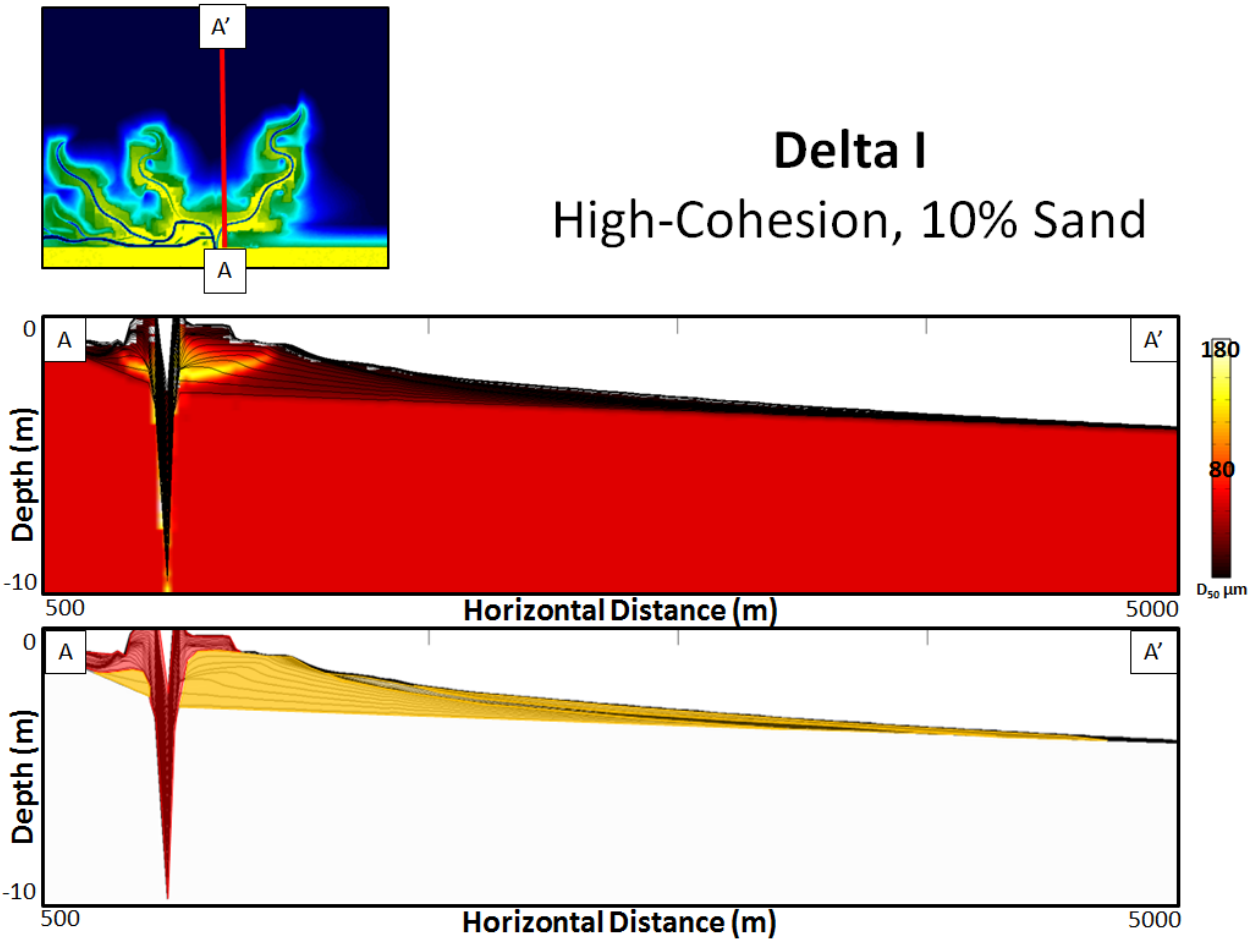
A'
A
Delta I
High-Cohesion, 10% Sand
0
-10
Depth (m)
A
A'
500
Horizontal Distance (m)
5000
180
80
D50 µm
0
-10
Depth (m)
A
A'
500
Horizontal Distance (m)
5000

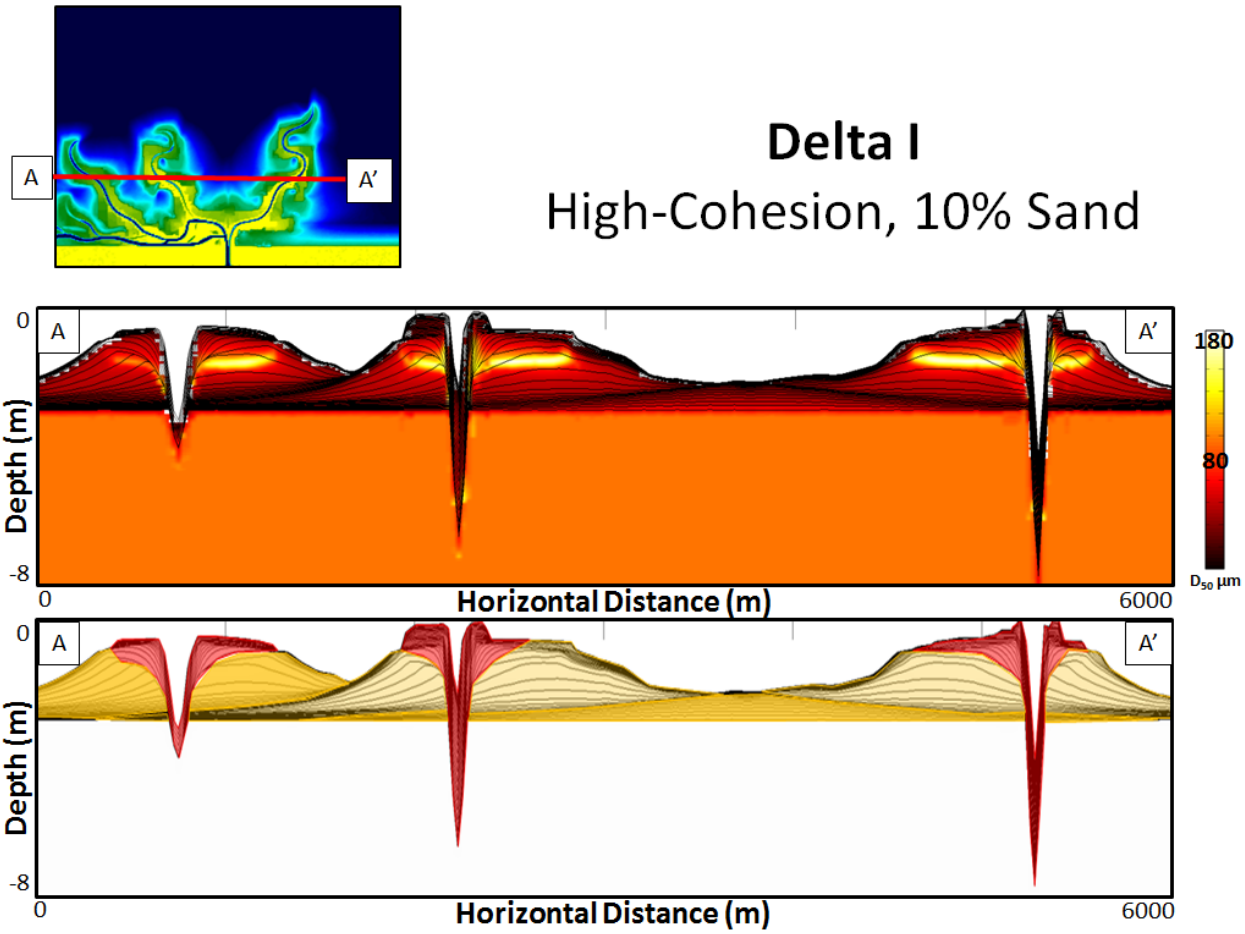
A
A'
Delta I
High-Cohesion, 10% Sand
0
A
A'
Depth (m)
-8
0
Horizontal Distance (m)
6000
180
80
D50 µm
0
A
A'
Depth (m)
-8
0
Horizontal Distance (m)
6000

APPENDIX J

```
%% Shoreline Extraction and Isoperimetric Quotient Calculation
%  APB June 14, 2012
%  Modified from the following:
%% Previous codes
%this m-file takes a cube of topography data from Delft3D output and
%converts each delta into a shoreline using the Open Angle Method (Shaw, et
%al, 2008).

%Code edited by APB and RLS 11/9/11
%Note:  When the delta has prograded to the edge of one of the open
%boundaries, this code will not compute the shoreline on the landward side
%of where the delta has prograded beyond the open boundary.
%%
clear all;
close all;
cd 'D:\BURPEE\NineTypeDeltas\Runs\Run3'  %  for different runs, change the
%  run number in this line, and in line 74 of code.
%%
%  1. Enter the number of time seps recorded for run [RUN SPECIFIC]:
timeslices = 52;
%%
%  2. Load bedlevel.mat "bed level in water level points" exported from
%  QUICKPLOT for all time steps:
load bedlevel; %
filename = 'temp';
%%
%  3. Enter the initial time step where morphodynamic change begins to
%  occur, or the time step where you would like to begin
%  calculating the shoreline [RUN SPECIFIC]:
for i=1:timeslices;
    z=data.Val;
    m=length(z(:,1,1));
        disp(['Computing shoreline for ' filename ' time slice ' num2str(i)])
        ztemp=squeeze(z(i,:,:));
        [r,c]=size(ztemp);
        ztemp=ztemp(2:r-1,23:c-1); %the '-1' and '2' is to get rid of the
collar of NaNs
        [r,c]=size(ztemp);
        mid=ceil(r/2);
        ztemp(mid-10:mid+10,1)=1;
        [r,c]=size(ztemp);
        zz=ztemp<-1; %  the land/water interface is defined as the -0.1 m
contour
        if nansum(nansum(zz))<50
        shore{1,i} = 0;
        else
        n=90;
        cd 'D:\BURPEE\Models\ShorelineCode'
        sl=Seaangles2(zz,n); %this calls the OAM script written by John Shaw,
et al 2008 GRL
        sl2=sparse(sl(2,:),sl(1,:),sl(3,:),r,c);
        sl2=sl2+0;
        angle = 25;
        c=contourc(sl2,[angle,angle]); %this is the NN degree OAM contour,
```

```
        % but the OAM method is imperfect and picks up other smaller,
        % artifical shorelines.  Thus, to find the real one we call contourc,
        % which exports the (x,y) for a given contour level then we sort
        % through that array and find the longest contour which is the
shoreline
        sep=seplines(c);
        % sep=sep(:,2:length(sep(1,:)));  %this cuts off the first contour
line
        % which is the border of the image and not the shoreline
        temp=sep(:,find(sep(1,:)==max(sep(1,:)))); %this returns the 3-row
vector of the
        % longest contour line, which corresponds to the shoreline
        c=c(:,temp(2):temp(3));
        shoretemp=[c(1,:); c(2,:)];
        shore=shoretemp; %this is the x coord of the shoreline at time i
        % Plot the shoreline:
        x=shore(1,:);
        y=shore(2,:);
        % To see both the delta and the shoreline, add the delta to the
        % figure:
        plot(x,y,'o')
        hold on
        contour(ztemp)
        end
%  4.  Save the shoreline file:
cd 'D:\BURPEE\NineTypeDeltas\Runs\Run3\Shoreline'
name=([filename(1:length(filename)-4) '_' num2str(i) '_OAM' num2str(angle)
]);
save(name,'shore')
%  5.  Calculate the area of the shoreline:
basin = zeros(225,300);
X = [];  %  determine the X,Y dimensions of the basin:
Y = [];
[rn,cn] = size(basin);
for j = 1:cn
    X(1:rn,j) = 1:rn;
    Y(1:rn,j) = j;
end
y=shore(1,:);
x=shore(2,:);
IN=inpolygon(X,Y,x,y); %this returns the logical "IN" matrix which is the
%  same size as X and Y with 1=yes this cell is within the shape, 0=no
%  this cell is outside the shape.
IN=+IN; %turns logical to numeric
total=sum(sum(IN));
DeltaArea = (total*(25*25))/(1000*1000)  %  This is the area of the Delta
[km^2]
%  6.   Calculate the perimeter of the shoreline:
sizextemp = size(x);
sizex  = sizextemp(2);
Perimeter = 0;
dist = zeros(1,sizex);
for k = 1:sizex-1;
    distx(k) = abs(x(k)*25 - x(k+1)*25);  %  horizontal distance [m]
    disty(k) = abs(y(k)*25 - y(k+1)*25);  %  vertical distance [m]
    if distx(k) == 0;
        dist(k) = disty(k);
```

```
    end
    if disty(k) == 0;
        dist(k) = distx(k);
    end
    if distx(k) ~= 0;
        if disty(k) ~=0;
            dist(k) = sqrt(distx(k)^2 + disty(k)^2);
        end
    end
    Perimeter = Perimeter + dist(k);  %  Perimeter recorded in [m]
end
%  Add in the distance along the beach!!!
DistBeach = abs(x(1)*25-x(sizex)*25);
PerimeterKM = (DistBeach+Perimeter)/1000  %  Perimeter length [km]
%  7.  Calculate the dimensionless Isoperimetric Quotient(IQ):
IQ(i) = (4*pi*DeltaArea)/(PerimeterKM^2)
end
%  8.  Plot IQ through time:
figure(2)
plot(IQ)
axis([0 55 0 1]);
xlabel('Time Step');
ylabel('Isoperimetric Quotient');
```

APPENDIX K

```
%%  Topset Roughness
%  We measure topset roughness on a strike line for each delta at y = 2000
%  and all x.  We use mean and standard deviation of bed elevation of the
%  topset to determine complexity.
%  APB September 13, 2012
%%
clear all; close all;
%  1.  Load bedlevel data and extract data for strike line:
cd D:\BURPEE\Models\Ferron\Run5
load bedlevel
%  2.  Extract data from file:
bed = data.Val;
strike = bed(52,:,80);
topset = rot90(strike);
%  3.  Copy the "topset" data from the variable editor and paste into an
Excel
%  spreadsheet.  Calculate mean and st dev for topset roughness at
%  different thresholds (-0.1, -0.5, etc).
```

APPENDIX L

```
% Program to extract clinoform dips and dip directions from Delft3D delta
% simulations
% Programmed by RSling and ABurpee
% FINAL VERSION: July 6th 2011
% NOTE:  BE SURE TO CHANGE ALL VALUES IN CODE WHICH ARE RUN AND/OR TIME
% SPECIFIC BEFORE RUNNING!
clear all; close all;

%---------------------- NECESSARY DATA -----------------------------------
% Bed elevation data stored in the bedlevel.mat file written from Quickplot
cd D:\BURPEE\Models\Ferron\Run5
load bedlevel
% The timestep of interest defined here:
TStep = 40;
%-------------------------------------------------------------------------
% Extract the bed elevation for a timestep (the timetep is the first number
% in the array counters)
Z=data.Val(TStep,:,:);
ZZ=squeeze(Z);
% We rotate the delta to prograde to the north because it makes the
% extraction of the clinoform slopes easier.  But note that this reverses
% the counters in the matrix.  The "flipdim" line corrects the error that
% results from bringing the Delft image from Delft to MatLab.  The image
% will come into MatLab as the mirror image of the Delft image.
ZZ=flipdim(ZZ,1);
ZZ=rot90(ZZ,3);
dem=ZZ;
dim = size(ZZ);
N=dim(2);
contour(ZZ,30)
hold on
% Contour the shoreline (actually the -0.1 m contour)as a thick black line
v=[-0.1];
contour(ZZ,v,'k','LineWidth', 2)
% Now define the region of the delta from which you want bed (clinoform
% surface) slopes.  Generally we want to exclude the top- and bottom-set
% region. Extract the bed elevations and bed slopes of interest by setting
all
% bed elevations and slopes landward of the region of interest to 0
for j = 1:302
    for i = 1:227
    if ZZ(i,j) >= -0.10 %Eliminates the topset, except for channels
        ZZ(i,j) = NaN;
    elseif i < 30
        ZZ(i,j) = NaN;  %Eliminates the feeder channel and non-deltaic
                        %shoreline; This line number (30) may change with
                        %different deltas
    end
    end
end
% Now define the toes of the delta clinoform. Hit enter when done.  Be sure
% your line extends from x=0 to to x = xmax and does NOT reverse itself in x.
[X,Y]=ginput;
X=round(X);
```

```
Y=round(Y);
XX=1:N;
YY = interp1(X,Y,XX,'linear');
hold on
YY=round(YY);
plot(XX,YY,'*')
% Define the topset region from which you want to remove bed elevations
% associated with channels
[Xtop,Ytop]=ginput;
Xtop=round(Xtop);
Ytop=round(Ytop);
XXtop=1:N;
YYtop = interp1(Xtop,Ytop,XXtop,'linear');
hold on
YYtop=round(YYtop);
plot(XXtop,YYtop,'o')
drawnow
% Make a vector of zeros and ones, with ones where YYtop is a NaN to
% control the loops below
ControlVec = isnan(YYtop);
% Extract the bed elevations and bed slopes of interest by setting all
% elevations and slopes seward of the region of interest to 0
for j = 1:302
    for i = 1:227
    if i > YY(j)
        ZZ(i,j) = NaN;
    end
    if ControlVec(j) ~= 1 && i < YYtop(j)
        ZZ(i,j) = NaN;
    end
    end
end
% contour the bathymetry of the delta clinoform in the region of study
hold off
subplot(2,2,1); contour(dem,30);
subplot(2,2,2);[CS, H]= contour(ZZ,30);
%clabel(CS,H);
% Calculate the aspect (dip direction), slope, and gradients (along the
% axes) of the delta foreset at every Delft3D cell. The reference vector
% converts the bathy elevation matric to actual geographic coordinates.
% The first number in the vector is the only important one; it gives the
% number of matrix entries per degree latitude.  Because our spacing is 25
% m, and there are 111000 meters per degree, the number of cells for us is
% 111000/25.
refvec = [111000/25 0 0];
[ASPECT, SLOPE, gradN, gradE] = gradientm(ZZ, refvec);
% Convert the aspect from a matrix to a column vector, while converting
% aspect to radians
k=0;
for i=1:227
    for j=1:302
        k=k+1;
        theta(k) = pi/180*ASPECT(i,j);
        dip(k) = SLOPE(i,j);
    end
end
% Remove NaNs
```

```
theta(isnan(theta)) = [];
dip(isnan(dip)) = [];
%Remove all slope data from the area of interest that are of a value less
%than what is observed in a foreset.
dimdip=size(dip);
increm = 0;
for counter=1:dimdip(2);
    if dip(counter) >= 0.08;
        increm = increm+1;
        newdip(increm) = dip(counter);
        newtheta(increm)=theta(counter);
    end
end
% Plot a rose diagram of clinoform dip direction
subplot(2,2,3);
nbins = 36;
h=rose(newtheta,nbins);
view(90,-90)
% Define some constants
num=size(newtheta);
x=0;
y=0;
% Calculate the mean dip direction and dispersion (the statistics below are
% derived from Doornkamp and King, 1971, "Numerical Analysis in
% Geomorphology", p. 208-213)
% VERSION 2 (from Jones, 2006)
C = sum(cos(newtheta));
S = sum(sin(newtheta));
thetabar = VectMean_arctan(S,C); % function from Jones
R = sqrt((S/(num(2))^2 + (C/num(2))^2));
% Large Rbar = small variance and vice versa
s1 = sqrt(2*(1-R)); % Angular dispersion (in radians)as given by Doornkamp
                    % and King
title(['Mean dip direction =',num2str(thetabar)],'FontSize',8)
subplot(2,2,4);
histbin=[0:0.05:8];
hist(newdip,histbin);
avedipmag=mean(newdip);
stdev = std(newdip);
text(1,200,['mean dip magnitude =',num2str(avedipmag)],'FontSize',8);
text(1,400,['dip std dev =',num2str(stdev)],'FontSize',8);
title('Mean Clinoform Bed Dip')
xlabel('dip (dg)')
ylabel('Frequency by Number')
% Run the Vector_Stats Package. Remember that newtheta is in radians
newtheta = newtheta';
Vector_Stats
```

APPENDIX M

```
%%  QUANTIFY CONCAVITY FOR DIP LINES OF DIFFERENT VERTICALLY EXAGGERATION
(VE)
%  APB  August 24, 2012
%%
clear all; close all;
%  1.  Read in and show your image:
%A =
open('D:\BURPEE\NineTypeDeltas\Runs\Run11\Stratigraphy\Run11_Dip_blank.fig');
open('D:\BURPEE\Models\Ferron\Run5\Stratigraphy\Run5_Ferron_Dip_blank.fig');
%imshow(A)
%  2.  Adjust image to zoom in on a clinoform, when image is adjusted,
%  type "return" in the command window:
keyboard
%  3.  Digitize the clinoform by clicking along the clinoform surface.
%  Start acquiring points at the rollover point, defined here as the point
%  where the clinoform changes from convex to concave.  The last point
%  along the clinoform should be acquired at its terminus where the slope
%  becomes zero and there is no more sediment deposition:
[X,Y] = ginput;
      hold on
      plot(X,Y,...
           '.','Color','r','MarkerSize',10)
%  4.  Make Y positive then vertically exaggerate Y:
Ypos = Y+100;
YVE50 = Ypos*50;
%  5.  Calculate the best fit equation of the clinoform:
pVE50 = polyfit(X,YVE50,2);
%  6.  Concavity is the second derivative of the polynomial, and we divide
%  by 50 to calculate the concavity of the clinoform without VE:
concavityVE50 = (pVE50(1)*2)/50
%  7.  %  Determine the misfit error of the polynomial compared to the
surface:
figure(2)
plot(X,YVE50,'o')
hold on
YfitVE50 = polyval(pVE50,X);
plot(X,YfitVE50)
%  8.  Calculate the dip magnitude (degrees) of the clinoform.  The dip
%  magnitude is calculated for the VE cross-section, so the true dip
%  magnitude is the dip magnitude divided by the VE:
M = size(Y);
N = M(1);
for n = 1:(N-1)
YVEchange(n) = YVE50(n+1) - YVE50(n);
YnoVEchange(n) = Ypos(n+1) - Ypos(n);
Xchange(n) = X(n+1) - X(n);
VESlopeAll(n) = YVEchange(n)/Xchange(n);
noVESlopeAll(n) = YnoVEchange(n)/Xchange(n);
end
VESlope = sum(VESlopeAll)/(N-1);
noVESlope = sum(noVESlopeAll)/(N-1);
VEDip = -atan(VESlope)*180/pi  %  this gives vertically exaggerated dip in
%  degrees.  The dip is assumed to be negative, so the dip magnitude is
%  presented as positive.
```

```
noVEDip = -atan(noVESlope)*180/pi  %  no vertical exaggeration
```

APPENDIX N

```
%% Process Laser Ranger Data
%Written by APB and RLS November 2011
%All values in meters or degrees azimuth
%%
clear all; close all;
%% Photomosaic Specific
%  1. Enter n number of shots and the HD VD and AZ for each shot in
%  sequential order.
n=3; %pts
V = [-51.2 -61.2 -50.7];
H = [495 493 473];
AZ = [203.2 202.5 208.6];
%%
%  2. Convert to spherical coordinates
R = sqrt(H.^2 + V.^2);
theta = (360-AZ) * pi/180;
phi = atan(V./H);
[x y z] = sph2cart(theta, phi, R);
%  3. Now calculate the direct line distance and then the horizontal distance
%  (in the plane of the face) between the two laser ranger points
for i = 1:n-1
Dist(i) = sqrt((x(i+1) - x(i))^2 + (y(i+1) - y(i))^2 + (z(i+1) - z(i))^2);
HDist(i) = sqrt(Dist(i)^2 - (z(i+1) - z(i))^2);
end
%  4. Open the corresponding photomosaic
%  Save file as a black and white image
%----------------------Photomosaic Specific-----------------------------
A =
imread('D:\mossy_disk\ALL_DELTA_WORK\BURPEE\FerronData\MatlabTrig\Photos\RC21
.jpg');
%-----------------------------------------------------------------------
B = rgb2gray(A);
C = histeq(B);
%  5.  ** OPTIONAL  If the beds in the photo are horizontal, vertically
exaggerate the image
%  with the following lines of code:
%[oldHeight oldWidth oldNumberOfColorChannels] = size(C);
%newWidth = int32(oldHeight * 2/1);
%newImage = imresize(C, [oldHeight newWidth]);
imshow(B);  %show "newImage" if vertically exaggerating, otherwise show B
%  6. To brighten or darken the image, use positive value btw 0 and 1 for
% brightening and negative value btw 0 and -1 for darkening.
brighten(0.2)
%  7. Pause the program to allow yourself to zoom the image.
keyboard
%  Once the image has been adequately zoomed, TYPE "return" into the
%  command window.
%  8. Tag the photomosaic where laser ranger shots were acquired.  You MUST
%  click the photomosaic in the same order as the points were acquired so
%  that each tagged point has the corresponding VD, HD, and AZ.
[Xopixels,Yopixels] = ginput;
      hold on
      plot(Xopixels,Yopixels,...
           '.','Color','r','MarkerSize',10)
```

```
%Hit "enter" when all laser ranger shots have been tagged
%want to use ginput to get the pixel coordinates of every point measured by
%the laser rangefinder.
%Now we have all of the information that we need to scale the pixels to a
%true horizontal and vertical distance (m).  These will not necessarily be
%the same length scales.  To determine the height of a pixel (m), consider
%the following.  The number of pixels between two laser ranger shots at
%different elevations is given by the abs difference between the Yopixel
%values of those two points.  The actual distance (m) between those two
%points is the abs difference of the z value of the two points from the
%laser ranger shots.  Therefore, the height of a pixel is the distance (m)
%divided by the number of pixels between the two points.  For the width of
%a pixel, we take the abs difference between the Xopixel values for two
%laser ranger points and divide that into HDist, the horizontal distance
%between those two points computed from the laser ranger data.
%ASSUMING YOU HAVE ORDERED YOUR LASER RANGER SHOTS AND YOUR X,Y,Z PIXELS IN
%SEQUENCE, THEN THE ABOVE IS ACCOMPLISHED BY:
Zdiff = abs(z(1)-z(2));
PixHeight = Zdiff/abs(Yopixels(1)-Yopixels(2));
PixWidth = HDist(1)/abs(Xopixels(1)-Xopixels(2));
%Now that the pixels have a value (m), you can again use ginput to acquire
%coordinates along the clinoform surface.  Click two points on the
%clinoformand press "enter".
[S,D] = ginput;
ClinSlope = ((abs(D(1)-D(2)))*PixHeight)/((abs(S(1)-S(2)))*PixWidth);
ClinDip = 180/pi*atan(ClinSlope)
```

APPENDIX O

```
%DEFINING THE AZIMUTH OF A CLIFF FACE
%RLS AND APB
%NOV 2011
%Process Laser Ranger Data to obtain best estimate of azimuth of a cliff
%face from laser ranger shots to face
clear all; close all;
%----------------------DATA-----------------------------------------------
%Ranger shots to a particular face
%All values in meters or degrees azimuth
V = [-16.5 -29.2 -15 -27.1];
H = [283 280 289 286];
AZ = [41.0 41.1 48.2 48.3];
%-------------------------------------------------------------------------
% Convert to spherical coordinates
R = sqrt(H.^2 + V.^2);
theta = (360-AZ) * pi/180;
phi = atan(V./H);
%Convert from spherical to Cartesian coordinates where the origin is at the
%laser ranger. Note that north is due east (i.e., uses math coordinate
%system with positive x to east
[X Y Z] = sph2cart(theta, phi, R);
% Throw away the Z (assume the face is vertical), and get a best fit line
% for the trend of the face in X Y space
p = polyfit(X,Y,1);
% The slope of the line in the horizontal plane is given by m in the
% equation y = mx + b. The arctan of that slope is the angle the line makes
% measured from x towards y, that is to say, its bearing. The bearing of
% this line is the strike bearing (angle beta below).
% We are using 19th century convention for strike, so if dip in in quandrant
% III or IV strike was corrected by adding 180 degrees
m=p(1);
if m > 0
    beta = 360 - 180/pi*atan(m);
elseif m < 0
        beta = 180/pi*atan(m);
end
fprintf('Strike of Cliff Face is %4.2f degrees\n', beta)
```

APPENDIX P

```
%Script to calculate the strike, dip, and dip direction of a clinoform
%(plane), given two vertical, non-parallel cliff faces on which the traces
% of (not necessarily the same) clinoforms can be seen.

%-------------------------------------------------------------------------
% Needed: the bearings of the two faces in the direction of the apparent dip
% (i.e., the trends of the clinoform traces) and their apparent dips
% (plunges). Always make the first trend the smaller bearing angle!
%-------------------------------------------------------------------------

% +y is due East--RSling 4/11
%Determine whether user wants to read a file or input data in a dialog box
clear all; close all
ButtonName=questdlg('How do you want to input your data?', ...
                        'Laser Ranger Data', ...
                        'An ASCII File','A Dialog Box', 'ASCII File');

   switch ButtonName,
     case 'An ASCII File',
     disp('ASCII');
     case 'A Dialog Box',
      disp('Dialog');
   end
A=length(ButtonName);
if A == 13
    load('data.txt','-ascii')
    Array = data;
else
    prompt = {'Enter: bearing1 plunge1', 'Enter: bearing2 plunge2'};
    dlg_title = 'Input Laser Ranger Data';
    num_lines= 1;
    def     = {'5 15','95 15'};
    answer = inputdlg(prompt,dlg_title,num_lines,def);
    row1 = str2num(answer{1});
    row2 = str2num(answer{2});

    Array = [row1; row2];
end
bearing = Array(:,1);
plunge = Array(:,2);
phi = pi/180*abs(bearing(1)-bearing(2));
alpha1 = plunge(1)*pi/180;
alpha2 = plunge(2)*pi/180;
theta = 180/pi*atan(-sin(phi)/(cos(phi)-(tan(alpha2)/tan(alpha1))));
%Calculate dip direction
dipdir = bearing(1)-theta +90;
% now calculate the true dip
delta = 180/pi*atan(tan(alpha1)/sin(theta*pi/180));
%Output the results as dip angle and dip direction (ie, European convention).
stringout=sprintf('The dip angle is %d degrees; the dip azimuth is %d
degrees',round(delta), round(dipdir));
disp(stringout)
```